Systematic Development and Validation of Predictive Models for the Removal of Indoor Gaseous Pollutants using Carbon-Based Filters

Mohamad Ghamangiz Khararoodi

A Thesis

In the Department

of

Building, Civil and Environmental Engineering

Presented in Partial Fulfillment of the Requirements

For the Degree of

Doctor of Philosophy (Civil Engineering) at

Concordia University

Montreal, Quebec, Canada

August 2023

CONCORDIA UNIVERSITY

SCHOOL OF GRADUATE STUDIES

This is to certify that the thesis prepared

By: Mohamad Ghamangiz Khararoodi

Entitled: Systematic Development and Validation of Predictive Models for the Removal of Indoor Gaseous Pollutants using Carbon-Based Filters

and submitted in partial fulfillment of the requirements for the degree of

Doctor of Philosophy (Civil Engineering)

complies with the regulations of the University and meets the accepted standards with respect to originality and quality.

Signed by the final examining committee:

_____ Chair
Dr. M. Reza Soleymani

_____ External Examiner
Dr. Jafar Soltan

_____ External to Program
Dr. Christian Moreau

_____ Examiner
Dr. Catherine Mulligan

_____ Examiner
Dr. Chunjiang An

_____ Thesis Co-Supervisor
Dr. Fariborz Haghighat

_____ Thesis Co-Supervisor
Dr. Chang-Seo Lee

Approved by_____
Dr. Chunjiang An, Graduate Program Director

August, 2023_____
Dr. Mourad Debbabi, Dean
Gina Cody School of Engineering & Computer Science

Abstract

Systematic Development and Validation of Predictive Models for the Removal of Indoor Gaseous Pollutants using Carbon-Based Filters

Mohamad Ghamangiz Khararoodi, Ph.D.

Concordia University, 2023

Adsorbent media, which utilize physisorption and/or chemisorption to remove gaseous pollutants, are the most commonly employed technology for indoor air purification. The primary challenge associated with this technology is the saturation or exhaustion of the filter. Since conducting tests at low indoor concentrations (ppb level) is time-consuming and costly, it is necessary to develop models that can predict the service life of adsorbent filters based on experimental data obtained at high concentrations.

The main purpose of this research is to estimate the performance of activated carbon filters in removing a mixture of ozone and VOCs. Three VOCs with various properties, namely limonene, toluene, and methyl ethyl ketone, were selected. To achieve the final goal, models were developed progressively for the individual components (ozone or VOC) as well as for the VOC binary mixture. The unknown parameters of these models were determined using experimental data obtained from a bench-scale setup at ppm concentration levels. Subsequently, the models were validated at lower concentrations, a higher velocity, and on a full-scale setup. Pore gas-phase and surface diffusion were the

dominant mass transfer steps for intraparticle mass transfer of zone and VOCs, respectively. On the other hand, axial dispersion was important in the interparticle mass transfer of all components. Furthermore, a first-order chemical reaction and a polynomial function effectively described the reactions involving fresh activated carbon and ozone, as well as the parallel deactivation of activated carbon through chemisorption and catalytic processes.

Using the information derived from modelling the removal of ozone, single VOCs, and binary mixtures of VOCs, the filter's performance was further modelled for the removal of binary and ternary mixtures of ozone and VOCs. The proposed model considers the generation of by-products resulting from the heterogeneous reaction between ozone and the reactive VOC (limonene) on the carbon surface. The rate constant for this heterogeneous reaction, formulated upon the Eley-Rideal mechanism, was determined by fitting the model to the experimental data. The obtained reaction constant was then used to validate the model's ability for binary and ternary mixtures of ozone and VOCs at typical indoor concentrations.

ACKNOWLEDGMENT

I would like to begin by conveying my utmost gratitude to my supervisors, Professor Fariborz Haghighat and Dr. Chang-Seo Lee, for their invaluable guidance, unwavering support, and remarkable patience during my doctoral studies. Their insightful counsel, innovative thinking, and meaningful conversations have consistently assisted and motivated me at various stages of this research.

I am grateful to Dr. Jiping Zhu and Dr. Jianjun Niu from Health Canada for their assistance and support in analyzing my samples using TD-GC/MS.

Also, I would like to express my gratitude to Mr. Luc Demers and Ms. Hong Guan for their technical support and dedication.

I would like to extend my heartfelt appreciation to the members of my thesis committee, Dr. Catherine Mulligan, Dr. Christian Moreau, Dr. Chunjiang An, and Dr. Jafar Soltan for their invaluable advice and suggestions that have greatly contributed to my research.

I would like to express my heartfelt appreciation to my colleagues and friends (Dr. Mojtaba Malayeri, Marzieh Namdari, Rasoul Rajabi Khamesi, Moein Dadollahi, Dr. Mohammad Esrafilian Najafabadi), whose unwavering support and insightful guidance have been invaluable throughout my journey of pursuing a Ph.D.

Lastly, I would like to convey my deepest gratitude to my parents, my brothers, and my uncle for their unwavering encouragement and support throughout my life. Their belief in me has been a constant source of strength, and I am incredibly grateful for their presence and influence. Without their unwavering faith, I would not have been able to achieve what I have accomplished thus far.

Table of Contents

List of Figures

List of Tables

List of Symbols

English Letters

A	surface area per mass of adsorbent $\left(\frac{m^2}{g}\right)$
a	activity function for the reaction between ozone and activated carbon
a_V	specific surface area of the bed $\left(\frac{m^2}{m^3}\right)$
Bi_p	relative resistance of pore diffusion to boundary layer mass transfer
Bi_s	relative resistance of surface diffusion to boundary layer mass transfer
C	concentration in bulk outside the boundary layer $\left(\frac{mg}{m^3}\right)$
C_{exp}	experimental value of outlet concentration $\left(\frac{mg}{m^3}\right)$
C_{in}	inlet concentration of the filter $\left(\frac{mg}{m^3}\right)$
C_{inlet}	inlet concentration of the duct $\left(\frac{mg}{m^3}\right)$
C_{mat}	concentration in the adsorbent particle $\left(\frac{mg}{m^3}\right)$
C_{out}	outlet concentration of the filter $\left(\frac{mg}{m^3}\right)$
C_{pred}	predicted value of outlet concentration $\left(\frac{mg}{m^3}\right)$
C_p	concentration in the gas-phase of adsorbent pores $\left(\frac{mg}{m^3}\right)$
C_S	saturation concentration $\left(\frac{mg}{m^3}\right)$
$C_{surface}$	ozone concentration at the external surface of activated carbon $\left(\frac{mg}{m^3}\right)$
C_{WP}	Weisz-Prater parameter
$\bar{C}$	dimensionless concentration
$\overline{C}_{\text{exp}}$	average experimental value of outlet concentration $\left(\frac{mg}{m^3}\right)$
$\bar{C}_p$	dimensionless concentration
$\bar{\bar{C}}_p$	average concentration in the gas-phase of adsorbent pores $\left(\frac{mg}{m^3}\right)$
C^*	concentration close to the external surface of adsorbents $\left(\frac{mg}{m^3}\right)$
D_e	effective diffusivity $\left(\frac{m^2}{s}\right)$
D_g	distribution parameter
D_K	Knudsen diffusion coefficient $\left(\frac{m^2}{s}\right)$
D_m	molecular diffusion coefficient $\left(\frac{m^2}{s}\right)$

D_p	effective gas-phase diffusion coefficient $\left(\frac{m^2}{s}\right)$
d_p	mean diameter of the activated carbon particle (m)
D_s	surface diffusion coefficient $\left(\frac{m^2}{s}\right)$
D_{s0}	surface diffusivity at zero loading $\left(\frac{m^2}{s}\right)$
D_x	axial dispersion coefficient $\left(\frac{m^2}{s}\right)$
$\overline{D}_s$	dimensionless surface diffusivity
E	characteristic energy $\left(\frac{J}{mol}\right)$
Ed_p	Diffusion Modulus based on the gas-phase diffusivity
Ed_s	Diffusion Modulus based on the surface diffusivity
$f'(C)$	slope of adsorption isotherm
g	number of experimental data
$g(a)$	a function of chemisorbent activity
H	height of the filter (m)
$h(C_p)$	functionality of rate of decay
J	rate of mass transfer $\left(\frac{mg}{s.m^2}\right)$
k	reaction constant $\left(\frac{1}{s}\right)$
K_C	external mass transfer coefficient $\left(\frac{m}{s}\right)$
k_d	specific decay constant for the reaction between ozone and activated carbon $\frac{1}{s}\left(\frac{m^3}{mg}\right)^m$
K_{DR}	D-R constant $\left(\frac{mol^2}{J^2}\right)$
K_m	ratio between the average concentration in the adsorbent particle and the gas-phase concentration at the interface $\left(\frac{m^3}{g}\right)$
K_p	partition coefficient in the linear adsorption model $\left(\frac{m^3}{g}\right)$
k_p	LDF model mass transfer coefficient $\left(\frac{1}{s}\right)$
k_1	reaction rate constant between ozone and activated carbon $\left(\frac{1}{s}\right)$
k_2	heterogeneous reaction rate constant $\left(\frac{m^3}{s.mg}\right)$
k_3	homogeneous reaction rate constant $\left(\frac{m^3}{s.mg}\right)$
L	thickness of the filters (m)
L_1	upstream length (m)
Pe	Peclet number

M	molecular weight of the diffusing system $\left(\frac{g}{mol}\right)$
m	exponent in the functionality of the rate of decay
M_{carbon}	mass of carbon per area $\left(\frac{mg}{m^2}\right)$
$M_{carbon.F}$	mass of carbon per filter (g)
M_r	removed pollutant mass at time t $\left(\frac{mg}{g}\right)$
M_0	maximum chemisorption capacity $\left(\frac{mg}{g}\right)$
N	total number of mixture compounds
n	order of decay
P	total pressure (Pa)
P_i^O	gas pressure when the only component i is present (Pa)
Q	airflow rate $\left(\frac{m^3}{s}\right)$
q	concentration in the adsorbed phase of activated carbon particles $\left(\frac{mg}{g}\right)$
q_{in}	concentration in the sorbed-phase in equilibrium with C_{in} $\left(\frac{mg}{g}\right)$
q_{max}	maximum adsorption capacity $\left(\frac{mg}{g}\right)$
q_t	total amount adsorbed $\left(\frac{mg}{g}\right)$
$\bar{q}$	dimensionless concentration
$\bar{q}^*$	concentration in the adsorbed phase in equilibrium with concentration in the fluid phase $\left(\frac{mg}{g}\right)$
$\bar{\bar{q}}$	average concentration in the adsorbed phase $\left(\frac{mg}{g}\right)$
q_i^O	equilibrium adsorbed-phase concentration of component i in its pure state $\left(\frac{mg}{g}\right)$
q^*	concentration at the particles' exterior surface $\left(\frac{mg}{g}\right)$
R	universal gas constant $(\frac{J}{Kmol.K})$
r	radial dimension (m)
$-r_{obs}$	observed reaction rate $\left(\frac{mg}{s.m^3}\right)$
R_p	mean radius of activated carbon particles (m)
r_p	mean pore radius of activated carbon particles (Å)
$\bar{r}$	dimensionless radius
R^2	determination coefficient
r_1	reaction rate between ozone and activated carbon surface $\left(\frac{mg}{s.m^3}\right)$

$r_1(t=0)$	reaction rate of fresh activated carbon with ozone $\left(\frac{1}{s}\frac{mg}{m^3}\right)$
r_2	heterogeneous reaction rate between ozone and limonene $\left(\frac{mg}{s.m^3}\right)$
r_3	homogeneous reaction rate between ozone and limonene $\left(\frac{mg}{s.m^3}\right)$
S	sum of squared residuals
S_{BET}	BET surface area $\left(\frac{m^2}{g}\right)$
St	Stanton number
T	absolute temperature of the system (K)
t	time (s)
$\bar{t}$	dimensionless time
u	superficial velocity $\left(\frac{m}{s}\right)$
u_b	interstitial velocity $\left(\frac{m}{s}\right)$
V	adsorbed volume of VOCs or by-products (m^3)
V_b	volume of the filter bed (m^3)
V_{max}	maximum adsorbed volume (m^3)
V_T	total pore volume of activated carbon (m^3)
W	width of the filter (m)
X	dimensionless length
x	axial dimension (m)
x_i	mole fraction of component i in the adsorbed phase
y_i	mole fraction of component i in the gas-phase

Greek Letters

β	equilibrium factor
λ	relative resistance of pore diffusion to surface diffusion
ε	adsorption potential $\left(\frac{J}{mol}\right)$
ε_b	filter bed porosity
ε_p	activated carbon particle porosity
ν	fluid kinematic viscosity $\left(\frac{m^2}{s}\right)$
π_i	dimensionless spreading pressure of the adsorbed phase
ρ_p	density of activated carbon particles $\left(\frac{g}{m^3}\right)$
τ	tortuosity
φ	porosity ratio

List of abbreviations

ANSI	American National Standards Institute
ARE	average relative error
ASHRAE	American Society of Heating, Refrigerating and Air-Conditioning Engineers
BDF	backward differentiation formula
BET	Brunauer–Emmett–Teller
BLCDM	boundary-layer-controlled diffusion model
C and D-MT-Chemi	convective and diffusive mass transfer chemisorption
C-MT-Chemi	convective mass transfer chemisorption
CONC	concentration
D-A	Dubinin-Astakhov
D-R	Dubinin-Radushkevich
D-Y	Doong and Yang
EI	electron impact
FD	Fick's diffusion
GC-MS	gas chromatography-mass spectrometry
HEPA	high efficiency particulate air
HSDM	homogeneous surface diffusion model
HVAC	Heating, Ventilation and Air Conditioning
IAST	Ideal Adsorbed Solution Theory
ISO	International Organization for Standardization
LDF	linear driving force
MDR	modified Dubinin-Radushkevich
MEK	methyl ethyl ketone
Min.	minimum
MIP	mercury intrusion porosimetry
MR	Mears number
MOL	method of lines
MTBE	methyl tert-butyl ether
MTZ	mass transfer zone
N/A	Not Applicable
NIOSH	National Institute for Occupational Safety and Health
ODEs	ordinary differential equations
PDEs	partial differential equations
PDM	pore diffusion model
PID	photoionization detector
ppb	parts per billion
ppm	parts per million
PSDM	pore surface diffusion model
R134a	1,1,1,2-Tetrafluoroethane

QDF	quadratic driving force
TDU	thermal desorption unit
TVOC	total volatile organic compounds
VOC	volatile organic compound
VSVO	variable-step, variable-order

1 Introduction

1.1 Background

The quality of the indoor air environment has a big impact on the occupants' health and productivity, so it has received considerable attention [1]. Indoor air pollutants are a complicated mixture of gases, vapours, and particles in the liquid or solid phase, and their source could be both the indoor and outdoor environment. Gaseous pollutants can be categorized into: a) inorganic gases (e.g. ozone, carbon monoxide, sulphur dioxide, nitrogen dioxide, nitric oxide, hydrogen sulphide, chloride, and so on), and b) organic gases such as VOCs [2]. Exposure to gaseous pollutants affects occupants' health (ranging from immediate effects – irritation of the eyes, nose, and throat, and headaches– to long-term effects – respiratory disease, heart disease, and cancer) [3].

There are different air treatment technologies for removing gaseous pollutants from the indoor environment. They include adsorption [4], photocatalytic oxidation [5–7], and cold plasma (non-thermal plasma) [8]. Photocatalyst technology works at room temperature, and a large portion of its final products are benign gases (CO_2 and H_2O). However, it may also produce byproducts (like formaldehyde, acetaldehyde, and ozone), which are more harmful than their parent compounds [9]. Also, several byproducts (like particles, ozone, nitrogen oxides, carbon monoxide, and formaldehyde) and low energy efficiency make non-thermal plasma inappropriate for indoor environment applications [9,10].

Adsorbent media is the most common technology used to remove gaseous pollutants from indoor air because of its high removal efficiency for many gaseous pollutants and the absence or insignificant generation of byproducts [11]. Capturing mechanisms for

removing gaseous contaminants through adsorption are physisorption and chemisorption. The most common adsorbent used for application in building heating, ventilation, and air conditioning (HVAC) systems is activated carbon, which has a high specific surface area (the typical surface area is from 800 to 1600 m^2/g) [11]. Activated carbon effectively removes hydrocarbons, many aldehydes, and organic acids by physisorption and ozone through chemisorption and catalytic reaction. However, it cannot remove oxides of sulphur, hydrogen sulphide, nitrogen oxide, and low molecular weight aldehydes (like formaldehyde) effectively [10,11].

Chemisorbent media, usually porous substrates (like activated alumina or carbon) coated or impregnated with a chemical reactant (like acids, bases, or oxidizing chemicals), are used to remove pollutants that cannot be removed effectively by activated carbon [11]. For indoor environment applications, activated carbon media, followed by permanganate-impregnated alumina media or a combination of them, are used [11].

The disadvantage of adsorbent media is that they need to be regenerated or replaced periodically. The breakthrough curve, which is the ratio of outlet to inlet concentration of the adsorbent bed versus the time profile, is employed to determine the service life of the filter. Experimental work with low indoor concentrations is quite time-consuming and expensive, particularly for granular or pelletized adsorbents, so researchers use simulation tools to predict filter performance. Developing a simulation model with an acceptable error range can enable estimating the filter's service life and enhance the understanding of the adsorption process. The model needs to be validated experimentally, and then it should employ independent parameters to predict the filter's performance at lower concentrations.

1.2 Problem statement

The existing models for predicting filter performance were only developed for a single component or a mixture of VOCs. However, in locations where gas-phase filters might be needed, in addition to indoor VOCs, other pollutants like SO_2, NO_2, and O_3 can be present and affect the performance of the filters. These pollutants are entered air handling systems at concentrations near their outdoor concentrations [12]. Mixing these pollutants with VOCs makes the removal of gaseous pollutants through filters even more complicated, and existing models fail to predict the filter's performance. Among these pollutants, ozone is the most critical oxidizer in some indoor environments (e.g., aircraft cabins, office environments, buildings exposed to high outdoor ozone concentrations, etc.). In contrast with VOCs, ozone destroys the activated carbon surface. Therefore, surface area and pore volume can be changed when activated carbon is exposed to ozone [13]. Also, the oxidation of the activated carbon by ozone can change its surface oxygen functional groups (increasing its polarity), so the affinity of activated carbon surface toward organic contaminants changes [13]. This can significantly reduce the filter's performance to remove those VOCs with a high affinity toward carbon filters [12]. Another possible interaction between ozone and VOCs is the heterogeneous reaction on the surface of activated carbon [14]. The reaction products can remain on the surface of the adsorbent [14], so they can poison the surface of activated carbon and affect its removal performance. Therefore, one of the most important shortcomings in the literature is the lack of a comprehensive model which can consider all the interactions mentioned above between ozone, VOCs, and the surface of activated carbon.

1.3 Applications

As mentioned, activated carbon filters are the most commonly used adsorbents in HVAC systems to remove gaseous pollutants. It removes most indoor gaseous pollutants effectively. Knowledge of the service life of the filter is necessary for both the building designers and the managers. The proposed model for the mixture of gaseous pollutants has great potential to estimate the life expectancy of the filter under realistic conditions.

1.4 Research objectives

Based on the facts mentioned above, the main objective of this work is to predict the operational lifespan of a carbon-based filter utilized for the removal of a mixture of ozone and VOCs from indoor environments. To achieve this goal, the following tasks will be accomplished:

1) Modeling and validation of the carbon-based adsorbent filters' performance for ozone removal.

2) Modeling and validation of filters' performance for removing a single VOC (limonene, toluene, and methyl ethyl ketone).

3) Modeling and validation of carbon-based filters to remove the mixture of VOCs.

4) Develop and validate a model for predicting a carbon-based filter's performance for the removal of a mixture of ozone and VOCs.

1.5 Thesis outline

Chapter 1 (Introduction) – In this chapter, an overview of the background, the problem statements, the application, and the main objectives of the research are presented.

Chapter 2 (Literature review) – This review covers the developed models to estimate the performance of adsorbent filters for indoor environment applications over the last two decades. For this purpose, the existing models are divided into interparticle mass transfer models and kinetic models. By systematically reviewing these models, their merits, useful applications, and limitations are highlighted. Specific emphasis is placed on determining the rate-limiting step(s) in the mass transfer process for both physisorbent and chemisorbent media. Then, the discussion highlights the strengths and weaknesses of currently used models for considering the effect of the gas mixture on the performance of the filters.

Chapter 3 (Methodology) – This chapter begins by providing detailed explanations of the experimental procedures and setups employed at both bench-scale and full-scale. Additionally, it provides a comprehensive explanation of the analysis instruments. Subsequently, models for the removal of ozone, single VOCs, VOC mixtures, and mixtures of VOCs and ozone through carbon-based filters are presented.

Chapter 4 (Removal of indoor air ozone using carbon-based filters: Systematic development and validation of a predictive model) – The focus of this chapter is on modelling the removal of ozone by filtering through chemisorption and catalytic reaction. First, the reaction rate parameters are measured by fitting the model onto the experimental data for all filters. This is followed by validating the model for lower concentrations. In addition, to show the model's validity for real-life applications, its prediction is compared with the experimental data collected using a full-scale experimental setup and a higher velocity. Furthermore, an inter-model comparison is performed to determine the importance of different mass transfer steps. Finally, a sensitivity analysis is conducted on

reaction kinetic parameters, axial dispersion coefficient, external mass transfer coefficient, and activated carbon particle porosity.

Chapter 5 (Develop and validate a mathematical model to estimate the removal of indoor VOCs by carbon filters) – In this chapter, first, the results of five experimental tests conducted on a bench-scale setup are used to compute the Dubinin-Radushkevich (D-R) isotherm parameters. Afterwards, the surface diffusivities at zero loading for various adsorbate-adsorbent systems are determined by fitting the developed model to the results of the experimental tests. Finally, the model is validated using experiments which are conducted at low concentrations, at a higher velocity, and on the full-scale. The inter-model comparison is carried out to show the importance of different mass transfer steps. In sensitivity analysis, dimensionless parameters are examined to investigate how they affect the filter's efficiency.

Chapter 6 (Dynamic modelling of removal of binary mixtures of VOCs from indoor air through a carbon-based filter) – In this chapter, iterative and non-iterative methods are applied to the D-R isotherm, and then they are incorporated into the mass transfer models to represent the adsorption behaviour of a binary mixture of VOCs. Afterwards, the model's predictions are compared with the experimental results at typical indoor concentrations. An inter-model comparison is conducted to show the importance of different mass transfer steps and the applicability of approximate solutions for intraparticle mass transfer. Finally, a parametric study is performed to evaluate the effect of some operational and design parameters on filter efficiency.

Chapter 7 (Removal of binary and ternary mixtures of ozone and VOCs by activated carbon filter: Mathematical modelling) – In this chapter, the mass transfer equations are employed to estimate the filter's dynamic behaviour by including the reaction rates of ozone with the carbon surface and the reactive VOC, as well as the adsorption isotherm for a single VOC or binary mixtures of VOCs. The reaction rate constant for the ozone-limonene reaction is calculated by fitting the model to the experiment results of their binary mixture. Additionally, the ozone-exposed filters are used to perform adsorption tests to determine the parameters of the D-R isotherm. The D-R isotherm is improved using the volume exclusion theory to consider the effect of by-products on the removal modelling of the binary mixture of ozone and limonene and the ternary mixture of ozone, limonene, and toluene. The inter-modal comparison assesses the importance of the by-products and the homogeneous reaction between ozone and limonene. A sensitivity analysis is carried out to evaluate the impacts of adsorption isotherm and reaction rate parameters on the filter's performance.

Chapter 8 (Conclusions and recommendations) – In this chapter, a comprehensive summary of the thesis findings is presented, along with recommendations for future research.

1.6 Current thesis type

This dissertation is a manuscript-based thesis in which the contents of chapters 2 to 7 are part of the published and submitted journal papers in the area of environmental chemical engineering:

Chapter 2:

Mohamad Ghamangiz Khararoodi, Chang-Seo Lee, and Fariborz Haghighat. "Modelling of sorbent-based gas filters for indoor environment: A comprehensive review." Building and Environment (2021): 108579.

Chapter 3 & 4:

Mohamad Ghamangiz Khararoodi, Fariborz Haghighat, and Chang-Seo Lee. "Removal of indoor air ozone using carbon-based filters: Systematic development and validation of a predictive model." Building and Environment (2022): 109157.

Chapter 3 & 5:

Mohamad Ghamangiz Khararoodi, Fariborz Haghighat, and Chang-Seo Lee. "Develop and validate a mathematical model to estimate the removal of indoor VOCs by carbon filters" Building and Environment 233 (2023): 110082.

Chapter 3 & 6:

Mohamad Ghamangiz Khararoodi, Jiping Zhu, Chang-Seo Lee, Jianjun Niu, and Fariborz Haghighat. "Dynamic modelling of removal of binary mixtures of VOCs from indoor air through a carbon-based filter." Chemical Engineering Journal (2023): 144792.

Chapter 3 & 7:

Mohamad Ghamangiz Khararoodi, Fariborz Haghighat, and Chang-Seo Lee. "Mathematical modelling of an activated carbon filter's performance in removing binary and ternary mixtures of ozone and VOCs." (Reviewer Comments Received).

2 Literature Review[1]

2.1 Adsorption process

Physical adsorption and chemisorption are two types of adsorption. For physisorption, intermolecular interactions between the filter surface and contaminants are responsible for capturing gaseous pollutants, in which multilayers of adsorbate can be formed on the adsorbents' surface, and pores could be filled. In chemisorption, chemical bonds are formed between the adsorbate and the absorbent. Compared with physisorption, chemisorption is slow, and it is not reversible [10,11]. Also, adsorption is site-specific for chemisorption and only takes place on the adsorbent's surface (monolayer adsorption) [15].

In general, the adsorption process includes the following steps: 1) transfer of adsorbate by airflow and diffusion, 2) transfer of adsorbate from bulk to the external surface of adsorbent (external or boundary layer mass transfer), 3) transfer of adsorbate from the exterior surface of adsorbent to the interior active sites (internal mass transfer), 4) adsorption of the adsorbate to the surface of the adsorbent, 5) chemical transformation of the adsorbate, 6) desorption of the physisorbed adsorbate or product species, 7) transfer of adsorbate or product species from the porous interstices of adsorbent to the external surface of adsorbent (internal mass transfer), 8) transfer of adsorbate or product species from the exterior surface of adsorbent to the bulk (external or boundary layer mass transfer), and 9) transfer of adsorbate or product species by airflow and diffusion (see Fig. 2.1) [16].

[1] M. G. Khararoodi, C.-S. Lee, and F. Haghighat, "Modelling of sorbent-based gas filters for indoor environment: A comprehensive review," Build. Environ., p. 108579, 2021.

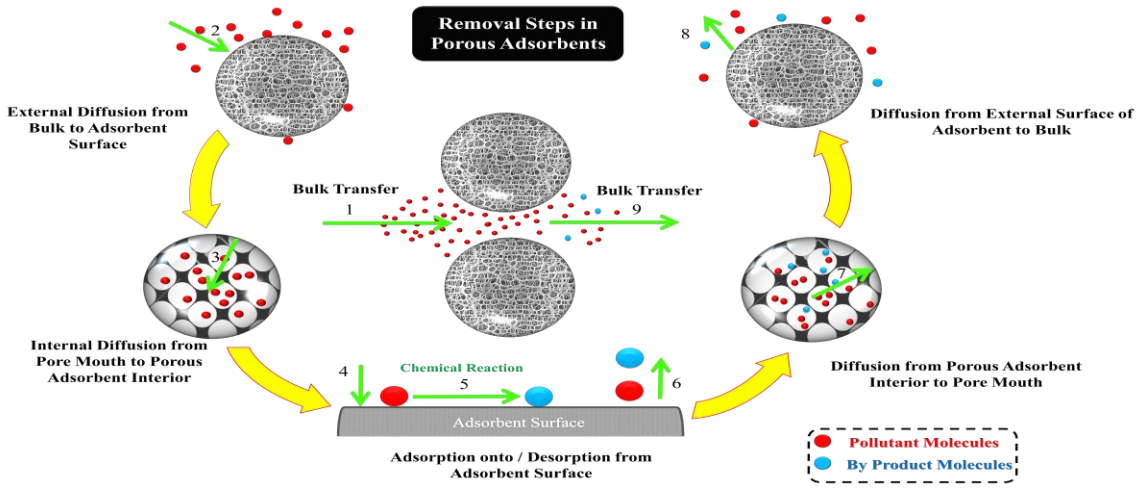

Fig. 2.1: Transfer steps for the removal of pollutants through adsorption.

2.2 Existing models for indoor air applications

A simultaneous solution of partial differential equations (PDEs) presenting mass, energy, and momentum balances is required to predict the adsorbent bed dynamics [17]. Assuming constant velocity and temperature simplifies the modelling of the purification through an adsorbent bed. One-dimensional mass transfer is another common assumption for modelling the adsorption process for indoor applications. Based on these assumptions, the mathematical model for the adsorption process includes a system of equations for interparticle mass transfer models and mass transfer kinetic models. The interparticle mass transfer consists of the diffusion term, the accumulation of species, the convection term, and the uptake term caused by the adsorption process. On the other hand, the kinetic models represent mass transfer mechanisms within the adsorbent particles [18].

Table 2.1 presents an overview of some modelling works for indoor air purposes and summarizes their critical assumptions and results. All models assumed isothermal and isobaric conditions, and the airflow pattern is represented by the plug flow or axially

dispersed plug-flow model. Most works used mass transfer controlling models for showing mass transfer mechanisms within the adsorbent particles. Fick's diffusion equations were widely utilized to describe the gas-solid mass transfer mechanism. The models considered a constant pore diffusion coefficient. Also, some models neglected surface diffusion at low concentrations, and some others considered a constant surface diffusion coefficient (no change by concentration). The majority of the models reviewed here used the linear isotherm model for ppb level concentration. In the next section, all models are explained in detail in two subsections of interparticle mass transfer models and kinetic models.

Table 2.1**:** Overview of mathematical models for removal of a single component by gas-phase filters.

Adsorbate/ Adsorbent	CONC (ppm)	Flow pattern	Interparticle mass transfer model	Isotherm model	Fitted parameters	Other assumptions	Ref.
MEK n-Hexane /25 g cylindrical activated carbon with a porosity of 0.4, a density of 450 kg/m^3, a diameter of 2.5 mm, and a length of 6 mm, in a cylinder with a 5.08 cm diameter and length of 3 cm	1-100 1-150	Axially dispersed Plug flow	PDM, HSDM, PSDM	Langmuir	N/A	1-Constant surface diffusion coefficient 2-Spherical and isotropic particles 3-Uniformly distributed particles 4-The LDF model for boundary layer mass transfer 5-Isothermal condition 6-Constant velocity 7-Dry condition 8-Negligible adsorption of the carrier gas	[19]

MEK n-Hexane /25 g cylindrical activated carbon with a porosity of 0.4, a density of 450 kg/m^3, a diameter of 2.5 mm, and a length of 6 mm, in a cylinder with a 5.08 cm diameter and length of 3 cm	15-200 15-300	Plug flow	LDF	Langmuir, Freundlich, D-R, BET	N/A	1-Negligible surface diffusion 2-Spherical and isotropic particles 3-The LDF model for boundary layer mass transfer 4-Isothermal condition 5-Constant velocity 6-Dry condition 7-Negligible adsorption of the carrier gas	[20]
Toluene /Two kinds of granular activated carbon (coconut-based with a porosity of 0.3 and a density of 450 kg/m^3 and coal-based with a porosity of 0.4 and a density of 490 kg/m^3) with a size of 1 mm in a cylinder with 4.8 cm diameter and 1 cm length	0.05, 0.1, 0.5, 5, and 50	Axially dispersed plug flow	PSDM	Linear	D_s	1-Spherical and isotropic particles 2-The LDF model for boundary layer mass transfer 3-Isothermal condition 4-Constant velocity 5-Negligible adsorption of the carrier gas	[21]
Ethanol Acetaldehyde Acetone Toluene Cyclohexane Tetrafluoroethane	10.93 0.39 0.4 0.32 0.25 1.21	Plug flow	PDM	Linear	N/A	1-Spherical and isotropic particles 2-Uniformly distributed particles 3-The LDF model for boundary layer mass transfer	[22]

/Coconut-based activated carbon with the S_{BET} of 1250 m^2/g, particle sizes ranging from 1.2 mm to 3.2 mm, and a pore volume of 0.1109 cm^3/g						4-Isothermal condition 5-Constant velocity 6-Dry condition 7-Negligible adsorption of the carrier gas	
Toluene /Flat shell activated carbon (coconut-based) with a size of 4.75×2.38 mm and a density of 450 kg/m^3, Cylindrical activated carbon (coal-based) with a diameter of 4 mm and a density of 490 kg/m^3, Ethylene urea treated granular activated carbon (coconut-based) with the size of 1.2×0.5 mm and the density of 450 kg/m^3 in a cylinder with 2.92 cm diameter and 2.54 cm length	0.067, 107	Axially dispersed plug flow	PSDM	Linear	K_c, D_e, partition coefficient	1-Constant surface diffusion coefficient 2-Spherical and isotropic particles 3-The LDF model for boundary layer mass transfer 4-Isothermal condition 5-Constant velocity 6-Negligible adsorption of the carrier gas	[23]
Toluene Limonene Decane /Bituminous coal activated carbon with a porosity of 0.4 and a diameter of 2.2 mm in	35 17 34	Axially dispersed plug flow	BLCDM, PSDM	Linear	K_c for BLCDM	1-Constant surface diffusion coefficient 2-Spherical and isotropic particles 3-The LDF model for boundary layer mass transfer	[24]

a cylinder with a 4.8 cm diameter						4-Isothermal condition 5-Constant velocity 6-Negligible adsorption of the carrier gas	
Toluene /Activated carbon fibre with a porosity of 0.072, a diameter of 26 μm, and a density of 87 kg/m^3 in cylinders with a diameter of 0.1 cm and a length of 6 mm and 8 mm	4.61	Axially dispersed plug flow	PSDM	Langmuir, Freundlich, D-R	D_p, D_s	1-ACFs are a cylinder of infinite length 2-The LDF model for boundary layer mass transfer 3-Isothermal condition 4-Constant velocity 5-Negligible adsorption of the carrier gas	[25]
Toluene Limonene / 1.4 g activated carbon fibre cloth (11.4×11.4 cm (Calgon Corporation, Type FM10) with a thickness of 0.5 mm	0.097 0.099	Axially dispersed plug flow	PSDM	Freundlich	K_c, D_p, D_s	1-Constant surface diffusion coefficient 2-Each bundle of activated carbon fibres is equivalent to a spherical particle 3-The LDF model for boundary layer mass transfer 4-Isothermal condition 5-Constant velocity 6-Negligible adsorption of the carrier gas	[26]

Formaldehyde / Ethylene urea treated granular activated carbon (coconut-based) with a size of 1.2×0.5 mm, and a density of 450 kg/m^3 in a cylinder with a 2.92 cm diameter and 2.54 cm length	0.075, 1.065	Axially dispersed plug flow	C and D-MT-Chemi	N/A	k, M_0	1-Pollutants in the sorbent exist in one overall phase 2-Spherical and homogeneous particles 3-The LDF model for boundary layer mass transfer 4-Isothermal condition 5-Constant velocity 6-First-order chemical reaction for fresh adsorbent	[23]
Formaldehyde /An activated carbon-based chemisorbent with a mesh size of 16×35, an S_{BET} of 970 m^2/g, and a pore volume of 0.451 cm^3/g and an activated carbon-based chemisorbent with a mesh size of 20×40, the S_{BET} of 1139 m^2/g, and the pore volume of 0.467 cm^3/g in a cylindrical bed with diameters between 0.5 to 1 cm and length ranging from 0.2 to 1.3 cm	2.6, 4.8	Axially dispersed plug flow	C-MT-Chemi, C and D-MT-Chemi	N/A	k, M_0	1-Pollutants in the sorbent exist in one overall phase 2-Spherical and homogeneous particles 3-The LDF model for boundary layer mass transfer 4-Isothermal condition 5-Constant velocity 6-First-order chemical reaction for fresh adsorbent	[27]

2.2.1 Interparticle mass balance

The interparticle (inter-pellet or inter-fibre) mass transfer equation describes the spatial and temporal variations of the concentration of adsorbates in the mainstream [28]. By assuming one-dimensional mass transfer, constant velocity, uniformly distributed particles, and using Fick's law for gas diffusion, the following equation can be written for the bulk gas in the bed [29].

$$\frac{\partial C}{\partial t} = -u_b \frac{\partial C}{\partial x} + D_x \frac{\partial^2 C}{\partial x^2} - \left(\frac{1-\varepsilon_b}{\varepsilon_b}\right)\frac{\partial \bar{\bar{q}}}{\partial t} \tag{2.1}$$

where C is the concentration in bulk outside the boundary layer, u_b is the interstitial velocity, D_x is the axial dispersion coefficient, ε_b is the bed porosity, $\bar{\bar{q}}$ is the average concentration in the adsorbent particle, t is the time, and x is the axial dimension. The associated initial and boundary conditions for the interparticle mass transfer model are as follows:

$$C(t=0,x) = 0 \tag{2.2}$$

$$D_x \frac{\partial C(t,x=0)}{\partial x} = -u_b\big(C_{in} - C(t,x=0)\big) \tag{2.3}$$

$$\frac{\partial C(t,x=L)}{\partial x} = 0 \tag{2.4}$$

where L is the length of the bed and C_{in} is the inlet concentration. The axially dispersed plug flow model (Eq. (2.1)) represents flow patterns in a system with a small deviation from plug flow [30]. The axial dispersion is caused by molecular diffusion and turbulent mixing [31]. The only parameter of this model is the axial dispersion coefficient. The coefficient can be measured experimentally using the tracer gas technique or empirical correlations [32–34]. The axial dispersion reduces the efficiency of the purification process

and leads to a broadening of the breakthrough curve [29]. The Peclet number (Pe) is used to compare the rate of advection to the rate of dispersion (diffusion) in the bed.

$$Pe = \frac{u_b L}{D_x} \tag{2.5}$$

Some researchers ignored the axial dispersion in their works (i.e. considered plug flow) [20,22]. Yao et al. [26] reported that for activated carbon fibre, even at low interstitial velocity (≈0.08 m/s), the axial dispersion did not affect toluene and limonene adsorption. However, the importance of axial dispersion needs to be investigated for each case study. Also, more study is required for determining the Peclet number range in which axial dispersion can be negligible.

2.2.2 Kinetic models

The kinetic model describes the mass transfer mechanisms within the adsorbent particles [18]. The main difference between existing models for indoor air purification has been centered on the kinetic models. The kinetic models can be categorized into equilibrium and mass transfer controlling models [17].

2.2.2.1 Equilibrium model

The equilibrium model assumes instantaneous equilibrium between the concentrations of contaminants in the adsorbent and fluid phases at each location in the bed [17]. Since there is no mass transfer resistance in this model, the amount of adsorption is equal to the amount of equilibrium adsorption [17].

$$\frac{\partial \bar{\bar{q}}}{\partial t} = \frac{\partial \bar{q}^*}{\partial t} \tag{2.6}$$

where $\bar{q}^*$ is the concentration in the adsorbed phase in equilibrium with the concentration in the fluid phase. Adsorption isotherms are utilized for quantifying this equilibrium.

$$\bar{q}^* = f(C) \tag{2.7}$$

The mass transfer equation for the equilibrium model is obtained by substituting Eq. (2.7) in Eq. (2.6) and then in Eq. (2.1).

$$\frac{\partial C}{\partial t} = \frac{1}{1 + f'(C)\left(\frac{1-\varepsilon_b}{\varepsilon_b}\right)}\left(-u_b \frac{\partial C}{\partial x} + D_x \frac{\partial^2 C}{\partial x^2}\right) \tag{2.8}$$

where $f'(C)$ is the slope of the adsorption isotherm. By using the initial and boundary conditions presented in section 2.2.1 and an isotherm model, the above PDE equation can be solved to predict the filter's performance. The model gives a first approximation for the adsorption process's behaviour [35]. This model can satisfactorily predict the filter's performance when both external and internal mass transfer resistances are negligible. The external resistance decreases by increasing the velocity or decreasing the adsorbent size (fibre or particle diameters). The small size of the adsorbent is also an advantage for internal mass transfer [36]. Fournel et al. [36] used the equilibrium model to simulate the removal of six VOCs (isopropanol, toluene, acetone, methyl ethyl ketone, ethyl acetate, and dichloromethane) through activated carbon fibres. The model could only predict the performance of the filter for the removal of dichloromethane. They showed that because of the high external surface area, external resistance was negligible. However, the internal diffusion of pollutants was not instantaneous despite the small diameter of fibres. Also, Yao et al. [26] showed the limitation in mass transfer steps in activated carbon fibres for

indoor environment application. They exhibited the importance of the external mass transfer at low velocities (≈0.08 m/s) and the internal mass transfer at higher velocities.

2.2.2.2 Mass transfer controlling models

As shown in Fig. 2.1, pollutants need to pass through the boundary layer to reach the external surface of adsorbents. All earlier indoor air adsorption modelling studies have employed film theory for representing this phenomenon. This theory assumes all mass transfer from the bulk fluid to the external surface of a particle happens in a hypothetical stagnant film next to the particle's surface [37]. Film theory, which is applicable for dilute concentrations of adsorbates, assumes a linear driving force for boundary layer mass transfer [38].

$$J = K_C(C - C^*) \tag{2.9}$$

where C^* is the concentration close to the external surface of adsorbents, K_C is the external mass transfer coefficient, and J is the rate of mass transfer. There are several empirical correlations for measuring the external mass transfer coefficient [39–42]. These correlations express the Sherwood number as a function of the Reynolds and Schmidt numbers.

After reaching the external surface, pollutants can transfer within the particles. Since there is negligible bulk flow inside the sorbent particle, diffusion is the dominant intraparticle mass transfer [35]. Because of the radial concentration gradient, adsorbates can diffuse through the gas-phase of pores through molecular and Knudsen diffusion. The presence of a concentration gradient within the gas-phase shows a similar concentration gradient in the

sorbed phase, which causes the diffusion of the adsorbed molecules (i.e., surface diffusion) [35].

Adsorbent type is one of the important factors that can control these mass transfer steps. Fig. 2.2-a shows the typical structures of granular activated carbon and activated carbon fibres. For granular (or pelletized) activated carbon, pollutants should pass through macropores and mesopores to reach the micropores; however, the micropores are directly connected to the external surface for activated carbon fibres [43,44]. Since there is more chance for pollutants to have surface diffusion within micropores, surface diffusion can play an important role in activated carbon fibres [45]. These two parallel resistances (pore gas-phase and surface diffusion resistances) are sequential with boundary layer mass transfer resistance (see Fig. 2.2-b). The importance of these three resistances on the filter's performance depends on the specific system and the conditions [29]. Accordingly, the mass transfer controlling models can be classified into the boundary layer resistance model and the intraparticle (intra-pellet or intra-fibre) resistance models.

Cheng et al. [25] employed the pore and surface diffusion model (PSDM) to predict the intra-fibre transfer of toluene by a cylindrical activated carbon fibre filter. The model is expressed below with the assumptions of one-dimensional mass transfer, negligible bulk flow inside the adsorbent, isotropic fibres, Fick's law for the diffusion, and constant pore gas-phase and surface diffusivities:

$$\varepsilon_p \frac{\partial C_p}{\partial t} + (1-\varepsilon_p)\frac{\partial q}{\partial t} = \varepsilon_p D_p \left(\frac{\partial^2 C_p}{\partial r^2} + \frac{1}{r}\frac{\partial C_p}{\partial r}\right) + (1-\varepsilon_p) D_s \left(\frac{\partial^2 q}{\partial r^2} + \frac{1}{r}\frac{\partial q}{\partial r}\right) \qquad (2.10)$$

The initial and boundary conditions are:

$$C_P(t=0,r) = q(t=0,r) = 0 \tag{2.11}$$

$$\frac{\partial C_P(t,r=0)}{\partial r} = \frac{\partial q(t,r=0)}{\partial r} = 0 \tag{2.12}$$

$$\varepsilon_p D_p \frac{\partial C_P(t,r=R_p)}{\partial r} + (1-\varepsilon_p) D_s \frac{\partial q(t,r=R_p)}{\partial r} = K_C\big(C - C_P(t,r=R_p)\big) \tag{2.13}$$

where C_p is the concentration in the gas-phase of pores, q is the concentration in the adsorbed phase, D_p is the effective gas-phase diffusion coefficient, D_s is the surface diffusion coefficient, ε_p is the sorbent porosity, R_p is the radius of the sorbent, and r is the radial dimension.

The PSDM considers both pore gas-phase and surface diffusions. Cheng et al. [25] used the linear driving force for boundary layer mass transfer in the axial dispersed plug flow model (Eq. (2.1)) for representing pollutant transfer in the adsorbent bed by assuming ACFs as cylinders of infinite length.

$$\frac{\partial C}{\partial t} = -u_b \frac{\partial C}{\partial x} + D_x \frac{\partial^2 C}{\partial x^2} - \frac{2(1-\varepsilon_b)}{R_p \varepsilon_b} K_C\big(C - C_p(r=R_p)\big) \tag{2.14}$$

The above equation with boundary and initial conditions presented in section 2.2.1 was coupled with Eq. (2.10) with its boundary and initial conditions to predict the filter's performance. In the work of Cheng et al. [25], the D-R model was utilized as an adsorption isotherm model to correlate the pore gas-phase concentration to the concentration in the adsorbed phase. The pore gas-phase and surface diffusion coefficients were measured by fitting the model into experimental data for the adsorbent with a thickness of 6 mm challenged with an inlet toluene concentration of 4.61 ppm. In another test, they retained the inlet concentration constant but increased the thickness of the filter to 8 mm. Then, they

could correctly predict the filter's performance by using the fitted values for the pore gas-phase and surface diffusion coefficients. However, since the surface diffusion coefficient is a concentration-dependent parameter, the fitted surface diffusion coefficient cannot be used for ppb level concentrations.

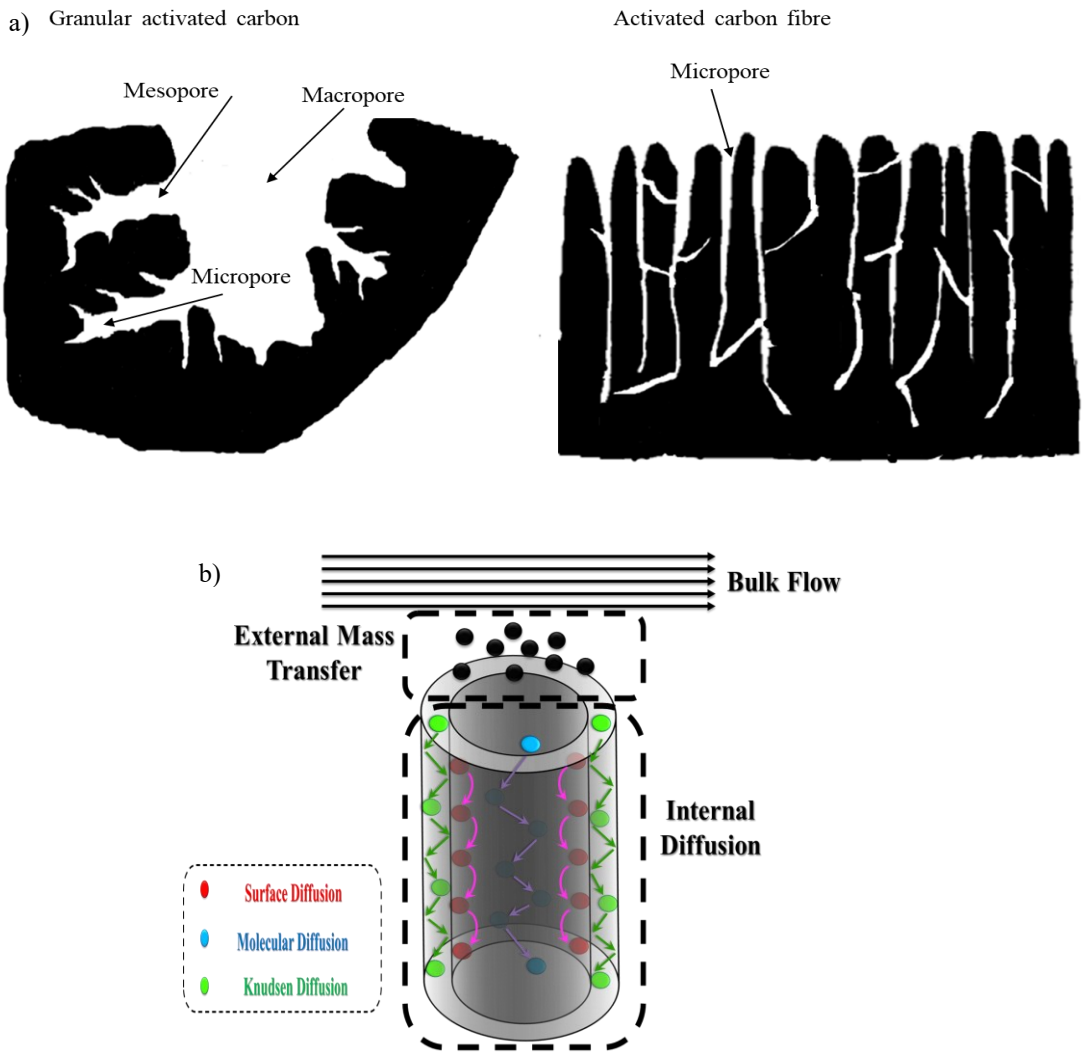

Fig. 2.2: a) Porous structure in granular activated carbon and carbon fibre (adapted from [43]) and b) external and internal mass transfer steps.

To solve this, Yao et al. [26] calculated surface diffusivity by fitting the PSDM model into experimental data of VOCs adsorption through a thin layer (0.5 mm) of a fibrous filter at

ppb concentration ranges. They assumed each bundle of activated carbon fibres is equivalent to a spherical particle, so Eqs (2.10) and (2.14) change to:

$$\varepsilon_p \frac{\partial C_p}{\partial t} + (1-\varepsilon_p)\frac{\partial q}{\partial t} = \varepsilon_p D_p \left(\frac{\partial^2 C_p}{\partial r^2} + \frac{2}{r}\frac{\partial C_p}{\partial r}\right) + (1-\varepsilon_p) D_s \left(\frac{\partial^2 q}{\partial r^2} + \frac{2}{r}\frac{\partial q}{\partial r}\right) \quad (2.15)$$

$$\frac{\partial C}{\partial t} = -u_b \frac{\partial C}{\partial x} + D_x \frac{\partial^2 C}{\partial x^2} - \frac{3(1-\varepsilon_b)}{R_p \varepsilon_b} K_C \big(C - C_p(r = R_p)\big) \quad (2.16)$$

The external mass transfer coefficient and pore gas-phase diffusivity were other parameters, which were measured by fitting into experimental results. The model was validated for another VOC and different airflow rates. They proposed that surface diffusion was the dominant intraparticle mass transfer. However, since they measured both pore and surface diffusivities by fitting the model into experimental data, it may cause an overestimation or underestimation in the fitted parameters.

Adsorption tests at ppb level concentrations need a very long time; they are also expensive. The ANSI/ASHRAE standard 145.1 [46], and the international standard ISO 10121-1 [47], were developed for testing adsorbents at ppm concentration to limit the test time. The results of these tests are used to compare adsorbent filters. Also, researchers have tried to use these results to predict the adsorbent filter's performance at the ppb level.

Based on ANSI/ASHRAE standard 145.1, Vizhemehr et al. [20] carried out experiments on the adsorption of two VOCs through a granular activated carbon filter at ppm levels. They also tried to use a linear driving force (LDF) approximation, a straightforward and applicable model for the intraparticle transfer of adsorbates. The model assumes that the uptake rate of adsorbate by adsorbent particles is linearly proportional to the difference

between the concentration close to the surface of materials and the air-phase concentration within the pores [16]:

$$\frac{\partial \bar{\bar{q}}}{\partial t} = k_p f'(C)(C^* - \bar{\bar{C}}_p) \tag{2.17}$$

The initial condition is:

$$\bar{\bar{q}}(t = 0) = 0 \tag{2.18}$$

where $\bar{\bar{C}}_p$ is the average concentration in the gas-phase of adsorbent pores, and k_p is the LDF model mass transfer coefficient, which was approximated by a theoretical correlation for spherical and isotropic particles. For the interparticle transfer, they assumed one-dimensional mass transfer, negligible axial dispersion, constant velocity, uniformly distributed particles, and a linear driving force for boundary layer mass transfer.

$$\frac{\partial C}{\partial t} = -u_b \frac{\partial C}{\partial x} - \frac{3(1 - \varepsilon_b)}{R_p \varepsilon_b} K_C (C - C^*) \tag{2.19}$$

The initial and boundary conditions are:

$$C(t = 0, x) = 0 \tag{2.20}$$

$$C(t, x = 0) = C_{in} \tag{2.21}$$

$$\frac{\partial C(t, x = L)}{\partial x} = 0 \tag{2.22}$$

The mass transfer rate in the boundary layer is assumed to be equal to the uptake rate of adsorbate by adsorbent particles at the surface of the particles:

$$k_p f'(C)\left(C^* - \bar{\bar{C}}_p\right) = \frac{3(1 - \varepsilon_b)}{R_p \varepsilon_b} K_C (C - C^*) \tag{2.23}$$

The Langmuir isotherm model was utilized as an adsorption isotherm model to correlate the average concentration in the adsorbent gas-phase to the average concentration in the adsorbent particle. The model matched experimental data only at concentrations higher than 100 ppm. They suggested that the probable reason was utilizing the LDF model for intraparticle mass transfer, which is less accurate than models based on Fick's diffusion equation.

In another work, they employed and compared the homogeneous surface diffusion model (HSDM), the pore diffusion model (PDM), and the PSDM to predict VOCs' removal by granular activated carbon [19]. The HSDM and PDM are used when surface diffusion and pore gas-phase diffusion are dominant intraparticle transfers, respectively, which can be derived from Eq. (2.15). All models predicted the filter's performance correctly for high concentrations (from 15 to 150 ppm). However, when the concentration was less than 15 ppm, there was some disagreement between the experimental data and the predictions made by the models. The first probable reason is using constant surface diffusivity for the whole concentration range. The second reason could be using Langmuir isotherm constants measured at ppm levels of concentration. This is why the deviation between the models and the experiment became considerable when the inlet concentration was 1 ppm.

The lack of equilibrium data at low concentration levels and the correlation for concentration dependency of surface diffusivity are critical issues for using the models mentioned above for indoor applications. Adsorption isotherm parameters and surface diffusion coefficients measured at high concentrations cannot be used for lower concentrations. Therefore, He et al. [21] developed a power-law empirical equation between gas-phase concentration and partition coefficient in the linear adsorption model

(K_p). They showed that the equation works appropriately for toluene with concentrations ranging between 0.05 and 50 ppm. They further showed that the PSDM, even by considering the concentration dependency of the surface diffusivity, cannot predict the filter breakthrough curve at ppb concentration levels. They proposed that this is because of considering the constant partition coefficient, which can change rapidly along the sorbent bed and particle radius at low concentrations. The high partition coefficient causes a steep concentration gradient in the mass transfer zone, so assuming a constant partition coefficient can cause a substantial error. Also, it is worth mentioning that the concentration dependency of the partition coefficient shows that other adsorption isotherms like the Freundlich isotherm and D-R may be able to describe the adsorption equilibrium even at low concentrations [26].

Intraparticle mass transfer equations are considered when there is a limitation in internal mass transfer. However, if boundary layer mass transfer limits the mass transfer process, there is no need to model internal transfer. Pei and Zhang. [24], compared the PSDM and the boundary-layer-controlled diffusion model (BLCDM), for predicting the activated carbon filter's performance. In the BLCDM, the particle concentration is considered a function of time (no resistance inside the particles) [16,24].

$$\frac{\partial \bar{\bar{q}}}{\partial t} = \left(\frac{K_C a_V}{1-\varepsilon_b}\right)\left(C - \frac{\bar{\bar{q}}}{K_m}\right) \tag{2.24}$$

where a_V is the specific surface area of the bed. The model assumes a linear driving force for boundary layer mass transfer, uniformly distributed particles, and equilibrium between the average concentration in the adsorbent particle and the gas-phase concentration at the interface. K_m is the ratio between these two concentrations. The initial condition is similar

to the initial condition of Eq. (2.17). For interparticle mass transfer, the last term on the right-hand side of Eq. (2.16) is substituted by $\left(\left(\frac{K_C a_V}{\varepsilon_b}\right)\left(C-\frac{\bar{\bar{q}}}{K_m}\right)\right)$. The external mass transfer coefficient was measured by fitting the BLCDM with an experimental test data. Then, they used the fitted value for predicting the filter's performance with the PSDM. The difference between these two models' results was quite small. They concluded that the BLCDM is adequately accurate for such an application. They posed that the surface diffusion is quite higher than the pore gas-phase diffusion within the adsorbent particle, so pore gas-phase diffusion can be neglected. Therefore, the boundary layer mass transfer is only in series with the surface diffusion. Also, the surface diffusion was higher than the boundary layer mass transfer. Accordingly, boundary layer mass transfer controls the mass transfer process. The importance of these three mass transfer steps can be shown by nondimensional numbers as follows:

$$\lambda = \frac{D_s \rho_p f'(C)}{\varepsilon_p D_p} \tag{2.25}$$

$$Bi_p = \frac{K_C R_p}{\varepsilon_p D_p} \tag{2.26}$$

$$Bi_s = \frac{K_C R_p}{D_s \rho_p f'(C)} \tag{2.27}$$

where λ is the relative resistance of pore diffusion to surface diffusion coefficient, Bi_p is the relative resistance of pore diffusion to boundary layer mass transfer, and Bi_s is the relative resistance of surface diffusion to boundary layer mass transfer. Table 2.2 shows that the values of λ is quite higher than 1 for the work of Pei and Zhang. [24], so surface

diffusion is the dominant intraparticle mass transfer mechanism. Also, the value of Bi_s is lower than 1 which indicates the boundary layer mass transfer is the most limiting step.

By decreasing concentration from ppm level to ppb level, the surface diffusivity and the slope of the adsorption isotherm decreases and increases, respectively. Therefore, the term of $D_s f'(C)$ changes and hence the rate-limiting step can change. Yao et al. [26] showed that the boundary layer mass transfer is the rate-limiting step mechanism only at low interstitial velocity (≈0.08 m/s). Also, the initial adsorption step is sensitive to the boundary layer mass transfer, where most adsorption occurs at the external surface of particles [29]. Therefore, the BLCDM can be fitted into the initial part of the breakthrough curve for calculating the mass transfer coefficient. Pei and Zhang. [24], showed that the fitted value was between values calculated by two well-known equations of Wakao and Funzkri [39] and Ranze and Marshall [41]. Also, when they employed that value in their modelling, it had better agreement with the experimental data than those models that used the Wakao and Funzkri or Ranze and Marshall's correlation.

Table 2.2 also depicts the effective diffusivities (D_e) which contain diffusion coefficients and the slope of the isotherm [48].

$$D_e = \frac{\varepsilon_p D_p}{\rho_p f'(C)} + D_s \tag{2.28}$$

The table shows that the effective diffusivity decreases with decreasing concentration. Therefore, it takes a longer time for the system to reach the true equilibrium condition, which differs from the local equilibrium condition. This can be because of a decrease in the mobility of species (the numerator in the above equation) and/or an increase in the capacity (the denominator in the above equation).

Based on the data obtained from the work of He [21], at the ppb concentration level, even with an effective pore diffusivity of 8×10^{-6} for toluene, the term of $\frac{\varepsilon_p D_p}{\rho_p f'(C)}$ is lower than the half of effective diffusivity. Therefore, if there was no overestimation of the partition coefficient, the results depict the importance of surface diffusion at low concentrations for the studied system. However, since it is difficult to measure surface diffusion experimentally, more investigation is required to confirm the importance of surface diffusion at low indoor concentrations.

Table 2.2**:** Nondimensional number measured for comparing the importance of mass transfer steps.

Pollutant(s)/ CONC (ppm)	Adsorbent type	$f'(C) \times 10^{-5}$	$D_s \times 10^{10}$ (m^2/s)	$D_p \times 10^{6}$ (m^2/s)	$D_e \times 10^{10}$ (m^2/s)	λ	Bi_p	Bi_s	Ref.
MEK 1-100	Activated carbon particle	9.2	1	2	1.0145	69	95.5	1.38	[19]
Toluene	Flat shell			8					[21]
0.05	activated	1150	0.00037		0.00066	1.24	23.0	18.5	
0.1	carbon	1070	0.00044		0.00076	1.37	15.8	11.5	
0.5		320	0.00050		0.00160	0.47	15.8	33.9	
5		76.1	0.00800		0.01250	1.78	15.8	8.9	
50		14.1	0.07000		0.09400	2.88	15.8	5.5	
	Activated		N/A			N/A	Min.	N/A	[22]
Ethanol 10.93	carbon particle	3.8		2.41	0.06000		14.1		
Acetaldehyde 0.39		8.3		3.10	0.00800		11.2		
Acetone 0.4		51.9		3.00	0.00127		11.1		
Toluene 0.32		772.0		2.92	0.00008		8.5		
Cyclohexane 0.25		161.0		1.90	0.00026		12.7		
Tetrafluoroethane 1.21		0.53		1.95	0.08000		14.9		
Toluene 35	Granular	8.5	5	0.088	5.0007	7244	1562	0.215	[24]
Limonene 17	activated	46		0.073	5.0001	47260	1582	0.033	
Decane 34	carbon	20		0.070	5.0002	21248	1532	0.072	
Toluene 4.61	Activated carbon fibre	N/A	200	0.0205	N/A	N/A	39.6	N/A	[25]

The existence of chemical reactions makes the adsorption of pollutants more complicated than simple physical adsorption. One of the most important steps in modelling this phenomenon is choosing the appropriate reaction rate model. Most works have been done for modelling the removal of toxic gases with impregnated adsorbent as a gas mask [49–51]. Some researchers assumed that removing adsorbate passing through a chemisorbent media follows two independent but simultaneous pathways: 1) physical adsorption, and 2) a second-order chemical reaction between the impregnant and adsorbate [50–53]. They used different intraparticle models (PDM and LDF) and interparticle models (plug flow and axially dispersed plug flow), and their modelling results were in good agreement with experimental data. However, the reaction models which they utilized are challenging to use.

Pei used a first-order reaction model for presenting the reaction between formaldehyde and fresh activated carbon-based chemisorbent [27]. The author used convective mass transfer chemisorption (C-MT-Chemi) and convective and diffusive mass transfer chemisorption (C and D-MT-Chemi) models for their work. The C-MT-Chemi model does not consider the internal diffusion like the BLCDM with the same assumptions, expresses as:

$$\frac{\partial \bar{\bar{q}}}{\partial t} = \left(\frac{K_C a_V}{1-\varepsilon_b}\right)(C - \bar{\bar{q}}\,) - (1 - \frac{M_r(t)}{M_0})k\bar{\bar{q}} \tag{2.29}$$

where k is the reaction constant, M_0 is the maximum chemisorption capacity, and M_r is the removed pollutant mass at time t. The adsorbent was assumed to be pure at the beginning of the test. For predicting the performance of the filter, the last term on the right-hand side of Eq. (2.16) is displaced by $\left(\frac{K_C a_V}{\varepsilon_b}\right)(C - \bar{\bar{q}})$, and then the new equation is coupled with Eq. (2.29). In the C and D-MT-Chemi model [27], pollutants in the sorbent

were assumed to exist in one overall phase (no distinction between the gas-phase in the pore and the sorbed phase at the adsorbate's surface). With this assumption, the model escapes the controversy of whether the reaction occurs in the gas or solid phase.

$$\frac{\partial C_{mat}}{\partial t} = D_p\left(\frac{\partial^2 C_{mat}}{\partial r^2} + \frac{2}{r}\frac{\partial C_{mat}}{\partial r}\right) - (1 - \frac{M_r(t)}{M_0})kC_{mat} \tag{2.30}$$

Other model assumptions are spherical and isotropic particles, uniformly distributed particles, and constant pore gas-phase diffusivity. The initial and boundary conditions are:

$$C_{mat}(t = 0, r) = 0 \tag{2.31}$$

$$\frac{\partial C_{mat}(t, r = 0)}{\partial r} = 0 \tag{2.32}$$

$$D_p\frac{\partial C_{mat}(t, r = R_p)}{\partial r} = K_C\big(C - C_{mat}(t, r = R_p)\big) \tag{2.33}$$

where C_{mat} is the concentration in the adsorbent particle. For this model, the interparticle mass transfer equation is derived by substituting the last term on the right-hand side of Eq. (2.16) by $\left(\frac{K_C a_V}{\varepsilon_b}\right)\big(C - C_{mat}(r = R_p)\big)$. The measured value of reaction rate constant by fitting C-MT-Chemi into experimental data was higher than that measured by the C and D-MT-Chemi model. This indicated that the internal diffusion was important and lumped into the reaction rate constant in the C-MT-Chemi model. Therefore, the gas-phase diffusion (intraparticle mass transfer) was a rate-limiting step for the transfer of the chemisorbed compound (formaldehyde), in agreement with other works [50,54]. This is because surface diffusion is negligible for chemisorption due to the strong bonds between adsorbates and adsorbents. Also, for most practical conditions for indoor air, the gas-phase diffusion resistance is higher than the boundary layer mass transfer resistance. He et al. [23] utilized

the C and D-MT-Chemi model by using the above-mentioned first-order reaction rate for the ppb level concentration and showed a good agreement between experimental data and the model prediction. However, the developed reaction rate failed to predict the filter's performance when the catalytic reaction occurred [23]. For example, for ozone, there are two reaction mechanisms for removal through activated carbon: a fast transformation into oxygen-containing surface functional groups followed by gasification of carbon, which releases CO and CO_2, and a slow catalytic transformation of ozone into molecular oxygen [55]. Therefore, the developed model cannot be used for modelling the removal of ozone through activated carbon [56].

2.3 Effect of the gas mixture

In the real indoor environment, there is always a mixture of gaseous pollutants. In the mixture, adsorbates interact in the gas-phase, and the interaction between adsorbates and the adsorbent becomes more complicated than in a single gas case. Therefore, using a single component as a challenge gas results in an inaccurate estimation of the filters' service life. To investigate the VOCs mixture's effect on carbon filters' performance, adsorption competition and displacement phenomena are two crucial characteristics [57]. Adsorption competition is the competition of different contaminants for the active sites on the adsorbent surface. It decreases the capacity and breakthrough time of the filter for each pollutant compared to those for individual pollutants. Displacement happens when less strongly adsorbed components are displaced by more strongly adsorbed components in the mixture. This results in their outlet concentrations becoming higher than their inlet concentrations for a certain period of time. This phenomenon is named roll-up or overshoot

[58]. Sidheswaran et al. [59] showed both adsorption competition and displacement phenomena for VOCs even at ppb level of concentration.

Molecular weight and polarity are two critical characteristics that affect the mixture's adsorption on the filters. Generally, VOCs with a higher molecular weight and lower polarity have higher adsorption on carbon filters [60]. Gas molecules with a higher molecular weight have a higher number of electrons, so their electron cloud is more polarizable, affecting their adsorption properties. The surface of activated carbon is non-polar with slightly polar groups, so it prefers to adsorb non-polar VOCs more than polar ones [60].

The experimental study of multicomponent adsorption is quite time-consuming, showing the importance of developing models for predicting adsorbent media's performance. Experiments are done for single components for measuring the required parameters for modelling the adsorption of the mixture. Diffusivities and sorption properties of adsorbate are two crucial parameters that are changed in the mixture [22]. Since the concentration of pollutants in the indoor air is quite low, one can assume that there is no interaction between contaminants during diffusion, and adsorbates only compete for adsorption sites on the adsorbent surface [22,61,62]. Adsorption isotherms are usually used for representing these interactions. Several models have been developed for multicomponent isotherms. Table 2.3 summarizes some of the commonly used multicomponent adsorption models.

Table 2.3: Multicomponent adsorption isotherm models.

Model name	Correlations	Model parameters	Ref.
Extended Langmuir	$q_i = \frac{q_{max,i} K_{L,i} C_{p,i}}{1 + \sum_{k=1}^{N} K_{L,k} C_{p,k}}$	q_{max}: Maximum adsorption capacity K_L: Langmuir constant	[35]
Jain and Snoeyink's Langmuir-like equation	$q_1 = \frac{(q_{max,1} - q_{max,2}) K_{L,1} C_{p,1}}{1 + K_{L,1} C_{p,1}} + \frac{q_{max,2} K_{L,1} C_{p,1}}{1 + K_{L,1} C_{p,1} + K_{L,2} C_{p,2}}$ $q_2 = \frac{q_{max,2} K_{L,2} C_{p,2}}{1 + K_{L,1} C_{p,1} + K_{L,2} C_{p,2}}$	q_{max}: Maximum adsorption capacity K_L: Langmuir constant	[63]
Extended Jain and Snoeyink's Langmuir-like equation	$q_i = \sum_{k=i}^{N} \frac{a_k K_{L,i} C_{p,i}}{1 + \sum_{j=1}^{k} K_{L,j} C_{p,j}}$	q_{max}: Maximum adsorption capacity K_L: Langmuir constant $a_k = (q_{max,k} - q_{max,k+1})$ for k= i to N-1, and $a_k = q_{max,N}$ for k= N	[64]
Ideal Adsorbed Solution Theory	$Py_i = P_i^O(\pi_i) x_i \quad \{i=1,2, \dots, N\}$ $\frac{\pi_i A}{RT} = \int_0^{P_i^O} \frac{q_i^O}{P_i^O} dP_i^O$ $\pi_1 = \pi_2 = \pi_N$ $\frac{1}{q_t} = \sum_{i=1}^{N} \frac{x_i}{q_i^O}$ $q_i = q_t x_i$	Dependent on the used isotherm	[65]

The simplest one is the extended Langmuir model [35], which is used frequently. This model is an extension of the original Langmuir model. One of the most important limitations of this model is that it assumes the presence of one species does not impact the coverage area of other species in absorption (no lateral interactions) [48]. Also, the extended Langmuir model can predict multicomponent adsorption equilibria of components if the adsorbent surfaces are equally available to all adsorbates, and the adsorbates compete for all active sites [63]. Therefore, if the adsorption of one component in the mixture happens on an active site that is not accessible for other components (e.g., because of molecular size), the extended Langmuir model is not applicable [66].

Jain and Snoeyink [63] improved the extended Langmuir model: The new model considers adsorption without competition at some active sites. The model assumes the number of active sites that can be occupied without competition is proportional to the difference

between the maximum adsorption capacities of adsorbates (see Table 2.3). Therefore, the surface concentration of the component with higher adsorption capacity (component 1 in the table) is estimated by two terms for a binary mixture. The first term is for the amount of component 1 that adsorbs without competition, and the second is for the amount of component 1 that adsorbs under competition with component 2. Tefera et al. [64] extended Jain and Snoeyink's Langmuir-like model for n-components; the new model was named extended Jain and Snoeyink's Langmuir-like equation. In this model, some active sites can be occupied without competition only by the component with the highest adsorption capacity (see Table 2.3).

Another widely used adsorption isotherm is the Ideal Adsorbed Solution Theory (IAST) [65]. This model considers the adsorbed phase forms an ideal solution (Raoult's law is valid). It assumes that the partial pressure of a component in the gas-phase above an adsorbed phase is equal to the multiplication of the mole fraction of that component in the adsorbed phase by the vapour pressure of the pure adsorbate (see Table 2.3) [65]. The IAST has limitations in showing the behaviour of mixtures of adsorbates with various adsorption affinities toward adsorbent [67].

By using a multicomponent adsorption isotherm model, all equations for the adsorption of a single component can be used for the mixture of pollutants. The mathematical models for multicomponent adsorption of different mixtures of gaseous pollutants by activated carbon filters are summarized in Table 2.4. Because of mathematical difficulties and the long computation time, the LDF model is usually used as a kinetic model for the multicomponent mixture [62,64,68,69]. Yun et al. [69] used the extended Langmuir model to predict the activated carbon's performance to remove binary and ternary mixtures of

benzene, toluene, and p-xylene. The only unknown parameter in their work was the LDF model mass transfer coefficient. They used single and binary mixture experimental data and correlated the LDF model mass transfer coefficient based on contaminant partial pressures and interstitial velocity. The model could correctly predict the binary mixtures' experimental data and only failed to predict the benzene roll-up amount in the benzene/toluene binary mixture. Also, they showed that the obtained correlation was valid for ternary mixtures. Table 2.4 reports that the accuracy of the modelling results for ternary mixtures was higher than 90% at 50% breakthrough time.

Gironi and Piemonte modelled the dynamic behaviour of an adsorbing bed to remove MTBE and cyclohexane [68]. The IAST was utilized as an adsorption isotherm for showing the equilibrium condition. Their modelling measured the LDF model mass transfer coefficient for the single system by fitting the LDF model with experimental data. They used the LDF model mass transfer coefficient values obtained from single contaminant cases for the binary system. They showed good agreement between modelling and experimental data. However, based on the theoretical correlation developed for the LDF model mass transfer coefficient [70], it is proportional to effective diffusivity. As Eq. (2.28) shows, the effective diffusivity depends on the slop of adsorption isotherm, which changes from a single component to a multicomponent. Therefore, using values obtained in single systems for a mixture can lead to inaccurate results, especially for the high number of pollutants.

When Popescu et al. [22] and Safari et al. [62] modelled the activated carbon filter's performance to remove VOCs mixtures with significantly various properties, their modelling works could predict the filter's performance to remove some of the mixture's

components, but not all of them (see Table 2.4). Neglecting surface diffusion and, more importantly, using the extended Langmuir model could be the reasons for these results.

To overcome this problem, Tefera et al. [64] utilized Extended Jain and Snoeyink's Langmuir-like equation model as an isotherm for multicomponent adsorption and modelled the activated carbon's performance to remove a mixture of VOCs. The average relative error (ARE) values in Table 2.4 show good agreement between the experimental data and the modelling results, except for compounds with low molecular weights.

Most of the work that has been done on the mixture of gaseous pollutants was at concentrations higher than the indoor level. For dynamic modelling of adsorbent filters, the adsorption isotherm is one of the most important factors. The Extended Jain and Snoeyink's Langmuir-like equation provided accurate predictions of the equilibrium behaviour of VOCs mixtures. However, the isotherm does not consider the effect of lateral interaction. On the other hand, it is difficult and time-consuming to conduct the experimental tests at the ppb level for finding accurate adsorption parameters. Moreover, in places that gas-phase filters are required, alongside indoor VOCs, other gaseous contaminants such as sulfur dioxide, nitrogen dioxide, and ozone can have a notable impact. These pollutants enter indoor spaces at levels similar to their outdoor concentrations [12]. The presence of these pollutants, combined with VOCs, further complicates the situation. For instance, unlike VOCs, ozone has the ability to damage the surface of activated carbon. When activated carbon is exposed to ozone, oxidation occurs, altering the oxygen functional groups on its surface. This process increases the polarity of the activated carbon surface, thereby modifying its affinity towards organic contaminants [13].

Table 2.4: Overview of mathematical models for multicomponent adsorption.

Adsorbate concentration (ppm)	Adsorbent	Flow pattern	Intraparticle and boundary layer mass transfer model	Isotherm model	Other assumptions	Error	Ref.
MEK (100) n-Hexane (100)	25 g cylindrical granular activated carbon with a diameter of 2.5 mm and a length of 6 mm in a cylinder with a diameter of 5 cm and a length of 2 cm	Plug flow	LDF	Extended Langmuir	1-Neglagible surface diffusion 2-Spherical and isotropic particles 3-No interaction between contaminants during diffusing 4-Isothermal condition 5-Negligible adsorption of the carrier gas	Around 25% at 50% breakthrough time for MEK. Around 50% at 50% breakthrough time for n-Hexane.	[62]
Ethanol (8.31) Acetaldehyde (0.6) Acetone (0.45) Toluene (0.28) cyclohexane (0.36) R134a (0.67)	12.95 g coconut-based activated carbon with S_{BET} of 1250 m^2/g, particle size of 1.2-3.2 mm and pore volume of 0.1109 cm^3/g	Plug flow	-PDM for intraparticle mass transfer -LDF model for boundary layer mass transfer	Extended Langmuir	1-Neglagible surface diffusion 2-Spherical and isotropic particles 3-No interaction between contaminants during diffusing 4-Isothermal condition 5-Dry condition 6-Negligible adsorption of the carrier gas	High accuracy at 50% breakthrough time for ethanol and R134a. Around 11% at 50% breakthrough time for cyclohexane. 20% at 50% breakthrough time for acetaldehyde. 300% at 50% breakthrough time for acetone.	[22]
(Benzene, Toluene, and p-xylene)(100-4000)	10 g beaded activated carbon in a column with a diameter of 1.82 cm and a height of about 10 cm.	Plug flow	LDF	Extended Langmuir	1-Ideal gas behaviour 2-Isothermal condition 3-Negligible adsorption of the carrier gas 4-Linear correlation between overall mass-transfer rate coefficients and the partial pressure of components	Less than 10% at 50% breakthrough time for most pollutants in the binary mixture. Only for toluene in the binary mixture of toluene/benzene at the concentration of 1300 ppm, the error was higher than 10% at different concentrations.	[69]

						Less than 10% at 50% breakthrough time for ternary mixtures at different concentrations.	
MTBE (20680-58780) Cyclohexane (12900-30320)	15 g granular activated carbon with a mean particle diameter of 1.6 mm, a specific surface area of 600 m^2/g, and the pore volume of 0.95 cm^3/g in a column with a diameter of 1.4 cm and height of about 37 cm.	Plug flow	LDF	Ideal adsorbed solution theory	1-Ideal gas behaviour 2-Spherical and isotropic pellets 3-Isothermal condition 4-Negligible adsorption of the carrier gas	Less than 10% at 100% breakthrough time for single systems Less than 20% at 100% breakthrough time for binary mixtures at different concentrations	[68]
n-butanol (62.5) n-butyl acetate (62.5) 2-heptanone (62.5) 2-butoxyethanol (62.5) n-decane (62.5) 1,2,4-trimethylbenzene (62.5) Indane (62.5) 2,2-dimethylpropylbenzene (62.5)	7.16 g beaded activated carbon with an average particle diameter of 0.75 and a pore volume of 0.57 cm^3/g in a cylinder with a diameter of 1.52 cm and a length of 6.5 cm	Two-dimensional with axial and radial dispersion	-LDF for intraparticle mass transfer -Negligible resistance for the external mass transfer	Extended Jain and Snoeyink's Langmuir-like	1-Neglagible surface diffusion 2-No interaction between contaminants during diffusing 3-Dry condition 4-Negligible adsorption of the carrier gas	n-butanol 600 n-butyl acetate 202 2-heptanone 9 2-butoxyethanol 12 n-decane 4 1,2,4-trimethylbenzene 1 indane 3 2,2-dimethylpropylbenzene 2	[64]

3 Methodology[1,2,3,4]

3.1 Experimental setup and analysis instrument

In this study, three commercial combined filters were employed. These filters consisted of coconut-based granular activated carbon, which was loaded at different weights (140, 200, and 500 g/m^2) between two layers of non-woven fibers. All physical properties of the tested filters are presented in Table 3.3. Fig. 3.1 shows the bench-scale experimental setup for testing filters that complies with ISO standard 10121-1 [47]. A description of the prequalification tests can be found in the Appendix. The bench-scale experimental setup was an aluminum duct measuring 1.3 meters in length with an inner cross-section area of 0.1×0.1 m^2. Compressed air is used as the carrier gas, and its flow rate was controlled by a mass flow controller (OMEGA, FMA5400/5500) at 30 and 60 litre/min. Tests were conducted at a temperature of 21±0.5 °C. Dry compressed air, which was purified with an activated carbon bed and particulate filter and controlled by a mass flow controller (OMEGA, FMA5400/5500), was used as the carrier gas. The airflow rate was also measured before and after each test using a calibrated flow meter (DryCal DC-Lite). A portion of compressed air was passed through two bubblers filled with distilled water to

[1] M. G. Khararoodi, F. Haghighat, and C.-S. Lee, "Removal of indoor air ozone using carbon-based filters: Systematic development and validation of a predictive model," Build. Environ., p. 109157, 2022.
[2] M. G. Khararoodi, F. Haghighat, and C.-S. Lee, "Develop and validate a mathematical model to estimate the removal of indoor VOCs by carbon filters," Build. Environ., p. 110082, 2023.
[3] Mohamad Ghamangiz Khararoodi, Jiping Zhu, Chang-Seo Lee, Jianjun Niu, and Fariborz Haghighat. "Dynamic modelling of removal of binary mixtures of VOCs from indoor air through a carbon-based filter." Chemical Engineering Journal (2023): 144792.
[4] Mohamad Ghamangiz Khararoodi, Fariborz Haghighat, and Chang-Seo Lee. "Mathematical modelling of an activated carbon filter's performance in removing binary and ternary mixtures of ozone and VOCs." (Reviewer Comments Received).

achieve a humidity of 50±1%. The airflow uniformity within the system was obtained by adding perforated metal sheets after the expansion zone and filter.

Toluene, methyl ethyl ketone (MEK), and limonene were selected as challenge VOCs. These VOCs have various physicochemical properties (see Table 3.1). A syringe pump (KD Scientific, Model 210) continuously introduced toluene and MEK into the system to produce target concentrations between 0.1 and 90 ppm. Also, the syringe injector was utilized to produce limonene in concentrations ranging from 0.1 to 9 ppm. [71] However, for concentrations between 30 and 90 ppm, gas-phase limonene was generated by passing compressed air (2 litre/min) through a cylinder (0.5 l) with limonene (0.2 l) followed by another cylinder (0.5 l) to trap condensed limonene. A rotameter was used to inject a certain amount of gas-phase limonene produced by the bubbling system. For single VOCs tests, the VOCs concentrations were measured by a photoionization detector (PID) (ppb3000 RAE, USA) for concentrations equal to or less than 1 ppm and an INNOVA 1312 Photoacoustic Multi-gas Monitor for greater concentrations. Each VOC within the binary mixture was injected individually into the mainstream using two separate syringe pumps. Following this, the VOCs were mixed within the mainstream air, allowing for a homogeneous distribution of the binary mixture. The target concentrations were 9 or 0.1 ppm for each compound in the mixture. For mixture tests, the VOCs and total volatile organic compound (TVOC) concentrations in the system were determined by PID.

The laboratory compressed air with a flow rate of 1.5 l/min controlled by a mass flow controller (Matheson Model 8270) passed through an ozone generator (ENALY Model 1KNT-24) to produce ozone. The outlet of the ozone generator was connected to a rotameter to inject certain amounts of the generated ozone into the test duct. The

experiments were carried out at seven ozone concentrations (0.1, 0.3, 0.5, 1, 5, 9 and 90 ppm). The ozone concentrations at the upstream and downstream of the filter were measured by an ozone monitor 2B Technologies Model scrubberless 211 for concentrations less than 1 ppm and 2B Technologies Model 202 for concentrations equal to or higher than 1 ppm. Also, the first ozone monitor was used for the mixture of ozone and VOCs. This was chosen based on its demonstrated ability to exhibit reduced susceptibility to the influence of VOCs [72].

To determine the exact concentration of each VOC in the binary and ternary mixtures, the compounds in the air from upstream and downstream of the duct were collected on Air Toxics tubes (1/4 inch × 9 cm, Supelco) using an air sampling pump with a 50 ml/min airflow rate for a premeditated durations (ranging from 45 seconds to 110 minutes) at certain time intervals (ranging from 15 minutes to 20 hours). The adsorbed pollutants in the tube were desorbed using a GERSTEL two-stage thermal desorption system comprising a thermal desorption unit (TDU) and a Cool Injection System (CIS) and subsequently transferred into a gas chromatography-mass spectrometry (GC-MS) system (Agilent GC 8890 coupled with Agilent 5977B). For the initial step of thermal desorption, the TDU was operated in split mode with a split ratio of 60:1 and rapidly heated to 250 °C and held for 10 minutes while the Cool Injection System (CIS) temperature was maintained at -20 °C to collect the desorbed analyte. The CIS was operated in split mode with a 10:1 split ratio during the second phase of thermal desorption. It was heated at a rate of 10 °C/s from -20 °C to 250 °C and held for 10 minutes. An Agilent DB-624 column (60 m long with 0.25 mm I.D., and 1.4 μm film thickness) was used for the separation of the analyte. The oven temperature program was set at an initial temperature of 35°C, which was maintained for

a period of 5 minutes, followed by a temperature ramping of 10°C/min until reaching 250°C. Finally, the temperature was maintained at 250°C for 10 minutes. A constant temperature of 250 °C was maintained in the transfer line that connects to the MS, while the ion source temperature and quadrupole temperature for the mass spectrometer were set at 230 °C and 150 °C, respectively, in positive electron impact (EI) mode. Full scan mode (30-350 amu) was used for signal detection. For the TD-GC/MS system, helium was utilized as the carrier gas.

For the mixture test of ozone and VOCs, the adsorbed pollutants on the surface of filters were extracted using a solution of methylene chloride (90%) and hexane (10%). An aliquot (1 uL) of the liquid sample was then pipetted into a glass thermal desorption tube that had been packed with glass wool and Tenax. The sample tube was flushed with pure nitrogen (N_2) gas at 0.03 l/min for 1 minute to remove the solvents. Subsequently, the analysis procedure remained identical to that used for the solid samples. Another aliquot (1 μL) of the extract was analyzed using a highly accurate mass spectrometer (Agilent 7200 Q-TOF) to determine the molecular formula of ozone-limonene reaction products under the following conditions: GC column: DB-5 MS UI column (30 m long with 0.25 mm internal I.D., and 0.25 μm film thickness); Injector: Split mode (50:1) at 280 °C; GC oven temperature program: 40 °C (held for 5 min), ramping at 15 °C/min to 220 °C, followed by a ramp to 300 °C at 10 °C/min, and held for 5 min; Temperature for the transfer line connecting to the MS: 280 °C; MS: positive EI mode with an ion source temperature of 230 °C and a quadrupole temperature of 150 °C, and a scan range of 30-600 amu.

To prevent any damage to the analyzers or sampling tubes and to avoid the production of artifacts resulting from the reaction between ozone and adsorbed pollutants, ozone

scrubbers were used for all analyzers except the ozone monitor. To prepare the scrubbers, a Teflon tube was packed with crystalline potassium iodide (KI). KI demonstrated high recovery of toluene, limonene, and the reaction products between ozone and limonene [73, 74].

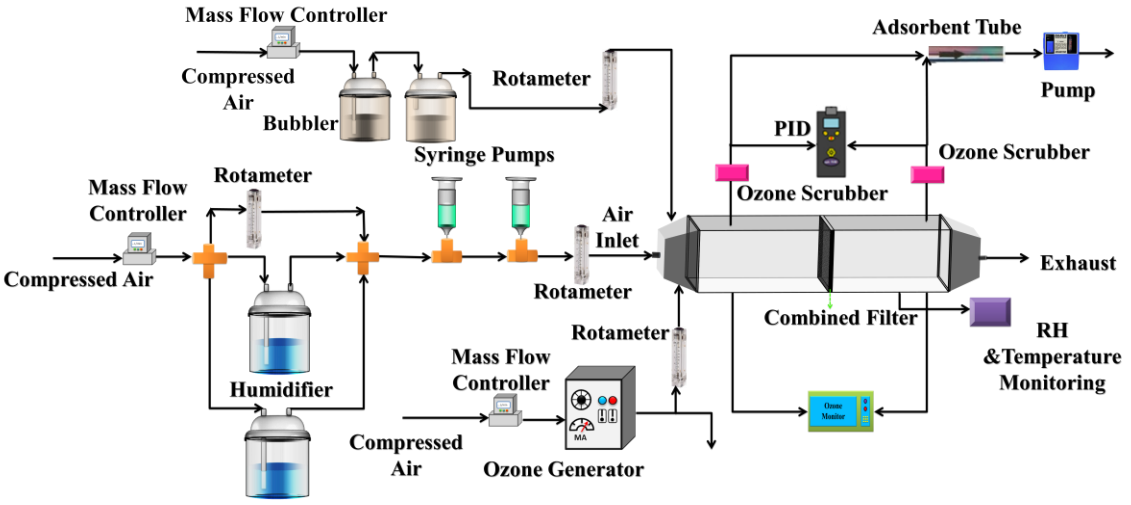

Fig. 3.1: Bench-scale setup for conducting dynamic experiments.

Table 3.1: Physicochemical properties of the selected VOCs [75–80].

Compound	Group	Mass of molecule (g/mol)	Boling point (°C)	Vapour pressure at 21°C (mmHg)	Kinetic diameter (Å)	Polarity	Polarizability $\times 10^{24}$ (cm^{-3})
Toluene	Aromatic	92.14	111.1	23.15	5.85	non-polar	12.3
MEK	Ketone	72.11	79.64	78.61	5.25	polar	8.13
Limonene	Terpene	136.24	176	1.52	6.70	non-polar	17.94

For filter type 1, single compound experiments were also conducted on a full-scale setup designed according to the ASHRAE standard 145.2 (see Fig. 3.2) [81]. It is worth mentioning that the prequalification tests (velocity uniformity, concentration uniformity, no filter, 100% efficiency) for ozone and toluene were conducted based on ASHRAE standard 145.2 prior to the main tests. The test duct is constructed of stainless steel, with a cross-sectional area of 0.61×0.61 m^2 and a total length of 23 m. A fan introduced laboratory air to the apparatus. A humidifier and cooling coil conditioned the supplied air, and then the supplied air passed through a clean-up bed and HEPA (high efficiency particulate air), which removed gaseous pollutants and particulate matter, respectively. The airflow rates of 1000 cfm (0.472 m^3/s) and 2000 cfm (0.944 m^3/s) were chosen for the experimental test on the full-scale setup. The ozone produced from pure oxygen within an ozone generator (BMT 803 N, BMT Messtechnik, Berlin) was injected into the conditioned air through an injection port, and then the polluted air passed through the filter. The target ozone concentration was 0.1 ppm when the airflow rate was 1000 cfm. The test was conducted 10 hours per day for 5 sequence days. Another test was conducted based on the test method recommended by ASHRAE standard 145.2 at an airflow rate of 2000 cfm. The initial performance is measured for an hour at the target concentration of 0.075 ppm. After the initial performance test, the capacity test at the target concentration of 0.5 ppm was done for 4 hours. The ozone concentration upstream and downstream of the filter was measured by an ozone monitor (2B Technologies Model scrubberless 211). For testing the toluene, an airflow rate of 1000 cfm (0.472 m^3/s) was used. A syringe injector generated toluene as a challenge VOC to produce a concentration of 0.1 ppm. The

PID analyzer measured the concentrations of toluene. Finally, the polluted air was exhausted from the system (open loop).

All tests were done at a relative humidity and temperature of 50±5% and 23±2 °C, respectively. All airflow measurement devices, as well as analyzers, were calibrated prior to usage.

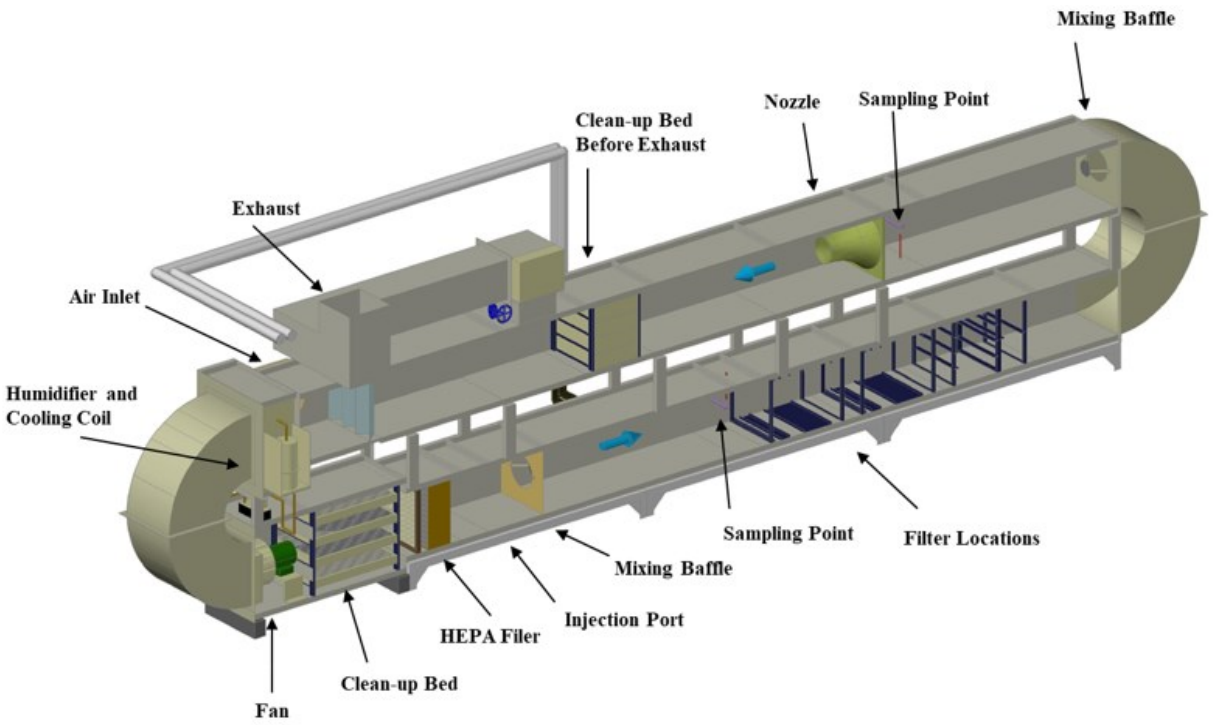

Fig. 3.2: Schematic diagram of the full-scale setup.

3.2 Model development

The developed model for each component includes a system of equations for interparticle mass transfer models and mass transfer kinetic models. The interparticle mass transfer is similar for all pollutants when the interaction between pollutants in the gas-phase is

negligible; however, the kinetic model can change by changing the type and number of pollutants.

3.2.1 Interparticle mass transfer model

As mentioned, the interparticle mass transfer equation describes variations of compounds concentrations in the mainstream over space and time (see Fig. 3.3) [28]. By assuming a one-dimensional mass transfer, negligible gas-phase reaction, uniformly distributed spherical particles, and an axially dispersed plug flow model, the differential fluid mass balance for all compounds is expressed by Eq. (2.1):

$$\frac{\partial C}{\partial t} = -u_b \frac{\partial C}{\partial x} + D_x \frac{\partial^2 C}{\partial x^2} - \left(\frac{1-\varepsilon_b}{\varepsilon_b}\right)\rho_p \frac{\partial \bar{\bar{q}}}{\partial t}$$

where $\frac{\partial \bar{\bar{q}}}{\partial t}$ is equal to boundary layer mass transfer.

$$\rho_p \frac{\partial \bar{\bar{q}}}{\partial t} = \left(\frac{K_C a_V}{1-\varepsilon_b}\right)\left(C - C_p(r = R_p)\right) \tag{3.1}$$

By assuming spherical pellets, the specific surface area is equal to:

$$a_V = \frac{3(1-\varepsilon_b)}{R_p} \tag{3.2}$$

Therefore the Eq. (2.1**)** change to:

$$\frac{\partial C}{\partial t} = -u_b \frac{\partial C}{\partial x} + D_x \frac{\partial^2 C}{\partial x^2} - \frac{3K_C(1-\varepsilon_b)}{R_p \varepsilon_b}\left(C - C_p(r = R_p)\right) \tag{3.3}$$

The associated initial and boundary conditions for the interparticle mass transfer model are as follows:

$$C(t = 0, x) = 0 \tag{3.4}$$

$$D_x \frac{\partial C(t, x = 0)}{\partial x} = -u_b\left(C_{in} - C(t, x = 0)\right) \tag{3.5}$$

$$\frac{\partial C(t, x = L)}{\partial x} = 0 \tag{3.6}$$

3.2.2 Kinetic model for removal of ozone

The following physical and chemical phenomena were considered in the development of the kinetic model for the removal of ozone through activated carbon: 1) Mass transfer of ozone from the bulk to the external surface of activated carbon through the boundary layer, 2) Reaction of ozone on the external surface of activated carbon, 3) Mass transfer of ozone from the external surface of activated carbon to the interior active sites, and 4) Reaction of ozone with the internal surface of the activated carbon (see Fig. 3.3).

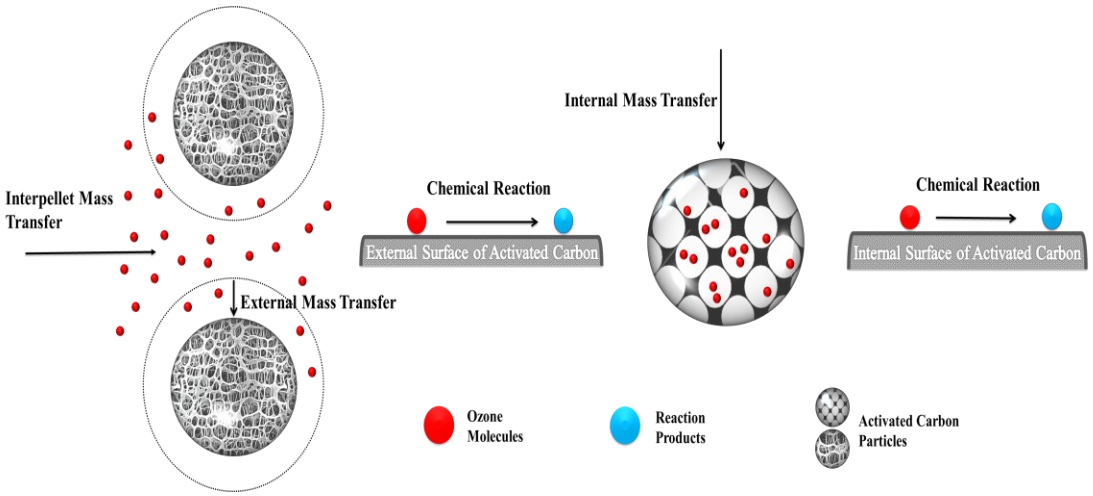

Fig. 3.3: Transfer steps for the removal of ozone through activated carbon.

By assuming spherical and isotropic particles, one-dimensional mass transfer within the activated carbon particles, negligible bulk flow inside the activated carbon particles, Fick's law for gas diffusion, constant gas-phase diffusivity, constant porosity, a negligible reaction between ozone and fibres compared to the reaction between ozone and activated carbon, a first-order chemical reaction for reaction between fresh activated carbon and ozone, separable kinetics, and the reaction taking place by the concentration of ozone in

the gas-phase, the kinetic model describing the mass transfer mechanisms within activated carbon particles can be expressed as:

$$\frac{\partial C_p}{\partial t} = D_p\left(\frac{\partial^2 C_p}{\partial r^2} + \frac{2}{r}\frac{\partial C_p}{\partial r}\right) - k_1 a C_p \tag{3.7}$$

where k_1 is the reaction rate constant for the reaction between ozone and activated carbon and a is the activity function for the reaction. The activity function is the ratio of the reaction rate of activated carbon at time t ($-r_1(t)$) to the reaction rate of fresh activated carbon ($-r_1(t=0)$) [37].

$$a = \frac{-r_1(t)}{-r_1(t=0)} \tag{3.8}$$

The activity function, a, can be expressed as follows [37]:

$$\frac{da}{dt} = -k_d g(a) h(C_p) \tag{3.9}$$

where k_d is the specific decay constant, $g(a)$ is a function of chemisorbent activity, and $h(C_p)$ is the functionality of the rate of decay on ozone concentration. By using the law of mass action for parallel deactivation of activated carbon through chemisorption and catalytic reaction, Eq. (3.9) can be written as [30,82]:

$$\frac{da}{dt} = -k_d a^n C_p^m \tag{3.10}$$

where n is the order of decay and m is the exponent in the functionality of the rate of decay. The initial and boundary conditions for Eqs. (3.7) and (3.10) are:

$$a(t=0, r) = 1 \tag{3.11}$$

$$C_P(t=0,r)=0 \tag{3.12}$$

$$\frac{\partial C_P(t,r=0)}{\partial r}=0 \tag{3.13}$$

$$D_p\frac{\partial C_P(t,r=R_p)}{\partial r}=K_C\left(C-C_P(r=R_p)\right) \tag{3.14}$$

3.2.3 Kinetic model for removal of single or mixture of VOCs

Fig. 3.4 illustrates all steps for the removal of VOCs through adsorbent filters. As VOC molecules transfer within adsorbent media, some can transfer to their external surfaces. While a certain amount of upcoming VOCs adsorb on the particles' exterior surface, others transport within the adsorbent particles. As these molecules are transferring within the particles, they adsorb on the internal surface of the adsorbent. For a mixture of VOC compounds, they may compete to be adsorbed on the surface.

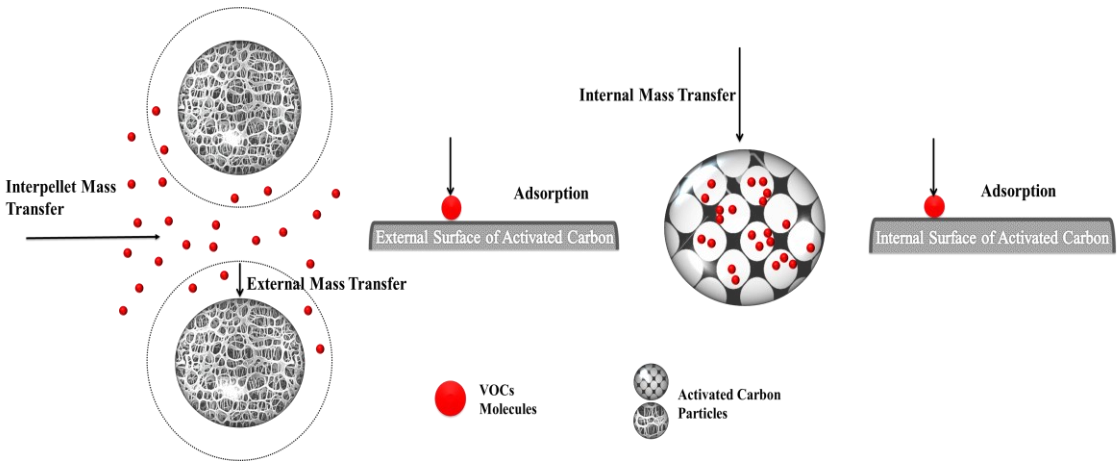

Fig. 3.4: Transport stages in the adsorption of VOCs.

With the assumptions of spheric particles, one-dimensional mass transfer within the particles, negligible bulk flow inside the adsorbent, Fick's first law of diffusion, and

concentration-independent gas-phase diffusivities, the kinetic model is expressed as follows [83]:

$$\varepsilon_p \frac{\partial C_p}{\partial t} + \rho_p \frac{\partial q}{\partial t} = \varepsilon_p D_p \left(\frac{\partial^2 C_p}{\partial r^2} + \frac{2}{r} \frac{\partial C_p}{\partial r} \right) + \rho_p \frac{1}{r^2} \frac{\partial}{\partial r} \left(D_s r^2 \frac{\partial q}{\partial r} \right) \tag{3.15}$$

By using the product rule:

$$\frac{1}{r^2} \frac{\partial}{\partial r} \left(D_s r^2 \frac{\partial q}{\partial r} \right) = \left(D_s \frac{\partial^2 q}{\partial r^2} + \frac{2D_s}{r} \frac{\partial q}{\partial r} + \frac{\partial D_s}{\partial r} \frac{\partial q}{\partial r} \right) \tag{3.16}$$

Finally, by using the chain rule, Eq. (3.15) changes into,

$$\varepsilon_p \frac{\partial C_p}{\partial t} + \rho_p \frac{\partial q}{\partial t} = \varepsilon_p D_p \left(\frac{\partial^2 C_p}{\partial r^2} + \frac{2}{r} \frac{\partial C_p}{\partial r} \right) \tag{3.17}$$

$$+\rho_p \left(D_s \frac{\partial^2 q}{\partial r^2} + \frac{2D_s}{r} \frac{\partial q}{\partial r} + \frac{\partial D_s}{\partial q} \left(\frac{\partial q}{\partial r} \right)^2 \right)$$

Eq. (3.17) is the pore surface diffusion model (PSDM) with a variable surface diffusion coefficient. The initial conditions at $t = 0$ and boundary conditions at the center ($r = 0$) and external surface of the particle ($r = R_p$) are:

$$C_P(t = 0, r) = q(t = 0, r) = 0 \tag{3.18}$$

$$\frac{\partial C_P(t, r = 0)}{\partial r} = \frac{\partial q(t, r = 0)}{\partial r} = 0 \tag{3.19}$$

$$\varepsilon_p D_p \frac{\partial C_P(r = R_p)}{dr} + \rho_p D_s \frac{\partial q(r = R_p)}{dr} = K_C \big(C - C_P(r = R_p) \big) \tag{3.20}$$

The concentrations on the adsorbent surface and in the gas-phase were assumed to be in local equilibrium. Two isotherm models (D-R and Langmuir) were tested against experimental data to quantify the equilibrium (see Table 3.2). Doong and Yang's (D-Y) model [84], which is based on the volume exclusion theory, was used for the extension of

the D-R isotherm to multi-component systems [85]. The model assumes that the maximum volume of accessible micropores is reduced from $V_{max,i}$ to $(V_{max,i} - \sum_1^N V_i)$, where N and V_i represent the total number of mixture compounds and the adsorbed volume in micropores, respectively. Applying the D-Y model to the D-R isotherm results in simple equations which can be solved analytically, contrary to two other frequently used models in the literature (Bering et al.'s [86] model or IAST [65]). Table 3.2 presents the equation for a binary mixture when the D-Y model is applied to the D-R isotherm [87].

Table 3.2: Adsorption isotherm model for a single and multi-component.

Model	$q = f(C_p)$	Model parameters
Langmuir	$q = \frac{q_{max} K_L C_p}{1 + K_L C_p}$	q_{max}: Maximum adsorption capacity K_L: Langmuir constant
D-R	$q = q_{max} \exp(-K_{DR} \varepsilon^2)$ $\varepsilon = \mathrm{RTln} \frac{C_S}{C_p}$	q_{max}: Maximum adsorption capacity K_{DR}: D-R constant
D-Y	$V_1 = \frac{\alpha_1 (V_{max,1} - V_{max,2}\alpha_2)}{1 - \alpha_1 \alpha_2}$ $V_2 = \frac{\alpha_2 (V_{max,2} - V_{max,1}\alpha_1)}{1 - \alpha_1 \alpha_2}$ $\alpha_1 = \exp\left(-K_{DR,1}\left(\mathrm{RTln}\frac{C_{S,1}}{C_{p,1}}\right)^2\right)$ $\alpha_2 = \exp\left(-K_{DR,2}\left(\mathrm{RTln}\frac{C_{S,2}}{C_{p,2}}\right)^2\right)$	V_{max}: Maximum adsorbed volume K_{DR}: D-R constant

ε: Adsorption potential, C_S: Saturation concentration, R: Universal gas constant, T: Temperature

3.2.4 Kinetic model for removal of ozone and VOC mixture

The kinetic model for the reactive VOC (limonene) with ozone, assuming one-dimensional transport, spherical and isotropic particles, constant porosity, constant gas-phase diffusivity, and insignificant bulk flow within the pore gas-phase of particles, is expressed by Eqs. (3.21) to (3.24) [31].

$$\varepsilon_p \frac{\partial C_{p,i}}{\partial t} + \rho_p \frac{\partial q_i}{\partial t} = \varepsilon_p D_{p,i} \left(\frac{\partial^2 C_{p,i}}{\partial r^2} + \frac{2}{r} \frac{\partial C_{p,i}}{\partial r} \right) \tag{3.21}$$

$$+\rho_p \left(D_{s,i} \frac{\partial^2 q_i}{\partial r^2} + \frac{2D_{s,i}}{r} \frac{\partial q_i}{\partial r} + \frac{\partial D_{s,i}}{\partial q_i} \left(\frac{\partial q_i}{\partial r} \right)^2 \right) + r_2$$

$$C_{p,i}(t = 0, r) = q_i(t = 0, r) = 0 \tag{3.22}$$

$$\frac{\partial C_{p,i}(t, r = 0)}{\partial r} = \frac{\partial q_i(t, r = 0)}{\partial r} = 0 \tag{3.23}$$

$$\varepsilon_p D_{p,i} \frac{\partial C_{p,i}(r = R_p)}{dr} + \rho_p D_{s,i} \frac{\partial q_i(r = R_p)}{dr} = K_{C,i}\left(C_i - C_{p,i}(r = R_p)\right) \tag{3.24}$$

where r_2 is the heterogeneous reaction rate for the ozone-limonene reaction on the activated carbon surface. Assuming an elementary bimolecular reaction on the activated carbon surface based on the Eley-Rideal (E-R) mechanism, r_2 is expressed as:

$$-r_2 = k_2 \rho_p q_{limonene} C_{p,ozone} \tag{3.25}$$

where k_2 is the heterogeneous reaction constant.

Assuming a negligible reaction rate between ozone and toluene, the above equations, by ignoring the reaction term (r_2), can be used for the intraparticle transfer of toluene. No reaction products were detected for the binary mixture of toluene and ozone, neither in the gas-phase nor from the extraction of the filter exposed to the mixture. It is worth

mentioning that the analytical methods used in this study were not able to detect highly volatile products (such as formaldehyde) and ultrafine particles. Nonetheless, toluene has a benzene ring and one methyl group attached to it. The benzene ring causes resonance stabilization in the structure of toluene, resulting in extremely low reactivity with ozone [88]. On the other hand, limonene can readily react with ozone because of two unsaturated carbon-carbon bonds (C=C) in its structure [89,90].

The kinetic model for ozone, assuming negligible surface diffusion, in addition to the assumption mentioned for intraparticle transfer of VOCs, can be presented by Eqs. (3.26) to (3.29) [91].

$$\varepsilon_p \frac{\partial C_{p,ozone}}{\partial t} = \varepsilon_p D_p \left(\frac{\partial^2 C_{p,ozone}}{\partial r^2} + \frac{2}{r} \frac{\partial C_{p,ozone}}{\partial r} \right) + \left(\frac{V_T - \sum V_i}{V_T} \right) \varepsilon_p r_1 + r_2 \tag{3.26}$$

$$C_{p,ozone}(t = 0, r) = 0 \tag{3.27}$$

$$\frac{\partial C_{p,ozone}(t, r = 0)}{\partial r} = 0 \tag{3.28}$$

$$D_p \frac{\partial C_{p,ozone}(r = R_p)}{dr} = K_C \left(C_{ozone} - C_{p,ozone}(r = R_p) \right) \tag{3.29}$$

where V_T is the total pore volume of activated carbon. The ratio of $\left(\frac{V_T - \sum V_i}{V_T}\right)$ shows that ozone can only react with those parts of the activated carbon surface which are not occupied by VOCs or by-products. It is worth mentioning that by assuming that the generation rate of all intermediates is equal to their consumption rate, the amount of produced by-products is equal to the amount of reacted ozone and limonene (or $r_{by-products} = r_2$). By using the weighted average density of reaction by-products, their total volume can be measured.

As mentioned, the D-R isotherm was used to show the equilibrium behaviour of a single VOC (toluene, limonene, and MEK). However, the generation of by-products can change the adsorption behaviour of VOCs and reduce the maximum available pore volume for VOCs adsorption. Using the volume exclusion theory similar to the D-Y model [84], and assuming that all of the reaction by-products remain on the activated carbon surface, the D-R isotherm is extended for the adsorption of limonene when ozone is present in the system.

$$V_{limonene} = (V_{max,limonene} - \sum V_{by-products})\exp\left(-K_{DR}(\mathrm{RTln}\frac{C_{S,limonene}}{C_{p,limonene}})^2\right) \quad (3.30)$$

Additionally, by applying the same assumption and theory, the D-R isotherm can be extended to a binary mixture of limonene and toluene in the presence of ozone.

$$V_{limonene} = (V_{max,limonene} - V_{toluene} - \sum V_{by-products})\exp\left(-K_{DR,limonene}(\mathrm{RTln}\frac{C_{S,limonene}}{C_{p,limonene}})^2\right) \quad (3.31)$$

$$V_{toluene} = (V_{max,toluene} - V_{limonene} - \sum V_{by-products})\exp\left(-K_{DR,toluene}(\mathrm{RTln}\frac{C_{S,toluene}}{C_{p,toluene}})^2\right) \quad (3.32)$$

3.3 Determination of model parameters

Several parameters are required to be estimated, and they are related to the operational conditions, filter bed, activated carbon particles, mass transfer, and reaction rate. The porosities of activated carbon particles and bed were measured experimentally through the

total pore volume obtained from the volume of N_2 adsorbed and mercury intrusion porosimetry (MIP). The average size of activated carbon particles was measured by the laser scattering particle size distribution analyzer LA-950V2. Table 3.3 shows the physical properties of filters.

Table 3.3: Physical properties of filters.

Parameters	Filter type 1	Filter type 2	Filter type 3
Filter dimensions for the bench-scale test (L×W×H) (mm)	0.8×100×100	0.8×100×100	2×100×100
Filter dimensions for the full-scale test (L×W×H) (cm)	2.5×61×61	N/A	N/A
Mass of activated carbon (M_{carbon}) ($\frac{g}{m^2}$)	140	200	500
BET surface area (S_{BET}) ($\frac{m^2}{g}$)	976	792	1130
Mean pore radius of activated carbon particles (r_p) (Å)	12.5	13.2	12.8
Filter bed porosity (ε_b)	0.75	0.58	0.60
Activated carbon particle average diameter (d_p) (mm)	0.560	0.632	0.620
Activated carbon particle porosity (ε_p)	0.47	0.4	0.54

The other parameters that need to be estimated are dispersion, diffusion, and external mass transfer coefficients. Axial dispersion is one of the three mass transfer steps limiting the removal process and broadening the breakthrough curve [92]. In order to estimate the axial dispersion coefficient within the bed of the activated carbon filter, the Wakao and Funazkri correlation [39], was utilized.

$$D_x = \frac{D_m}{\varepsilon_b}\left(20 + 0.5\frac{u_b d_p}{D_m}\right) \tag{3.33}$$

where D_m is the molecular diffusion coefficient obtained from the literature [93], and d_p is mean diameter of the activated carbon particle. The external mass transfer coefficient was measured by applying the Wakao and Funzkri equation [39].

$$\frac{K_c d_p}{D_m} = 2 + 1.1\left(\frac{u_b d_p}{\nu}\right)^{0.6}\left(\frac{\nu}{D_m}\right)^{\frac{1}{3}} \tag{3.34}$$

where ν is the fluid's kinematic viscosity. The axial dispersion was considered in mass balance equations for developing the Wakao and Funzkri correlation, so a high mass transfer coefficient is obtained by using this correlation [35]. The correlation can be an indirect way of accounting for the potential impact of axial dispersion [62]. Therefore, the Wakao and Funzkri equation should be used when there is axial dispersion in the filter bed [35]. The Bosanquet correlation was used to calculate the effective gas-phase diffusion coefficient (D_p) [48]:

$$D_p = \frac{1}{\tau}\left(\frac{1}{D_m} + \frac{1}{D_K}\right)^{-1} \tag{3.35}$$

where τ is the tortuosity factor of the particles and D_K is the Knudsen diffusion coefficient. They can be determined by [29,94]:

$$\tau = \frac{1}{\varepsilon_p} \tag{3.36}$$

$$D_K = 97 r_p \left(\frac{T}{M}\right)^{\frac{1}{2}} \tag{3.37}$$

where r_p is the mean pore radius of activated carbon particles measured by the Barrett, Joyner and Halenda (BJH) technique, and M is the molecular weight of the compound.

The concentration dependence of surface diffusion was estimated by the well-known Darken model [48]. According to the Darken Model, surface diffusivity at each concentration equals surface diffusivity at zero loading (D_{s0}) times by a thermodynamic correction factor derived based on chemical potential [95].

$$D_s = D_{s0} \frac{\partial \ln C_p}{\partial \ln q} \tag{3.38}$$

3.4 Model implementation

The developed model includes a system of equations for interparticle mass transfer models and mass transfer kinetic models. The filter bed was discretized into N slices, and particles were discretized into M slices (see Fig. 3.5). The PDEs for interparticle mass transfer and the kinetic model were converted to ordinary differential equations (ODEs) using the method of lines (MOL), and then the ODE15S function in MATLAB R2018a was used to solve them. The ODE15S is a variable-step, variable-order (VSVO) solver that is based on the backward differentiation formula (BDF) of orders 1 to 5 [96,97]. As a result of the flexibility in choosing the step size, simulations are more efficient than those using fixed-step integration algorithms [98]. This code is specifically designed to solve stiff differential equations [96].

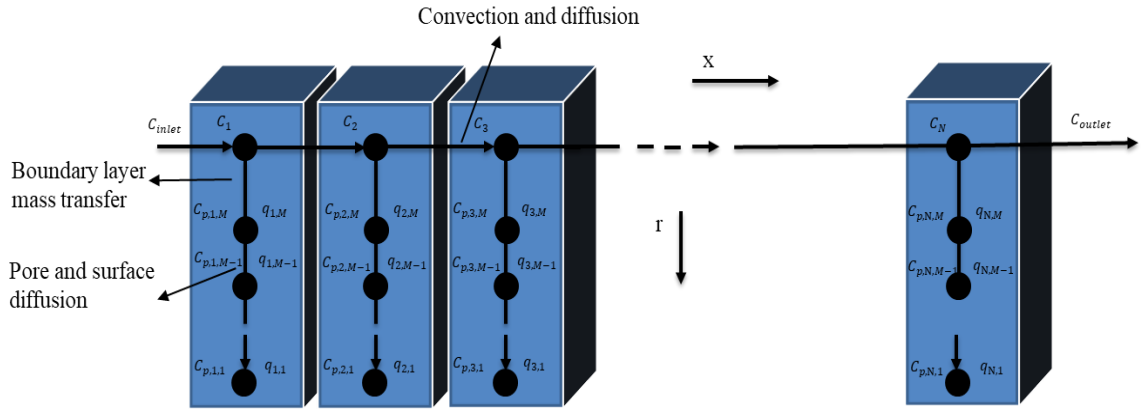

Fig. 3.5: Discrete representation of the adsorbent filter (adapted from Ref. [19]).

The main method for using the developed models was to calculate reaction kinetic parameters, isotherm constants, and surface diffusivities at zero loading by using experimental data at high concentrations and then employing them to predict the filter's performance at low concentrations. Also, the models were validated for a higher flow rate and binary mixtures of VOC at ppb level concentrations. The next step was the experimental test for the binary mixture of ozone and a VOC. Then, the model for binary mixtures was fitted to experimental data to find the kinetic parameters for the reaction between ozone and VOC. Finally, the models for binary and ternary mixtures of ozone and VOCs were validated at low concentrations. The fitted parameters were also used for scale-up purposes (see Fig. 3.6).

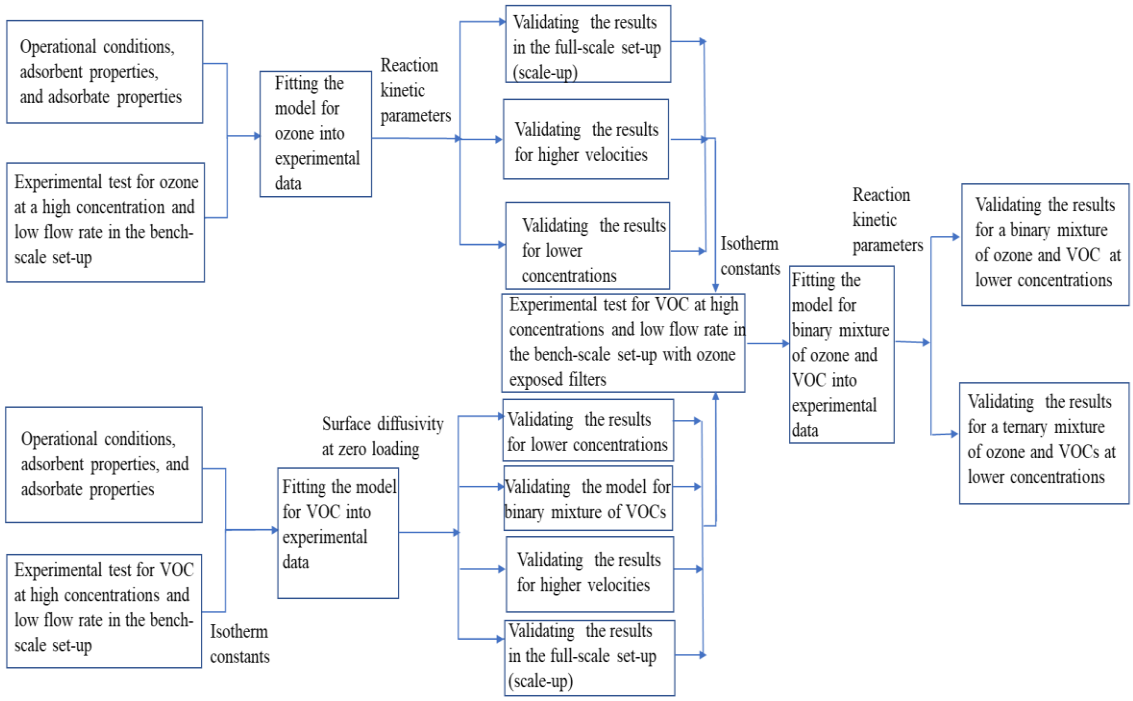

Fig. 3.6: Structure of the simulation program.

4 Removal of Indoor Air Ozone Using Carbon-based Filters: Systematic Validation of a Predictive Model[1]

Ozone has been reported to be one of the most important air pollutants, and it can originate indoors or outdoors. The indoor sources are photocopiers, laser printers, fax machines, scanners, ozone generators, and ion generators [90]. Outdoor ozone is generated by the photochemical reaction products of nitrogen oxides (NO_x) and volatile organic compounds (VOCs) [99]. Usually, the ozone concentration in the indoor environment is 20% to 70% of the outdoor ozone concentration [2]. Average ozone concentrations in the indoor environment are between 10 and 100 parts per billion (ppb) [90], and its peak concentration can be as high as 200 ppb [100]. Moreover, the high levels (500–800 ppb) of ozone at high altitudes (>10000 m) lead to high concentrations of ozone inside aircraft cabins, which can reach up to 300 ppb [101]. According to Health Canada's guideline for residential buildings, the recommended maximum ozone exposure level for eight hours is 20 ppb [102], and the National Institute for Occupational Safety and Health (NIOSH) recommends that workplace ozone exposure be less than 100 ppb [75]. Exposure to ozone can cause cough and chest pain on deep inhalation, shortness of breath, and eye, throat and nose irritation [103]. Also, ozone reacts with organic compounds that contain unsaturated carbon-carbon bonds from different sources, such as skin oils, personal care products, carpets, certain paints, cleaning products, air fresheners, etc. and produces hazardous by-products (like ultrafine particles, formaldehyde, ketones, and organic acids) [89].

[1] M. G. Khararoodi, F. Haghighat, and C.-S. Lee, "Removal of indoor air ozone using carbon-based filters: Systematic development and validation of a predictive model," Build. Environ., p. 109157, 2022.

Carbon-based filters are the most common media used in HVAC systems for the removal of ozone along with other gaseous pollutants [11]. Several experimental works have been conducted to remove ozone through activated carbon [55,104–106]. The results showed two reaction mechanisms for ozone removal through activated carbon: a rapid transformation into oxygen-containing surface functional groups followed by carbon gasification, which releases CO and CO_2, and a slow catalytic transformation of ozone into molecular oxygen [55,106]. As a result of these reaction mechanisms, activated carbon becomes exhausted and needs to be replaced periodically. Thus, accurate information about its performance is needed to plan for service and maintenance scheduling.

Conducting experiments at low indoor concentrations (ppb level) is time-consuming and costly. ISO 10121–1 recommends gaseous pollutants with a concentration of 9 or 90 ppm for testing media to speed up the experimental time. The challenge concentration should be chosen in such a way that the filter shows a breakthrough between 0.5 and 0.9 within 12 hours. This information can be used to compare different filters [47]. However, the challenge concentrations are quite higher than those that can be found in indoor environments. Therefore, researchers have tried to simulate the filter's performance at ppb levels based on experimental data obtained at high concentrations [19,20,23,107]. In the case of reactive pollutants, the reaction parameters are neither concentration- nor flow-dependent, so they were extracted from experiment data at high concentrations [23]. Then, the measured parameters were used in the model to predict filters' performance at ppb level concentrations.

Air velocity is another factor that influences the performance of the filters in removing gaseous pollutants. HVAC systems operate at a wide range of airflow rates, resulting in various air velocities within the filter bed. Therefore, the developed models should accurately estimate the performance of filters at different velocities.

One of the most important steps in predicting the removal of pollutants through reactive media is choosing a suitable reaction rate model. Alvarez et al. [54] considered reaction rates for both routes of ozone removal through activated carbon. Applying reaction rate parameters from their work to other concentrations requires knowledge of the transition time between two routes at different concentrations. Additionally, the reaction rate model developed by Pei [27], for showing the reaction between gaseous components and chemisorbents, failed to predict the filter's performance when the catalytic reaction was present [56]. This chapter validates the developed model (Eqs. (3.3) to (3.7), Eqs. (3.10) to (3.14), and Eqs. (3.33) to (3.37)) to study ozone removal through activated carbon filters using an appropriate reaction rate by integrating the two reaction mechanisms.

4.1 Methodology

The following four steps were taken for modelling the removal of ozone through filters: First, experimental tests were performed in the bench-scale setup at 9 or 90 ppm ozone concentration and an airflow rate of 30 l/min. The developed model for ozone removal was then fitted to experimental data to determine reaction kinetic parameters. The reaction kinetic parameters, if measured correctly, are neither concentration- nor airflow rate-dependent. Therefore, the fitted parameters can be used in the developed model to predict filter performance at lower concentrations, higher flow rates, and the full-scale setup (see

Fig. 4.1). As part of the inter-model comparison, the developed model was compared to three other models to investigate the importance of various mass transfer steps. Finally, a sensitivity analysis was conducted to determine the effects of reaction rate, external mass transfer, axial dispersion, and activated carbon particle porosity on the removal process.

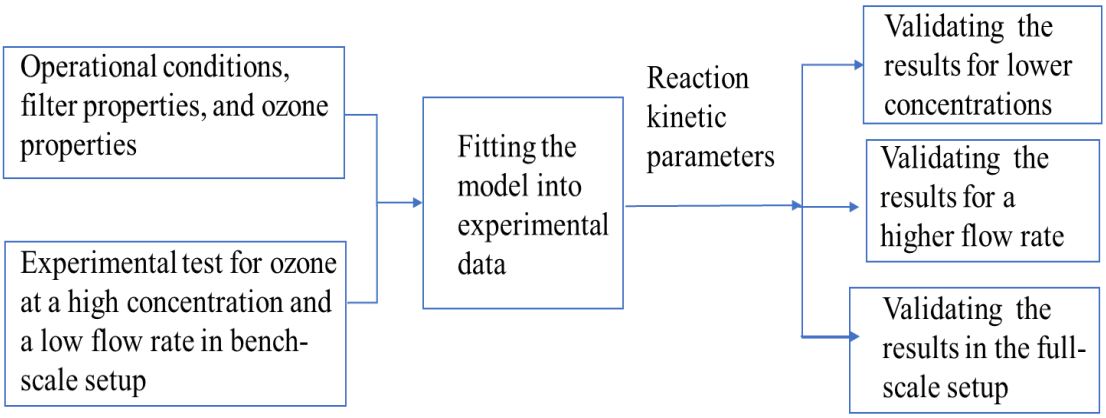

Fig. 4.1: Structure of the simulation program for ozone.

4.2 Results and discussion

4.2.1 Reaction kinetic parameters determination

The reaction kinetic parameters were measured by fitting the model into experimental results at a high concentration conducted in the bench-scale setup. The applied ozone concentrations were 9 ppm, 9 ppm, and 90 ppm for filters type 1, type 2, and type 3, respectively. The parameters were obtained by minimizing the sum of the differences of the squares between outlet ozone concentrations of the experimental data and the prediction made by the model.

$$S = \sum_{i=1}^{g} \left(C_{exp} - C_{pred}\right)^2 \tag{4.1}$$

where S is the sum of squared residuals, g is the number of experimental data, C_{exp} is the experimental value of outlet concentration, and C_{pred} is the predicted value of outlet concentration. The global minimum of the function was found using a hybrid particle swarm and pattern search optimization algorithm [108]. Fig. 4.2 shows the results of curve fitting for all filters, and Table 4.1 depicts the reaction kinetic parameters for the reaction between ozone and different filters, and the determination coefficient (R^2).

$$R^2 = 1 - \frac{\sum_{i=1}^{g}\left(C_{exp} - C_{pred}\right)^2}{\sum_{i=1}^{g}\left(C_{exp} - \bar{C}_{exp}\right)^2} \tag{4.2}$$

where $\bar{C}_{exp}$ is the average experimental value of outlet concentrations. The high values of R^2 and randomly scattered residuals, as seen in Fig. 4.2, indicate that the model is well fitted.

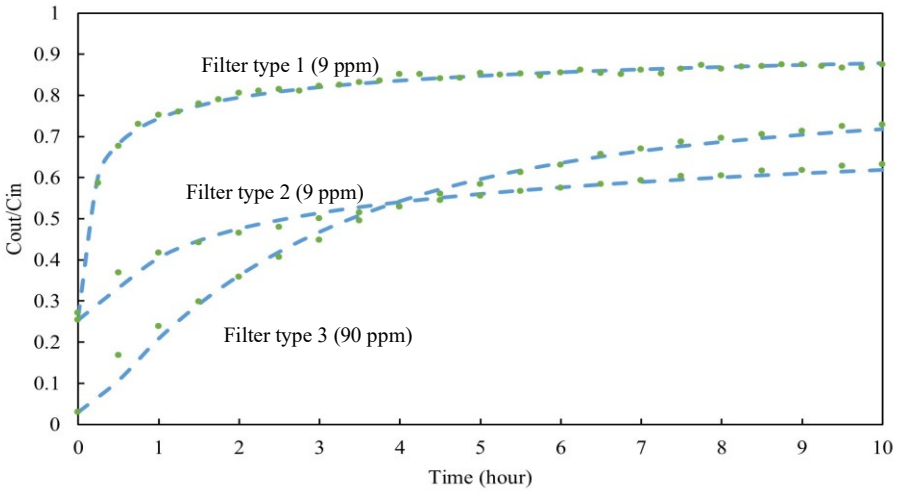

Fig. 4.2: Experimental data and model fitted into experimental data (green dots: experimental data, and dashed lines: fitted model).

Table 4.1: Reaction kinetic parameters for removal of ozone through activated carbon.

Parameters	Filter type 1	Filter type 2	Filter type 3
Reaction constant $k_1\left(\frac{1}{s}\right)$	802	1260	1120
Specific decay constant $k_d\left(\left(\frac{1}{s}\right)\left(\frac{m^3}{mg}\right)^m\right)$	3.12	1.52	1.71
Order of decay (n)	1.62	1.44	1
Exponent in the functionality of rate of decay (m)	4	3.48	3.3
R^2	0.998	0.999	0.999

4.2.2 Model validation

In order to validate the developed model, the unknown parameters measured by fitting the model into experimental data at high concentrations and low velocities were used to predict the filter performance at lower concentrations and a higher velocity. Further validation was done to predict the filter's performance using the experimental data from a full-scale setup. Also, an inter-model comparison was performed to investigate the importance of axial dispersion, external mass transfer, and internal mass transfer.

4.2.2.1 Validation for lower ozone concentrations

The tested ozone concentrations based on the ISO standard (9 or 90 ppm) are substantially higher than those that can be found in an indoor environment (ppb level), so the developed model needs to be verified for lower concentrations. Using the reaction kinetic parameters measured at 9 ppm for filter types 1 and 2, and 90 ppm for filter type 3 (see Table 4.1), the performance of the filters was predicted at concentrations of 9, 5, 1, 0.5, 0.3 and 0.1 ppm. Fig. 4.3 compares the experimental results and predicted breakthroughs for different filters. The average relative error (ARE) is utilized to evaluate the prediction results [109].

$$ARE=\frac{100\%}{g}\sum_{i=1}^{g}\left|\frac{C_{exp}-C_{pred}}{C_{exp}}\right| \quad (4.3)$$

The results show a good agreement between the experimental results and model predictions for all three filters. The model predicts breakthrough curves with less than 5.0% ARE for most cases. There are slight deviations between the model prediction and experimental result, especially at the early stage of the process. The probable reason for this is estimating both removal mechanisms (chemisorption and catalytic reaction) by one reaction rate. This can cause overestimation in the early removal phase and underestimation when the catalytic reaction is the dominant removal mechanism.

At each concentration, the removal is highest at the beginning of the process, but the activated carbon is being slowly deactivated as time progressed. As mentioned, chemisorption and catalytic reaction are two pathways for removing ozone through activated carbon [55,106]. Fig. 4.3 shows that the initial parts of the breakthrough curves are steeper because of the consumption of chemisorption sites. However, after the initial period, the removal is mainly because of a catalytic reaction where some active sites can be regenerated, resulting in a less steep breakthrough curve [54,110]. By increasing the inlet concentration, the breakthrough time decreases. As shown in Fig. 4.3-a, after 4 hours, the breakthrough curves for inlet concentrations of 5, 1, 0.5 and 0.3 ppm reach 0.78, 0.64, 0.51 and 0.42, respectively. This phenomenon can be explained by the fact that the driving forces for mass transfer and deactivation rates are enhanced as concentration increases. As a result, breakthrough curves become sharper [111].

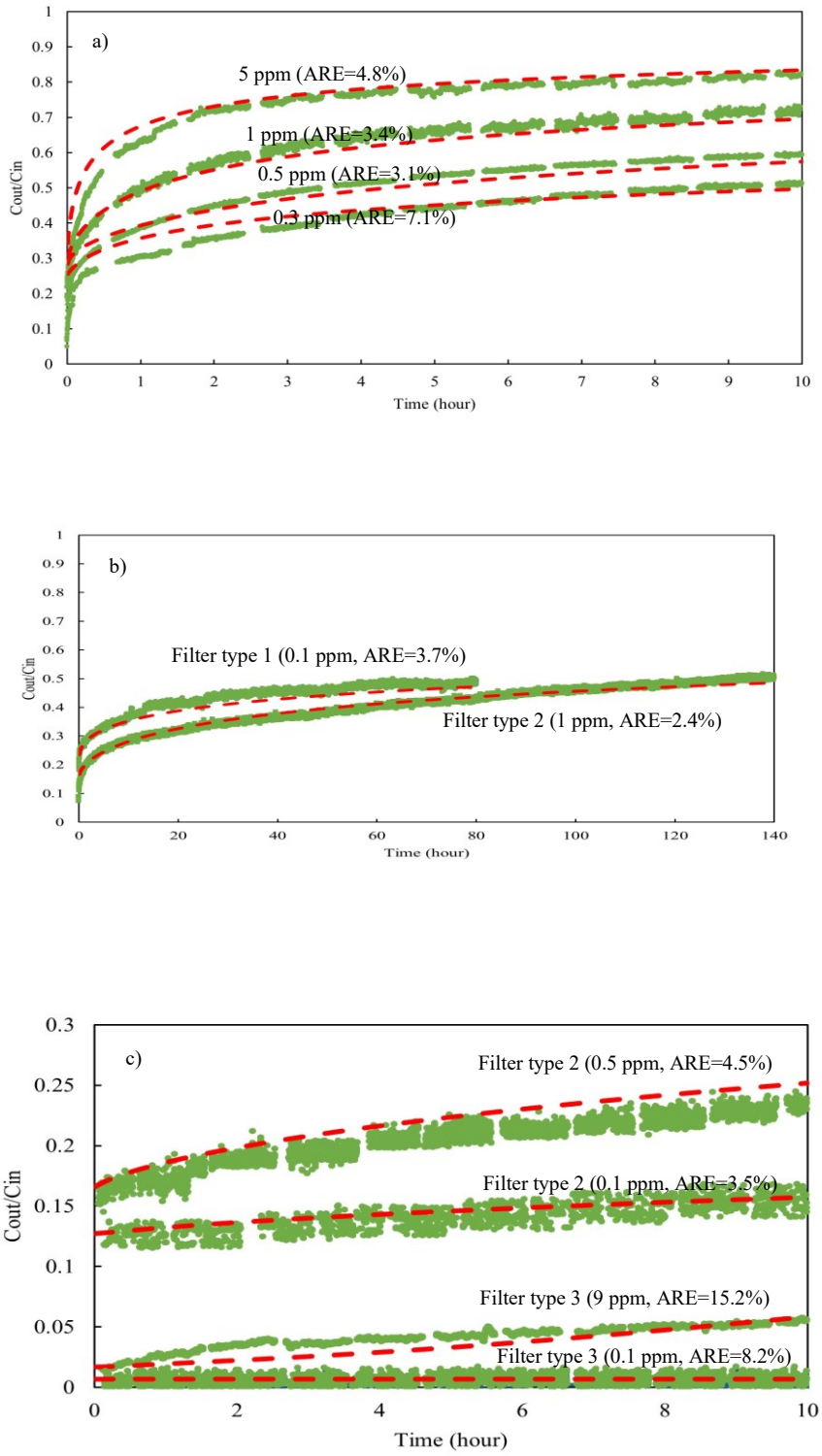

Fig. 4.3: Breakthrough of the filter to remove ozone (green lines: experimental data, and red lines: model prediction). a) filter type 1, b) filter types 1 and 2 for long-term testing, and c) filter types 2 and 3.

4.2.2.2 Validation for higher velocity

As filters are exposed to a wide range of velocities in HVAC systems, the developed model must accurately predict the performance of filters at different airflow rates. Therefore, the validation of the model was also done for a higher flow rate (60 l/min) by using the reaction parameters measured at the airflow rate of 30 l/min. Fig. 4.4 compares the results of experimental data and model prediction for all filters. There is good agreement between the results predicted by the model and the experimental results.

Increasing air velocity can affect the performance of the filter in two ways: 1) Reducing residence time (less time is available for ozone to be removed through activated carbon) and 2) Increasing the external mass transfer coefficient [19,24,112]. The developed model considers these two phenomena. As expected, the comparison between Fig. 4.2 and Fig. 4.4 shows that the filter efficiency decreases by increasing the airflow rate, which is because of a shorter contact (residence) time. For instance, for filter type 2, the efficiencies after 5 hours are 45% and 24% for 30 and 60 l/min, respectively. Also, at higher airflow rates, the first part of the breakthrough curve is steeper, mainly because of lower external mass transfer resistance.

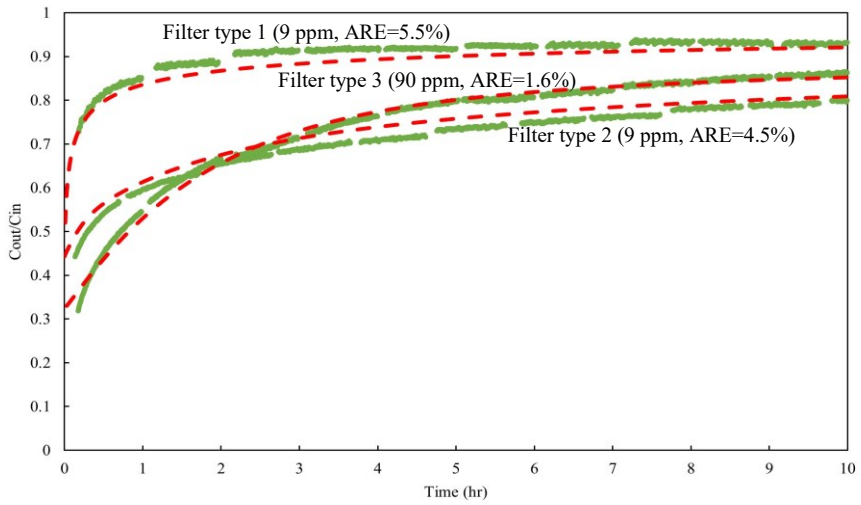

Fig. 4.4: Measured and simulated breakthrough at the flow rate of 60 l/min (green lines: experimental data, and red lines: model prediction).

4.2.2.3 Validation with full-scale results

The developed model needs to be tested for a large-scale system in order to verify its ability to work for real-built duct systems. Therefore, the model for ozone removal with the parameters measured at 9 ppm was used to predict the performance of the pleated filter (type 1) installed in the full-scale setup. As mentioned earlier, the experiment was carried out 10 hours/day for 5 days at the airflow rate of 1000 cfm. According to the experiments' results, the filter's initial efficiency is slightly higher at the beginning than the final efficiency of the previous day. This could be because of the regeneration of a few active sites due to the desorption of oxygen [104,113]. Also, the ASHRAE standard 145.2 test method was used for the second test at the airflow rate of 2000 cfm. Fig. 4.5 shows that the model prediction agrees well with the experimental results. Only a slight deviation is observed at the early stage. As mentioned earlier, possibly the main reason is using a single reaction rate for two ozone removal mechanisms (chemisorption and catalytic reaction).

This assumption results in a lower estimation for the removal rate at the early stage of the process, where chemisorption is the dominant removal mechanism.

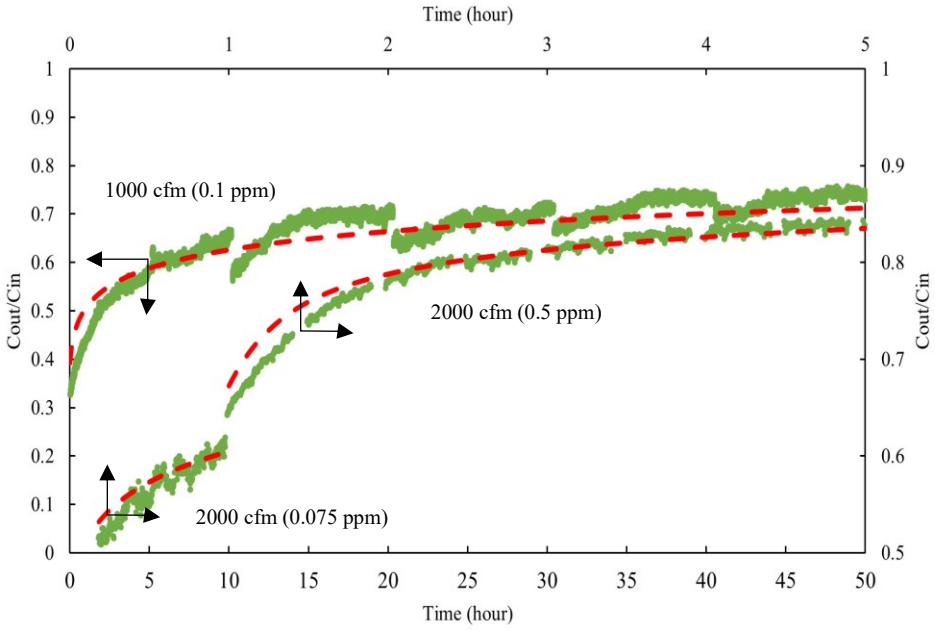

Fig. 4.5: Measured and simulated breakthrough (green lines: experimental data, and red lines: model prediction).

4.2.2.4 Inter-model comparison

For investigating the importance of axial dispersion and external and internal mass transfer considered in the comprehensive model (Model O-A), three other models were developed. Like the comprehensive model, other models were fitted into the experimental data to find the reaction parameters (k_1, k_d, n and m). Finally, the models' predictions were compared to show the importance of different mass transfer steps.

4.2.2.4.1 Effect of axial dispersion

In order to study the importance of axial dispersion, Young and Finlayson developed a criterion [37]. They proposed that when the term $\frac{-r_{obs}D_x}{u^2C}$ (u is the superficial velocity and $-r_{obs}$ is the observed reaction rate), named here Y-F number, is less than 1, the axial dispersion is ignorable. The following equation can measure the observed reaction rate.

$$-r_{obs} = \frac{(C_{in} - C_{out})Q}{V_b(1-\varepsilon_b)} \tag{4.4}$$

where C_{out}, Q, and V_b are the outlet concentration of filter, the volume metric airflow rate, and the filter bed volume, respectively. Another way to examine the effect of axial dispersion is by comparing axial dispersion with forced axial convection using the Peclet number (see Eq. (2.5). Axial dispersion is insignificant when the Peclet number is much higher than 1 [37]. However, employing these numbers requires the exact value of the axial dispersion coefficient. Using existing empirical correlations can produce biased estimates of the Y-F and Peclet numbers. A comprehensive study of axial dispersion was performed by comparing the simulation results of the proposed model with predictions made by two other models. Model O-B considers interparticle mass transfer by plug flow, while Model O-C considers dispersion by molecular diffusion only. There is no difference in the kinetic model across all models, but there are differences in the interparticle mass transfer models and boundary conditions. Table 4.2 lists the differences between the models.

Table 4.2: Differences between Model O-A, O-B, and O-C.

Model name	Intraparticle mass transfer model	Boundary conditions
O-A	$\frac{\partial C}{\partial t} = -u_b \frac{\partial C}{\partial x} + D_x \frac{\partial^2 C}{\partial x^2} - \frac{3K_C(1-\varepsilon_b)}{R_p \varepsilon_b}\left(C - C_p(r = R_p)\right)$	$D_x \frac{\partial C(t, x=0)}{\partial x} = -u_b\left(C_{in} - C(t, x=0)\right)$
O-B	$\frac{\partial C}{\partial t} = -u_b \frac{\partial C}{\partial x} - \frac{3K_C(1-\varepsilon_b)}{R_p \varepsilon_b}\left(C - C_p(r = R_p)\right)$	$C(t, x=0) = C_{in}$
O-C	$\frac{\partial C}{\partial t} = -u_b \frac{\partial C}{\partial x} + D_m \frac{\partial^2 C}{\partial x^2} - \frac{3K_C(1-\varepsilon_b)}{R_p \varepsilon_b}\left(C - C_p(r = R_p)\right)$	$C(t, x=0) = C_{in}$

The fitted values measured by these three models were used to predict the performance of filter type 1 at 0.1 ppm, filter type 2 at 1 ppm, and filter type 3 at 9 ppm (see Fig. 4.6). It is found that model O-A has the best prediction, confirming the role of axial dispersion.

As a result of dispersion, the unreacted ozone in the filter bed of activated carbon mixes with reaction products (like molecular oxygen, CO, and CO_2), so the ozone concentration decreases, causing a lower reaction rate [32]. Therefore, the filter's performance decreases when dispersion increases [112]. It is worth mentioning that since the reaction rate is highest in the case of plug flow, the filter will be deactivated sooner. The reaction kinetic parameters calculated by Models O-B and O-C are flow rate-dependent, so they are not true constants. Fig. 4.7-a shows that the axial dispersion is more important for filter type 3, consistent with the results of the inter-model comparison.

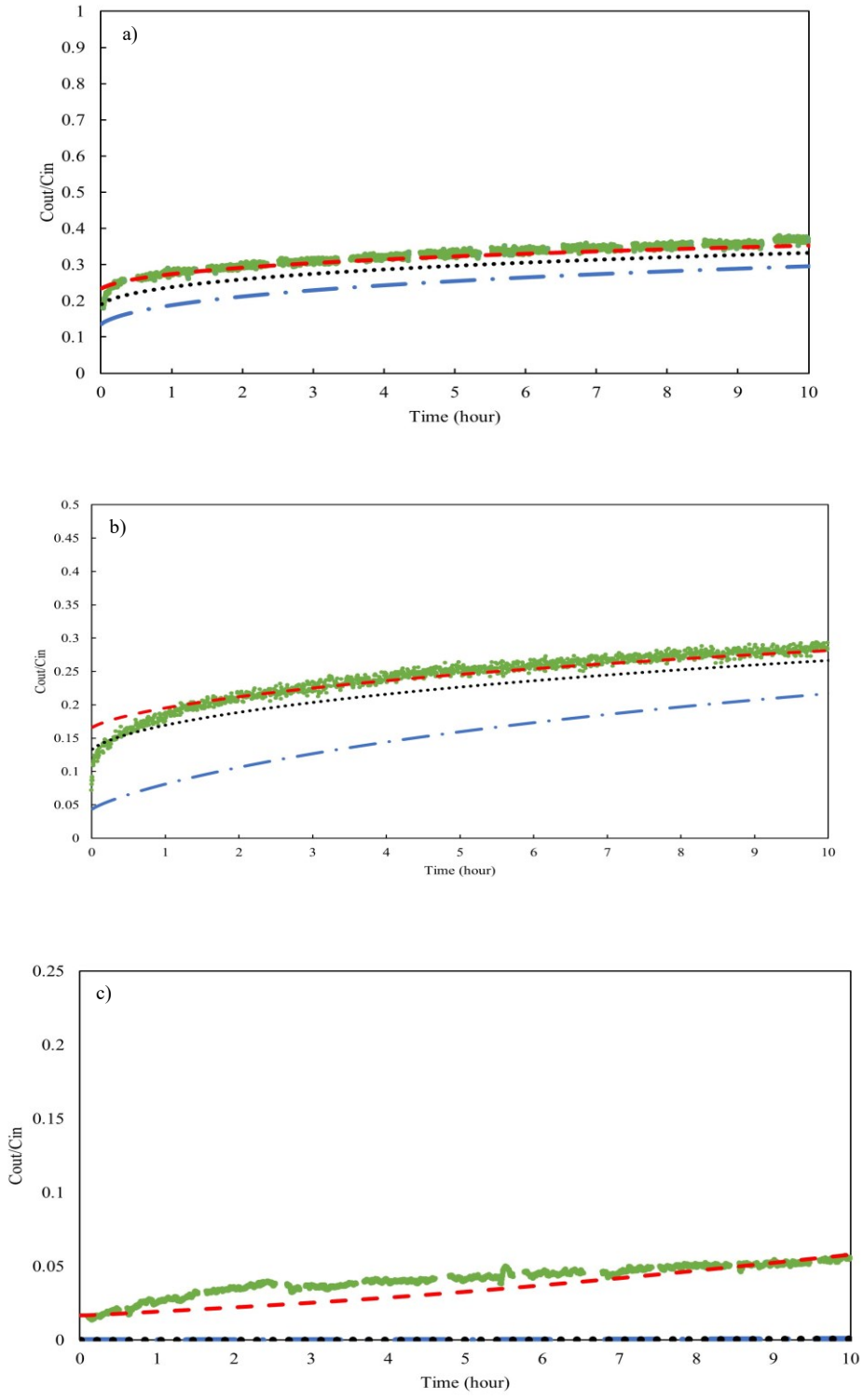

Fig. 4.6: Comparison of Models O-A, O-B, and O-C (green lines: experimental data, red lines: Model O-A, blue lines: Model O-B, and black dots: Model O-C). a) filter type 1, b) filter type 2, and c) filter type 3.

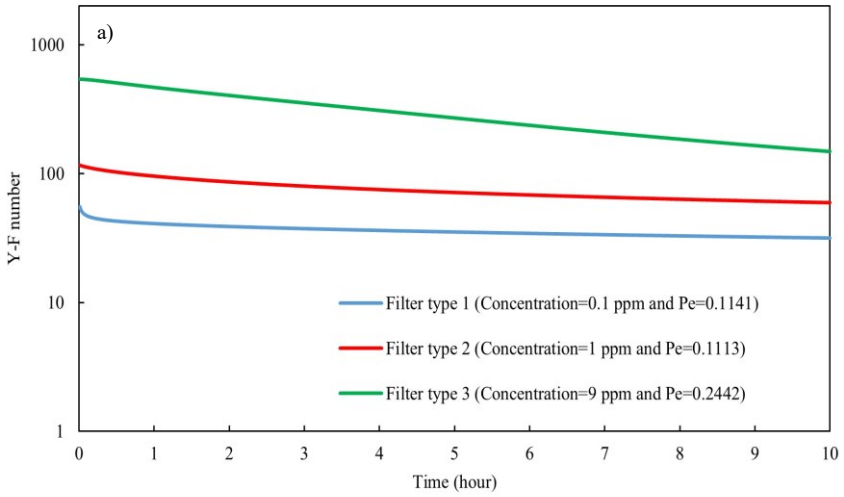

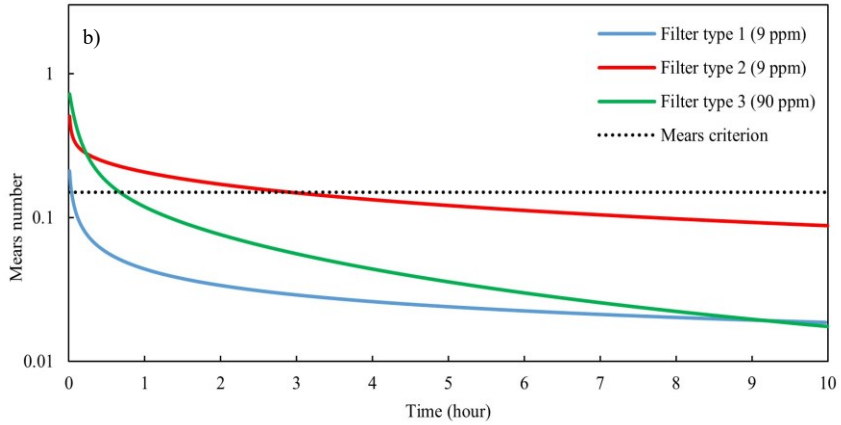

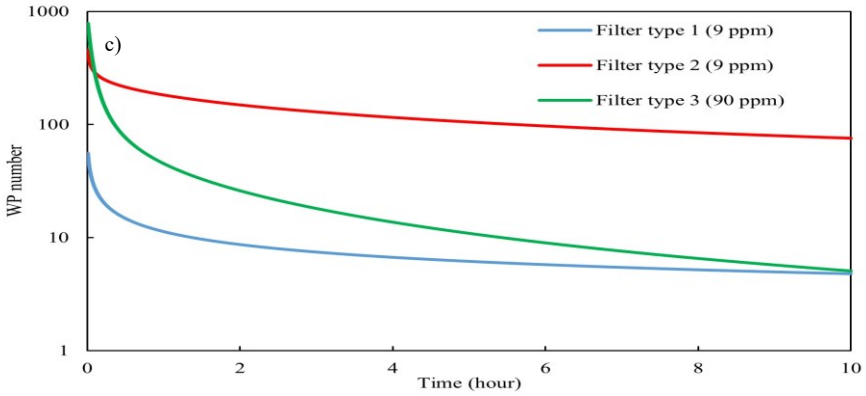

Fig. 4.7: a) Y-F and Peclet numbers, b) Mears numbers, and 3) Weisz-Prater parameter for various filters.

4.2.2.4.2 Effect of external mass transfer

The external mass transfer is the transfer of pollutants from bulk to the external surface of activated carbon particles. Mears criterion can be used to show if the external mass transfer can be neglected. Mears number (MR) is expressed [37]:

$$MR = \frac{-r_{obs}(1-\varepsilon_b)R_p}{K_C C} \tag{4.5}$$

The external mass transfer can be ignored when the Mears number is less than 0.15. Fig. 4.7-b shows the values of Mears number for all types of filters. During the early stages of the process, Mears number is higher than 0.15. For filter type 1, the value drops to below 0.15 earlier than other filters. The reason is that this filter has the lowest observed reaction rate because of its low carbon content (see Table 3.3). Initially, filter type 3 has the highest Mears number due to its high carbon content (see Table 3.3). However, because of the high challenge concentration (90 ppm), the filter is deactivated faster than other filters. As a result, the Mears number for filter type 3 finally reaches the lowest value compared to filters type 1 and 2.

4.2.2.4.3 Effect of internal diffusion

Internal diffusion is the last mass transfer step that can limit the reaction. If it is ignored incorrectly, it will result in a significant error in the measured reaction rate parameters. The Weisz-Prater criterion is used to prove that internal diffusion limits the reaction. Weisz–Prater parameter can be calculated as [37]:

$$C_{WP} = \frac{-r_{obs}R_p^2}{D_p C_{surface}(1-\varepsilon_b)} \tag{4.6}$$

where C_{WP} is the Weisz-Prater parameter, and $C_{surface}$ is the ozone concentration at the external surface of activated carbon, which is assumed to be equal to $C_P(r = R_p)$. If C_{WP} is about 1 or above, the effect of internal diffusion is important, but if C_{WP} is much less than 1, the internal diffusion can be ignored. Fig. 4.7-c depicts the amount of C_{WP} for the three kinds of filters as a function of time. The figure shows that its values are always greater than 1, confirming the importance of internal diffusion. Also, in the first steps of the reaction, because of the higher reaction rate, the C_{WP} has its maximum value. Then, due to the deactivation of the activated carbon, it decreases.

In addition, the simulation result of the comprehensive model (Model O-A) was compared to the prediction made by another model (Model O-D) in order to assess the impact of the mass transfer process. The internal and external mass transfers were ignored in Model O-D.

$$\frac{\partial C}{\partial t} = -u_b \frac{\partial C}{\partial x} + D_x \frac{\partial^2 C}{\partial x^2} - k_1 a C \tag{4.7}$$

The initial and boundary conditions were similar to the initial and boundary conditions of Eq. (3.3). The fitted values measured by Models O-A and O-D were used to predict the performance of filter type 1 at 100 ppb, filter type 2 at 1 ppm, and filter type 3 at 9 ppm (see Fig. 4.8). It can be seen that Model O-A has the best prediction, confirming the importance of mass transfer resistances. Applying Model O-D results in higher initial efficiencies and steeper breakthrough curves because it considers that mass transfer steps do not limit the reaction. Since Model O-D ignores the importance of mass transfer, the kinetic parameters measured by this model are not the intrinsic ones. The results also confirm that the mass transfer is more significant for filter type 2 than for two other filters.

The main reason is the low activated carbon particle porosity in filter 2 (see Table 3.3), which led to the smallest effective gas-phase diffusion coefficient.

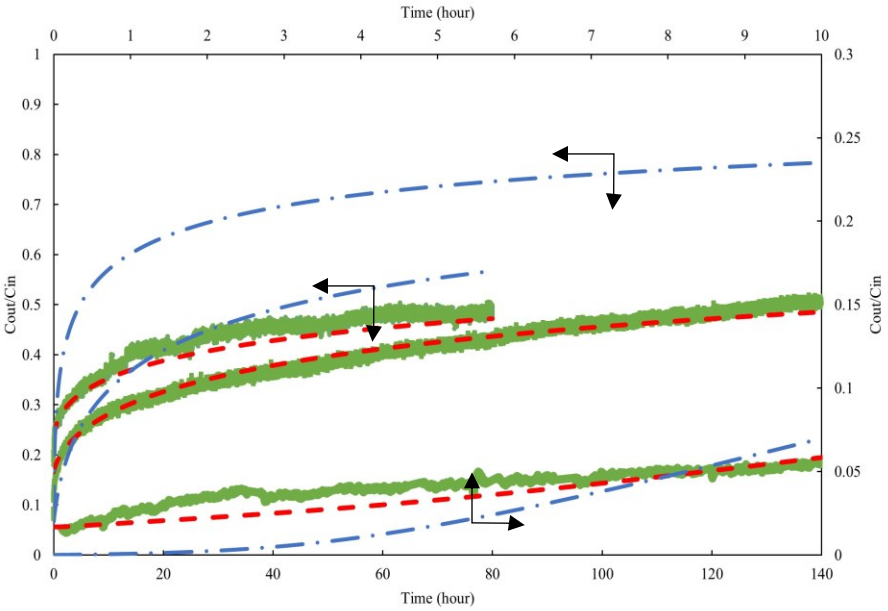

Fig. 4.8: Comparison of the results of Models O-A and O-D. (green lines: experimental data, red lines: Model O-A prediction, and blue line Model O-D prediction).

4.2.3 Sensitivity analysis

As part of evaluating the robustness of the developed model, sensitivity analysis was performed on parameters that are subjected to measurement errors. These parameters can be grouped into parameters measured by fitting into experimental data (reaction kinetic parameters), time-dependent parameters (porosity of the particles) and those measured by empirical correlations (external mass transfer and axial dispersion coefficients).

4.2.3.1 Reaction kinetic parameters

The reaction kinetic parameters were measured by fitting the model into experimental data. In the sensitivity analysis, the value of each reaction parameter was changed from 80 % to 120 % of its fitted value, while the values of other reaction parameters were kept constant.

Fig. 4.9 shows that the model is sensitive to the variation of all reaction parameters. The sensitivity is highest and lowest for the order of decay and decay constants, respectively. The figure exhibits that a 20% decrease in order of decay (from 100% to 80% of fitted value) results in around 44%, 90%, and 30% increase in error for filter types 1, 2 and 3, respectively. Therefore, it is important to measure the reaction parameter accurately since it limits the removal rate significantly.

4.2.3.2 Porosity of the activated carbon particles

For the modelling, the porosity of the particles was assumed to be constant (equal to the initial porosity). However, the reaction between ozone and the activated carbon surface can alter the porosity of the particle in several ways [114]. For example, the porosity of particles in filter type 1 was decreased from 47% to 40% after exposure to 9 ppm of ozone for 10 hours. This is probably due to the surface functional groups covering the pore walls [55,114,115]. In order to investigate the importance of this time-dependent parameter, the fitting procedure was repeated using the final porosity for filter type 1, and the predictions were compared with previous results (see Fig. 4.10-a). Modelling results based on two porosities show a negligible difference up to 80 hours. However, the difference gradually increases with time, which needs further investigation.

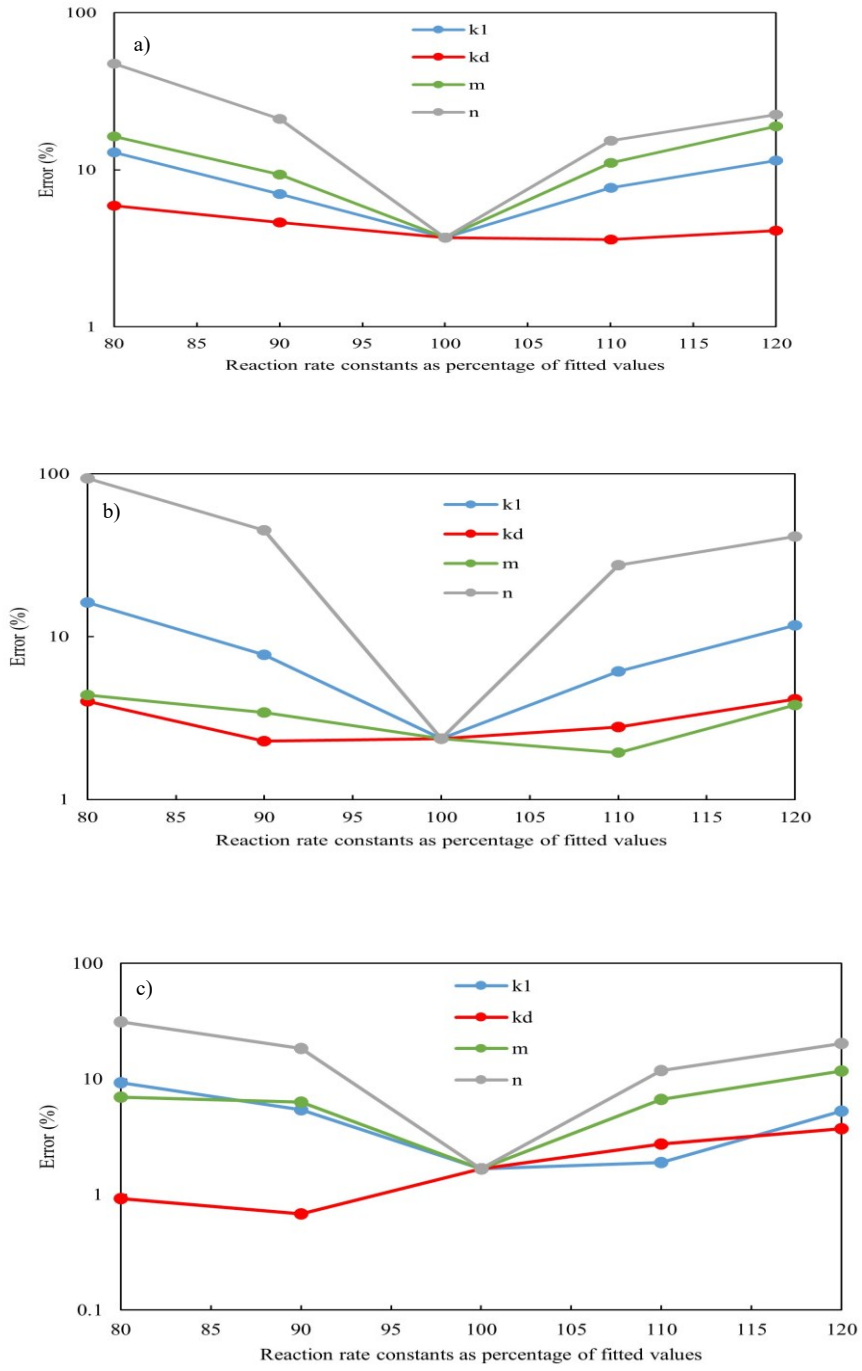

Fig. 4.9: Sensitivity analysis of the reaction kinetic parameters. a) filter type 1 at 100 ppb and 30 l/min, b) filter type 2 at 1 ppm and 30 l/min, and c) filter type 3 at 90 ppm and 60 l/min.

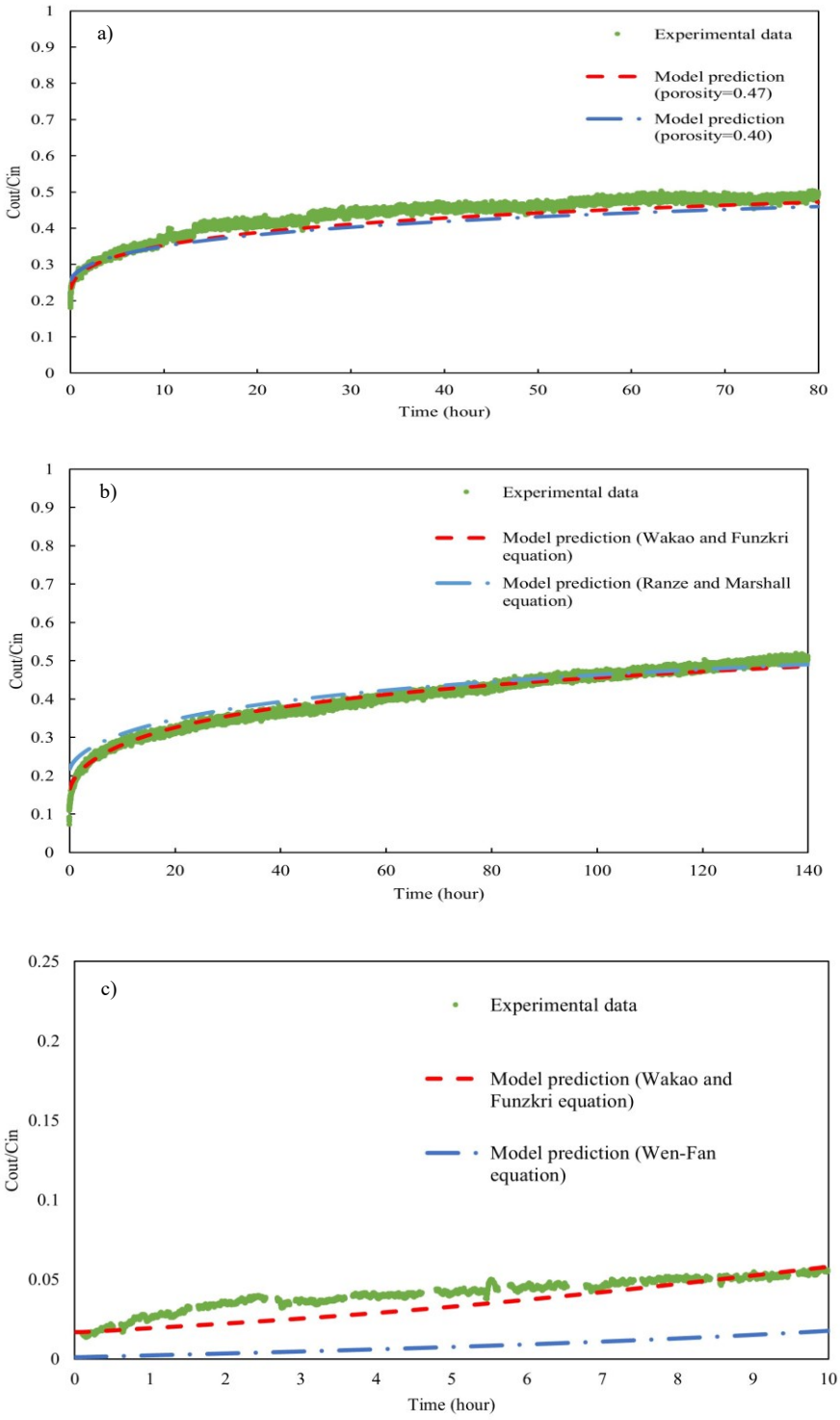

Fig. 4.10: Sensitivity analysis of a) porosity of the particles for filter type 1 at 0.1 ppm, b) external mass transfer coefficient for filter type 2 at 1 ppm, and c) axial dispersion coefficient for filter type 3 at 9 ppm.

4.2.3.3 External mass transfer coefficient

The external mass transfer coefficient is measured by the Wakao and Funzkri equation (Eq. (3.34)) [39]. Another widely used correlation is the Ranze and Marshall correlation [41].

$$\frac{K_c d_p}{D_m} = 2 + 0.6\left(\frac{u_b d_p}{\nu}\right)^{0.5}\left(\frac{\nu}{D_m}\right)^{\frac{1}{3}} \tag{4.8}$$

This correlation was developed for single spheres, giving relatively lower mass transfer coefficient values than most empirical correlations [41]. Therefore, these two equations give a wide external mass transfer coefficient range. The modelling procedure was repeated with Ranze and Marshall correlation for filter type 2, which showed the highest Mears numbers. Fig. 4.10-b exhibits a slight difference between models' predictions at the early stage of ozone removal, where the reaction rate is highest and mainly occurred on the external surface of activated carbon particles.

4.2.3.4 Axial dispersion coefficient

The importance of axial dispersion was further validated by conducting a sensitivity analysis of the model on the axial dispersion coefficient. The new set of reaction kinetic parameters was measured by fitting the model into experimental data, while the Wen-Fan [116] equation was used for calculating the axial dispersion coefficient. The Wen-Fan equation is shown in Eq. (4.9).

$$\frac{D_x \varepsilon_b}{D_m} = 0.3\varepsilon_b + \frac{0.5\left(\frac{u_b d_p}{D_m}\right)}{1 + \frac{3.8 D_m}{u_b d_p}} \tag{4.9}$$

Fig. 4.10-c compares the model prediction when Wakao and Funzkri (Eq. (3.33)) [39], and Wen-Fan [116], equations are used to calculate the axial dispersion coefficient. Filter type

3 was selected for this study because it has the highest Y-F numbers. The figure shows that the breakthrough curve is sensitive to the value of the axial dispersion coefficient. The Wakao and Funzkri correlation has better prediction results, which give a higher axial dispersion coefficient than the Wen-Fan equation.

4.3 Summary

This chapter reported the systematic validation of a dynamic model to predict the service life of carbon-based filters to remove ozone from indoor environments. Models of axially dispersed plug flow and pore diffusion were considered for interparticle and intraparticle mass transfer, respectively. The axially dispersed plug flow incorporates convection, dispersion, accumulation within the pores of the filter, and mass transfer across the boundary layer. On the other hand, the pore diffusion model considered accumulation and diffusion in the pores of particles. Also, it was augmented by a reaction rate that considered the deactivation of activated carbon.

The prediction made by the model was in good agreement with the experimental data for the concentration level observed indoors for all tested filters. Additionally, the model correctly predicted the experimental results collected at a higher velocity and using a full-scale setup.

The inter-model comparison between the axially dispersed plug flow model, the plug flow model, and the model that considers dispersion only by molecular diffusion for interparticle mass transfer indicated the importance of axial dispersion. Therefore, the reaction kinetic parameters measured by models other than the axially dispersed plug flow were not intrinsic. Moreover, the results of the comprehensive model were compared with a model that ignored the boundary layer and internal mass transfer resistances. It was found that the

internal mass transfer limited ozone removal through activated carbon particles even with particle diameters below 1 mm.

According to the sensitivity analysis, the external mass transfer showed a subtle effect only at the beginning of the removal process, which was also shown by the values of Mears number. Furthermore, changing the porosity of the activated carbon particle because of the reaction with ozone did not significantly affect the model prediction. Meanwhile, comparing different empirical correlations for the axial dispersion coefficient revealed that the Funzkri and Wakao correlation results in the best model prediction. The sensitivity analysis also showed that the reaction rate significantly limits the removal process.

5 Validate a Mathematical Model to Estimate the Removal of Indoor VOCs by Carbon Filters[1]

VOCs, which tend to have higher concentrations in indoor air compared with outdoor air, are considered important hazardous chemicals [117,118]. There are many different sources of VOC in the indoor environment, such as building materials, furnishings, office equipment, personal care products, paint, and cleaning agents [97,118]. Various types of VOCs, including n-alkanes, aliphatic hydrocarbons, cyclo-alkanes, halogenated compounds, alcohols, aldehydes, ketones, esters, aromatic hydrocarbons, and terpenes, may be found in the indoor environment [119]. Exposure to VOCs can cause eye, nose, and throat irritation, liver and kidney dysfunction, headaches, and damage to the central nervous system [118,120]. Also, some VOCs - such as formaldehyde, acetaldehyde, benzene, naphthalene, and chloroform - are suspected or proven to be carcinogenic [121].

Integrating adsorbent filters into ventilation systems is a way to reduce indoor VOC concentrations. The majority of VOCs are usually removed from buildings using carbon-based filters [11]: VOCs are physically adsorbed on the adsorptive filter surface, and the filter will eventually become saturated. Therefore, they require periodic regeneration or replacement. Consequently, building engineers and designers need information about the service life of filters.

[1] M. G. Khararoodi, F. Haghighat, and C.-S. Lee, "Develop and validate a mathematical model to estimate the removal of indoor VOCs by carbon filters," Build. Environ., p. 110082, 2023.

Different standards recommend experimental testing at ppm level concentrations to remove VOCs through adsorbent media. It is deliberately set at significantly higher concentrations than indoor concentrations of VOCs (ppb level) to limit the experimental time and associated cost. Experimental results at high concentrations have been widely utilized for estimating the efficiency of adsorptive media at low indoor concentrations using mathematical models [19,22]. This can be done by measuring the unknown parameters of the model by fitting the model into experimental data at tested concentrations (usually ppm level) and applying them to predict the efficiency of the filter at ppb level concentrations.

Developing an appropriate mathematical model requires knowledge of controlling mass transfer steps at various concentrations. Vizhemehr et al. [19] modelled the performance of granular activated carbon by considering all possible mass transfer steps (internal diffusions and external mass transfer). However, their model only had a correct prediction of breakthrough curves of the filter when the concentrations of VOCs were higher than 15 ppm. The main reason for the deviation of the prediction of their model from experimental data was applying Langmuir isotherm constants obtained at high ppm concentrations (15-300 ppm) in the dynamic modelling of the filter's efficiency for concentrations less than 15 ppm. In addition, the use of a constant surface diffusion coefficient may be another factor. By using an inter-model comparison, Pei and Zhang [24] proposed that the surface diffusion rate was quite higher than the external mass transfer, and the external mass transfer was greater than the gas-phase diffusion rate for the tested granular activated carbon at the ppm level. It means that there was no need to model the internal mass transfer, and the mass transfer was only controlled by the external transfer. However, they did not validate their model for low indoor concentrations. Also, their conclusion was based on

assuming constant surface diffusivity. On the other hand, Yao et al. [26] depicted that the external resistance is only important at low velocities and in the early stages of the removal process for activated carbon fibres, which are highly microporous. Also, they argued that the intrafibre diffusion was only controlled by surface diffusion. He et al. [21] measured a significantly lower surface diffusivity for the adsorption of toluene into granular activated carbon at ppb levels compared with ppm levels. For their tested system, the external mass transfer was quite higher than the internal diffusion mechanisms. However, the gas-phase and surface diffusion were comparable for both ppb and ppm concentration levels for the tested adsorbent. The most important limitation of these two works was measuring the surface diffusivity by utilizing the experimental results at ppb concentration levels, which is demanding.

Various pore size distributions and adsorbent sizes for the tested carbon adsorbents were the main reason for disagreement between the earlier works on the dominant mass transfer steps at low indoor concentrations. By decreasing the pore size of the adsorbent (granular, pellet, or fibre), VOCs molecules are more likely to diffuse through the surface than through the gas-phase. Therefore, the ratio of surface diffusion to gas-phase diffusion increases. Additionally, a longer diffusion path for molecules within the adsorbent particles is expected for adsorbents with a greater diameter [122]. Therefore, the ratio of internal to external resistance increases. Also, concentration-dependent parameters like adsorption isotherm parameters and surface diffusivity hindered the application of previously developed models for low indoor concentrations. This chapter examines the validity of the developed model (Eqs. (3.3) to (3.6), Eqs. (3.17) to (3.20), Eqs. (3.33) to (3.38), and D-R isotherm) to study VOCs removal through activated carbon filters.

5.1 Methodology

The methodology involves the following four steps. 1) Experiments were conducted in the small-scale system at five concentrations of VOCs ranging from 9 to 90 ppm and an airflow rate of 30 l/min with filter types 1 and 3. 2) Two adsorption isotherms were fitted to the five experimental points to find the most appropriate isotherm model and estimate its unknown parameters. 3) The developed model for VOC removal was fitted into the dynamic experimental data of different adsorbate-adsorbent systems at ppm level concentrations to find the surface diffusivities at zero loading. 4) The model was utilized for estimating the efficiency at lower concentrations, a higher airflow rate, and a larger scale configuration using adjusted parameters (see Fig. 5.1). Also, the model was compared with a variety of different mathematical models in order to investigate the significance of each stage of the transfer process. Finally, the controlling stages in the adsorption systems at various conditions were determined using the dimensionless version of the transfer equations.

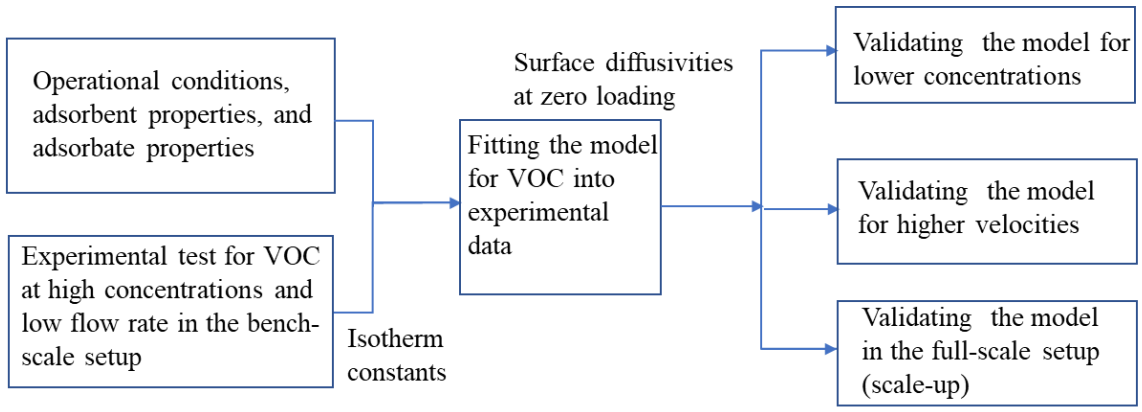

Fig. 5.1: Structure of the simulation program for VOCs.

5.2 Dimensionless model

The Peclet number (Pe), Stanton number (St), Diffusion Modulus (Ed_p and Ed_s), dimensionless surface diffusivity ($\bar{D}_s$), distribution parameter (D_g), porosity ratio (φ), dimensionless time ($\bar{t}$), dimensionless length (X), dimensionless radius ($\bar{r}$), and dimensionless concentrations ($\bar{C}$, $\bar{C}_p$, and $\bar{q}$) were used to derive the dimensionless equations [123]:

$$\bar{C} = \frac{C}{C_{in}}, \bar{C}_p = \frac{C_p}{C_{in}}, \bar{q} = \frac{q}{q_{in}}, \bar{D}_s = \frac{D_s}{D_{s0}}, X = \frac{x}{L}, \bar{r} = \frac{r}{R_p}, \bar{t} = \frac{u_b t}{L}, Pe = \frac{u_b L}{D_x},$$

$$Ed_p = \frac{D_p L}{u_b R_p^2}, Ed_s = \frac{D_{s0} L D_g}{u_b R_p^2}, St = \frac{K_C L}{\varepsilon_p R_p u_b}, \varphi = \frac{\varepsilon_p (1-\varepsilon_b)}{\varepsilon_b}, D_g = \frac{\rho_p q_{in}}{\varepsilon_p C_{in}}$$

Eqs. (3.3) and (3.17) can be rewritten as below:

$$\frac{\partial \bar{C}}{\partial \bar{t}} = -\frac{\partial \bar{C}}{\partial X} + \frac{1}{Pe}\frac{\partial^2 \bar{C}}{\partial X^2} - 3\varphi St\left(\bar{C} - \bar{C}_p(\bar{r}=1)\right) \tag{5.1}$$

$$\frac{\partial \bar{C}_p}{\partial \bar{t}} = \frac{Ed_p}{1 + D_g f'(\bar{C}_p)}\left(\frac{\partial^2 \bar{C}_p}{\partial \bar{r}^2} + \frac{2}{R}\frac{\partial \bar{C}_p}{\partial \bar{r}}\right) \tag{5.2}$$

$$+ \frac{Ed_s f'(\bar{C}_p)}{1 + D_g f'(\bar{C}_p)}\left(\bar{D}_s \frac{\partial^2 \bar{C}_p}{\partial \bar{r}^2} + \frac{2\bar{D}_s}{\bar{r}}\frac{\partial \bar{C}_p}{\partial \bar{r}} + \frac{\partial \bar{D}_s}{\partial \bar{C}_p}\left(\frac{\partial \bar{C}_p}{\partial \bar{r}}\right)^2\right)$$

The associated initial and boundary conditions are:

$$\bar{C}(\bar{t}=0, X) = 0 \tag{5.3}$$

$$\frac{\partial \bar{C}(\bar{t}, X=0)}{\partial X} = -Pe\left(1 - \bar{C}(\bar{t}, X=0)\right) \tag{5.4}$$

$$\frac{\partial \bar{C}(\bar{t}, X=1)}{\partial X} = 0 \tag{5.5}$$

$$\bar{C}_p(\bar{t}=0,\bar{r})=0 \tag{5.6}$$

$$\frac{\partial \bar{C}_p(\bar{t},\bar{r}=0)}{\partial \bar{r}}=0 \tag{5.7}$$

$$\frac{\partial \bar{C}_p(\bar{t},\bar{r}=1)}{\partial \bar{r}}=\frac{St}{Ed_p+Ed_s\bar{D}_s f'(\bar{C}_p)}\left(\bar{C}-\bar{C}_p(\bar{r}=1)\right) \tag{5.8}$$

5.3 Results and discussion

5.3.1 Adsorption isotherm parameters determination

Adsorption isotherms are utilized to quantify the adsorption process. They correlate the amount of equilibrium sorbed-phase concentration (capacity) and the concentration (or pressure) on the gas-phase at a constant temperature. Adsorption studies on the bench-scale setup were employed to identify the proper adsorption isotherm for VOCs onto activated carbon filters. The tests were carried out for toluene, limonene, and MEK at five concentrations between 9-90 ppm. The adsorption test was run till the downstream and upstream concentrations become equal (100% breakthrough). The adsorption capacity is calculated by:

$$q(t)=\frac{\int_0^t Q(C_{in}(t)-C_{out}(t))dt}{M_{carbon.F}} \tag{5.9}$$

where $M_{carbon.F}$ is the mass of carbon per filter. Fig. 5.2 depicts the fitted Langmuir and D-R curves together with the experimental data, and Table 5.1 summarizes the various isotherms parameters and their corresponding R^2.

It can be seen that the D-R isotherms fit better fit to the experimental data compared with the Langmuir model. It is worth mentioning that although Freundlich isotherm can be

considered as a potential isotherm for representing the adsorption data of organic compounds into carbonaceous adsorbent, one of the most important limitations of this isotherm for indoor application is the concentration dependency of its constants [124,125]. For example, Yao et al. [126] showed that the Freundlich exponent for VOCs at ppb concentration levels was significantly higher than that at ppm levels. Therefore, using adsorption parameters measured in the concentration range of 9 to 90 ppm in the dynamic model can result in an inaccurate estimation of filter service life. The D-R equation, derived from the Polanyi potential theory, was used to overcome this [125]. Adsorption occurs as a pore-filling process for this isotherm rather than as a layer-covering process, and adsorption parameters are only dependent on adsorbate and adsorbent types [26].

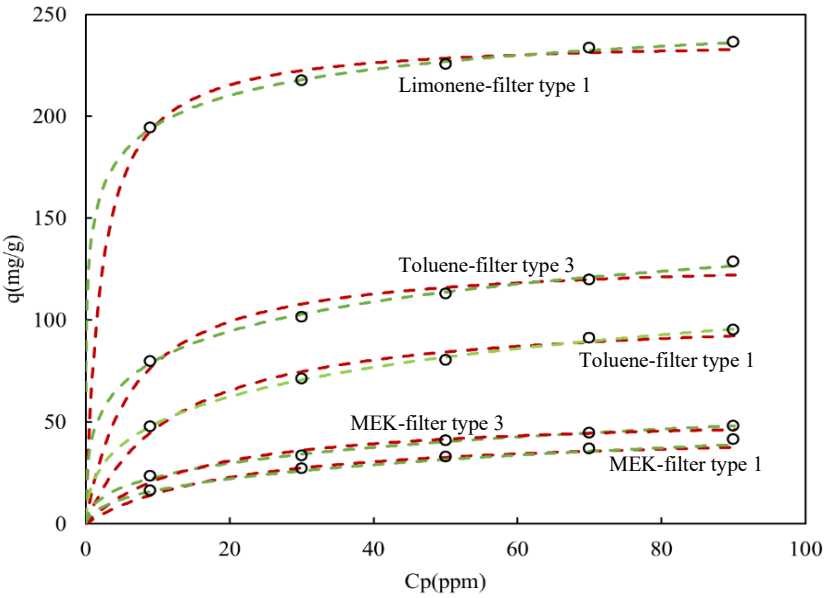

Fig. 5.2: Experiments and isotherm models. (black dots: experiments, green lines: D-R isotherm and red lines: Langmuir isotherm).

Table 5.1: Isotherm parameters for various filters and VOCs.

Isotherm model	Parameters	Filter type 1 for toluene	Filter type 3 for toluene	Filter type 1 for MEK	Filter type 3 for MEK	Filter type 1 for limonene
D-R	$K_{DR} \times 10^9$	3.50	2.40	3.68	3.15	1.76
	q_{max}	205	213	143	149	258
	R^2	0.9969	0.9933	0.9979	0.9973	0.9967
Langmuir	K_L	0.0221	0.0414	0.0166	0.0228	0.0845
	q_{max}	105	131	46.1	53.9	238
	R^2	0.9658	0.9274	0.9607	0.9639	0.9522

5.3.2 Surface diffusivity determination

The surface diffusivities at zero loading were obtained by fitting the developed model into experimental data of toluene, limonene and MEK adsorption into filter types 1 and MEK adsorption into filter types 3 at 9 ppm and experimental data of toluene adsorption into filter types 3 at 30 ppm. Depending on the types of adsorbates and adsorbents, various concentrations were chosen to achieve at least 50% breakthrough time after 10 hours of testing. Therefore, the test time was sufficient to generate useful data for measuring surface diffusivities. In other words, it is enough to pass the initial step which is controlled by external mass transfer [24]. Fig. 5.3 shows the fitting results for various adsorbate-adsorbent systems, and Table 5.2 reports the surface diffusivities at zero loading and the R^2. As evidenced by high R^2 values and randomly scattered residuals, the model fits well.

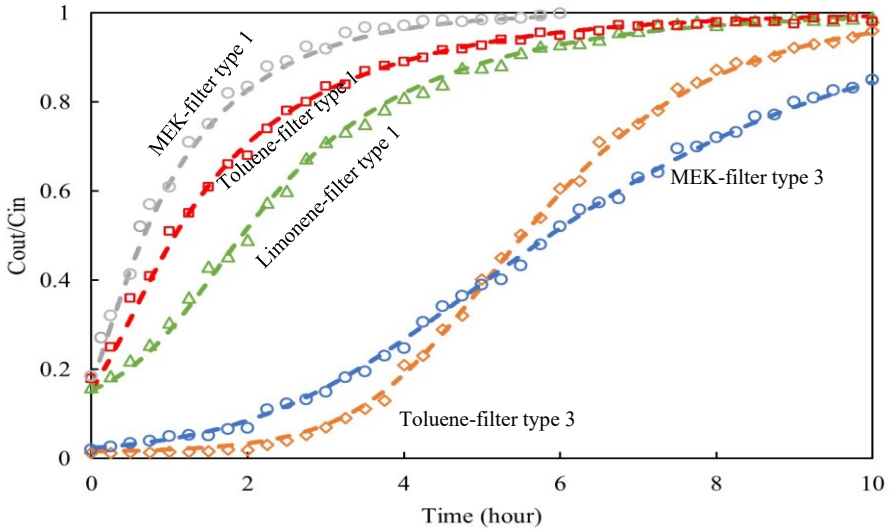

Fig. 5.3: Experiments and the fitted model. (dots: experimental data and lines: model's prediction).

Table 5.2: Surface diffusivities at zero loading for various adsorbate-adsorbent systems.

Parameters	Filter type 1 for toluene	Filter type 3 for toluene	Filter type 1 for MEK	Filter type 3 for MEK	Filter type 1 for limonene
$D_{s0} \times 10^{13}$	6.6	5.4	10.6	9.1	1.2
R^2	0.9983	0.9985	0.9966	0.9977	0.9975

5.3.3 Model validation

The validation of the model was conducted in two steps. First, it was performed by employing the model to predict the efficiency of the adsorptive filter at lower concentrations and a higher airflow rate. Also, the simulation and experimental results for the large-scale system were compared for further validation of the model. A comparative of the models was performed for further validation by examining the significance of boundary layer transport, gas-phase diffusion, and surface diffusion.

5.3.3.1 Evaluation at lower VOCs concentrations

The indoor concentration of single VOCs is in the ppb range, so verifying the model for lower concentrations is necessary. The adsorption isotherm parameters and surface diffusivities at zero loading that were calculated at ppm level concentrations were used to estimate the filters' performance at concentrations of 5, 1, and 0.1 ppm. Fig. 5.4 compares the experimental data and model prediction and shows that the model follows the experimental results closely at low concentrations.

The acceptable model prediction up to the upstream concentration of 0.1 ppm shows that the concentration range is not in Henry's law region. The D-R isotherm does not have a valid Henry's law region, so this isotherm model will fail to present the equilibrium condition at upstream concentrations lower than 0.1 ppm. The modified Dubinin-Radushkevich (MDR) isotherm equation, which reduces to the linear equation at low concentrations and D-R isotherm at higher concentrations, may be able to present the equilibrium condition when there is a limitation for D-R isotherm [127].

Filter type 3 shows approximately s-shaped breakthrough curves, while filter type 1 follows convex shape breakthrough curves with high initial breakthroughs. The reason is that filter type 1 has low carbon content and small thickness (quite less than the length of the mass-transfer zone (MTZ)) (see Table 3.3). Therefore, there is less chance for VOCs molecule to come into contact with filter type 1 compared to filter type 3 [107].

The adsorption performance of filters is highest for limonene and lowest for MEK. For example, for filter type 1, the efficiencies after 4 hours for the inlet concentration of 5 ppm are around 45%, 28%, and 3% for limonene, toluene, and MEK, respectively. Also, the

efficiencies after 6 hours for the inlet concentration of 1 ppm for filter type 3 are about 98% and 94% for toluene and MEK, respectively. This behaviour can be described by the physical properties of gaseous contaminants and the surface properties of activated carbon. The activated carbon surface is non-polar, so it adsorbs non-polar VOCs (limonene and toluene) rather than polar ones (MEK) [128]. Also, limonene molecules have a higher electron number content and are larger (electrons are further away from the nucleus charge) than toluene molecules, resulting in less controlled charge distribution [129]. Therefore, limonene molecules possess higher polarizability, which means they have a greater tendency to generate induced electric dipole moments than toluene molecules when approaching the activated carbon surface [129]. Consequently, limonene and MEK have the strongest and weakest induced dipole-induced dipole attraction on the surface of activated carbons. This can also justify the greater surface diffusivity at zero loading of MEK compared with toluene and limonene on filter type 1 or compared with toluene on filter type 3.

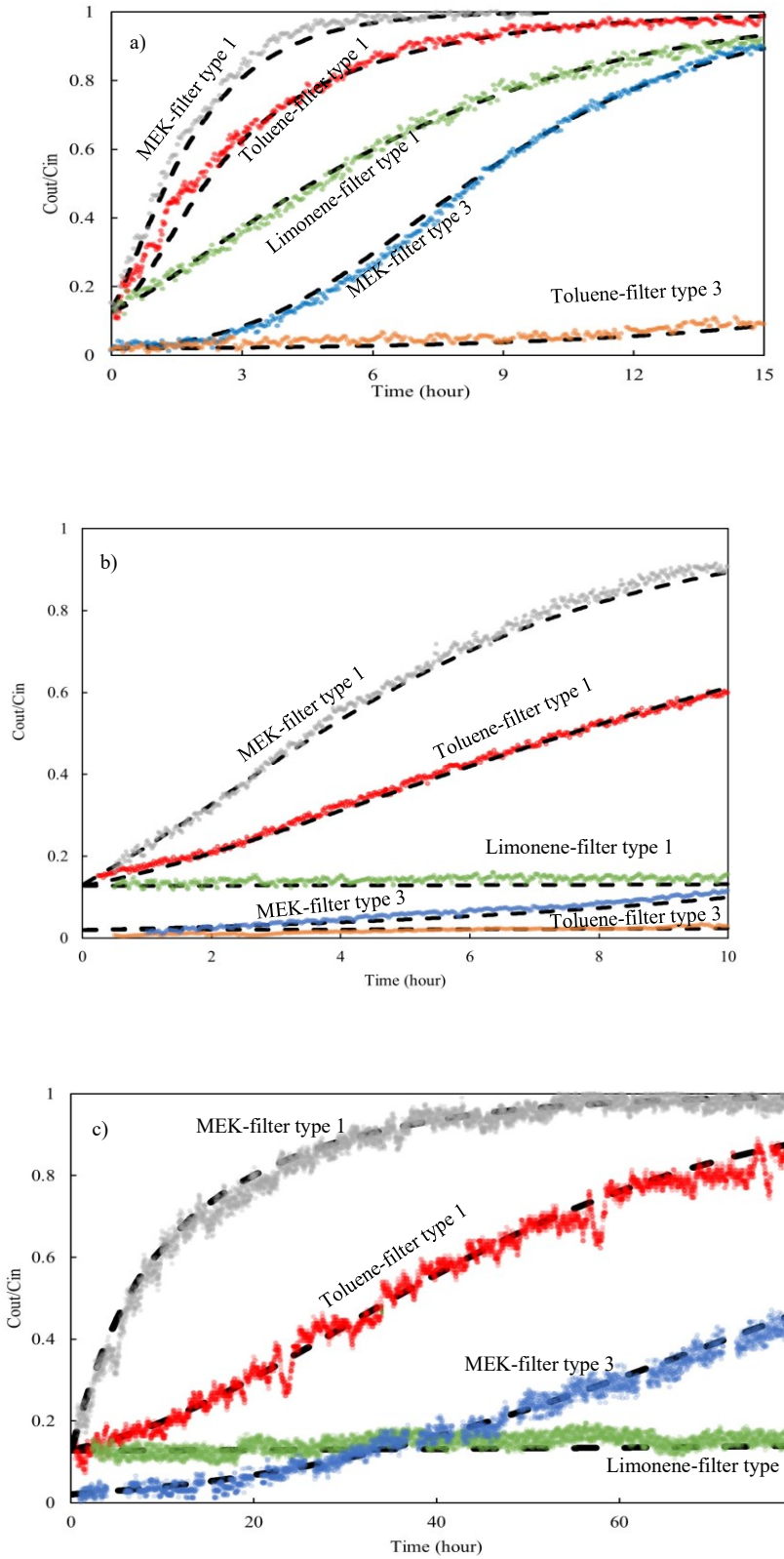

Fig. 5.4: Breakthrough curves of filters for removal of VOCs (dots: experiments and lines: model). a) 5 ppm, b) 1 ppm, and c) 0.1 ppm (long-term testing).

5.3.3.2 Evaluation at a higher airflow rate and with full-scale results

The developed model must estimate the filter breakthrough curve at various airflow rates to be applicable for indoor environment applications. The surface diffusivity at zero loading (D_{s0}) and D-R isotherm parameters (K_{DR} and q_{max}), are not a function of airflow rate. Therefore, the constants calculated at the tested airflow rate (30 l/min), were employed in the prediction of the performance of the filters at 60 l/min. Fig. 5.5 shows that the deviation of the model from experimental data is insignificant. The comparison between Fig. 5.3 and Fig. 5.5 reveals that the efficiency of all filters decreases as the airflow rate increases. For example, to remove toluene through filter type 1, 50% breakthrough changes from 60 minutes to 40 minutes when the airflow rate doubled. The reason is that by increasing the airflow rate, VOC molecules have less time (shorter residence time) to be removed. Also, 100% breakthrough occurs sooner when the airflow rate rises, which is because the mass flow rate of VOCs is higher at the higher airflow rates; however, the total capacity of the adsorbent is constant [24].

To verify the ability of the developed model for real application, the model prediction was compared with the experimental results of filter type 1 (pleated form) exposed to toluene with the concentration of 0.1 ppm in the full-scale experimental setup (see Fig. 5.5). This figure shows there is a good agreement between the model prediction and the experimental results.

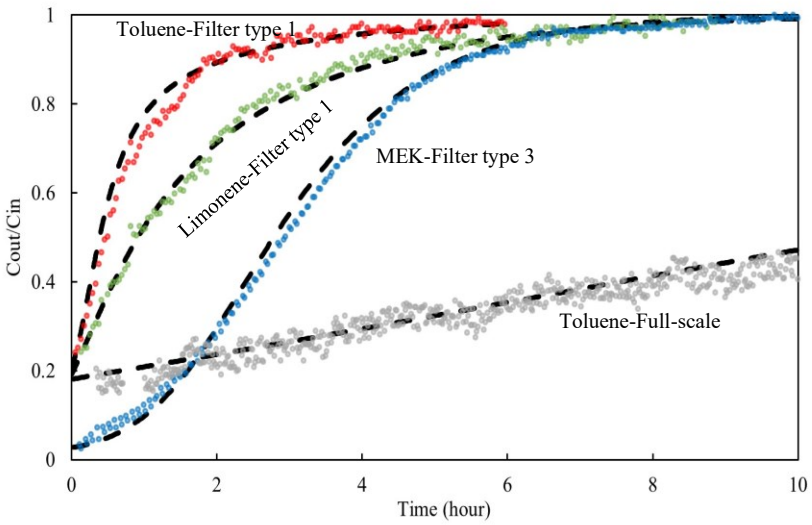

Fig. 5.5: Experiment (dots) and model prediction (lines) for a higher flow rate and large-scale setup.

5.3.3.3 Inter-model comparison

The significance of various mass transfer stages was examined by comparing the prediction made by the developed model for VOCs with four others. For all models, Eq. (3.3) with its corresponding initial and boundary condition was used for the transport of VOCs between the particles; also, the D-R isotherm was utilized to show adsorption equilibrium. The unknown parameters of models were calculated at ppm concentration level like the procedure used for the comprehensive model. Also, the models' results were compared by using the average relative error.

5.3.3.3.1 Internal diffusion

As mentioned, by assuming negligible bulk flow, diffusion through the gas-phase and adsorbed phase (surface diffusion) are two pathways for transferring pollutants inside the adsorbent particle (see Fig. 5.6). The comprehensive model (PSDM with variable surface diffusivity (Model V-A)) considered both gas and surface diffusion for the internal mass

transfer. Two other models: HSDM with variable surface diffusivity (Model V-B), and PDM (Model V-C) were used to investigate the importance of each mass transfer pathway.

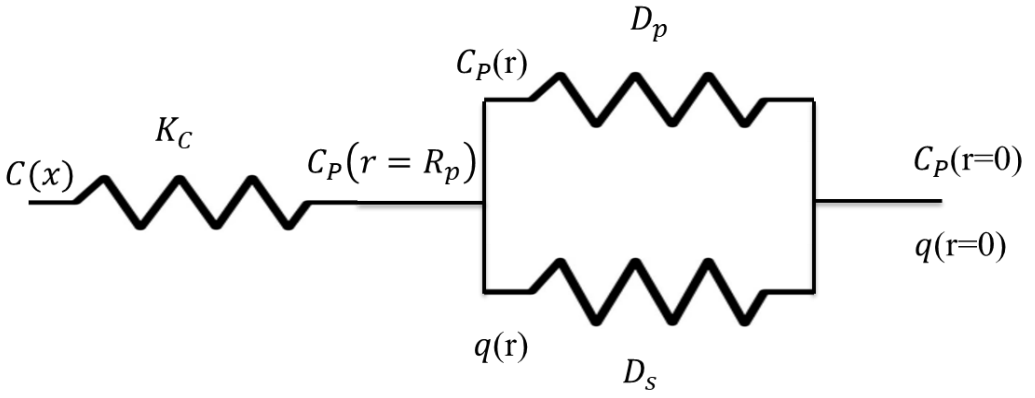

Fig. 5.6: Transport resistances in the adsorption process (adapted from Ref. [19])

As mentioned, the HSDM is used when diffusion in the adsorbed-phase is the predominant way of transport within particles [18]. The transport occurs by jumping adsorbate molecules between adsorption sites called surface diffusion, and the diffusion through the pore air phase can be neglected [130]. For the HSDM with variable surface diffusivity, the intraparticle mass transfer is described by the following equation [131]:

$$\frac{\partial q}{\partial t} = D_s \frac{\partial^2 q}{\partial r^2} + \frac{2D_s}{r}\frac{\partial q}{\partial r} + \frac{\partial D_s}{\partial q}\left(\frac{\partial q}{\partial r}\right)^2 \tag{5.10}$$

The initial and boundary conditions are:

$$q(t = 0, r) = 0 \tag{5.11}$$

$$\frac{\partial q(t, r = 0)}{\partial r} = 0 \tag{5.12}$$

$$\rho_p D_s \frac{\partial q(r = R_p)}{dr} = K_C(C - C^*) \tag{5.13}$$

On the other hand, the PDM is employed when gas phase diffusion is the dominant intraparticle mass transfer [18]. It assumes that adsorbate molecules escape from the adsorbent surface's force field during diffusion, so for this model, the pollutants diffuse through the particles' pores and then adsorb on the internal surface of the particle [132]. For one-dimensional mass transfer, the macroscopic conservation equation is given as [31]:

$$\varepsilon_p \frac{\partial C_p}{\partial t} + \rho_p \frac{\partial q}{\partial t} = \varepsilon_p D_p \left(\frac{\partial^2 C_p}{\partial r^2} + \frac{2}{r} \frac{\partial C_p}{\partial r} \right) \tag{5.14}$$

The initial and boundary conditions are:

$$C_P(t = 0, r) = 0 \tag{5.15}$$

$$\frac{\partial C_P(t, r = 0)}{\partial r} = 0 \tag{5.16}$$

$$D_p \frac{\partial C_P(r = R_p)}{dr} = K_C\big(C - C_P(r = R_p)\big) \tag{5.17}$$

Similar to the comprehensive model, the surface diffusivities at zero loading for HSDM with variable surface diffusivity were calculated using the model fitting to the measured breakthrough curve. However, for the PDM, all input parameters are known. Fig. 5.7 shows the prediction of PSDM and HSDM with variable surface diffusivity and PDM for different adsorbate-adsorbent systems, and Table 5.3 compares their ARE up to 80 hours. The PDM cannot predict the experimental data correctly, and HSDM with variable surface diffusivity results in predictions similar to PSDM with variable surface diffusivity. Therefore, the internal transfer is controlled by surface diffusion. This can be explained by the small pore size of tested activated carbons (see Fig. 5.8), where surface diffusion is more likely to happen for VOCs than gas-phase diffusion. This can be further shown by measuring λ_0 number, which is the ratio of adsorbed-phase diffusion to gas-phase diffusion as follow:

$$\lambda_0 = \frac{Ed_s}{Ed_p} = \frac{D_{s0}D_g}{D_p} \tag{5.18}$$

The values of λ_0 number for systems of toluene-filter type 1, toluene-filter type 3, limonene-filter type 1, MEK filter type 1, and MEK filter type 3, at the concentration of 100 ppb, are 263, 726, 326, 102, and 171, respectively. These values show that the internal mass transfer is mainly because of surface diffusion.

Table 5.3: Average relative error for various adsorbate-adsorbent systems at a concentration of 0.1 ppm up to 80 hours.

Models	Filter type 1 for toluene (%)	Filter type 1 for MEK (%)	Filter type 3 for MEK (%)	Filter type 1 for limonene (%)
V-A and V-B	4.8	4.1	4.6	6.7
V-C	62.5	20.1	240.7	6.5
V-D and V-E	12.2	14.3	42.1	6.7

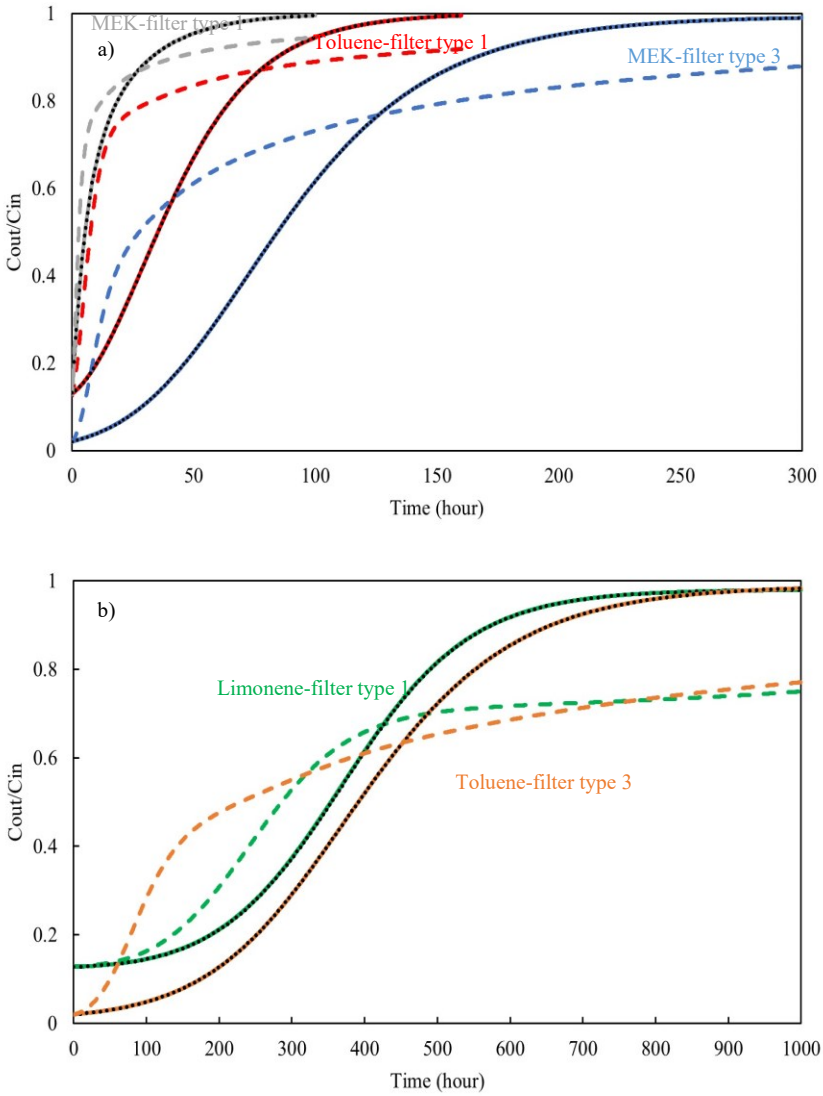

Fig. 5.7: Comparing model predictions for models V-A (dots), V-B (solid lines) and V-C (dashed lines). a) MEK-filter type 1 and 3 and Toluene-filter type 1 and b) Toluene and Limonene-filter type 3.

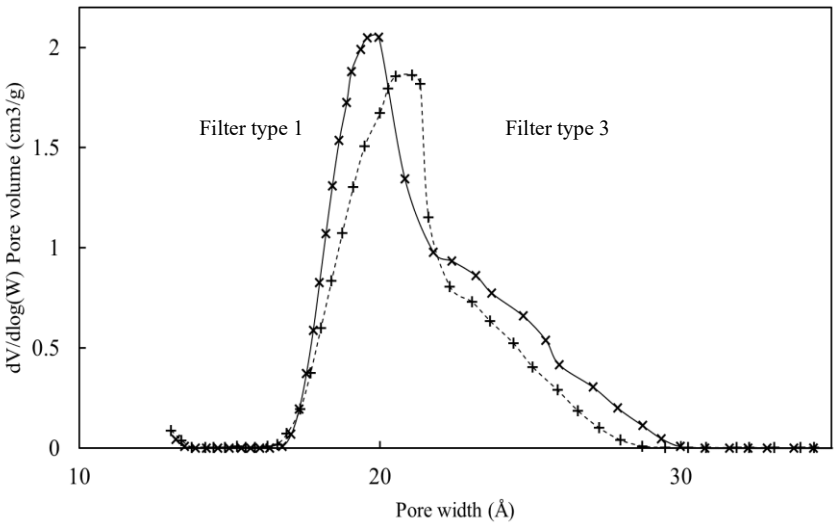

Fig. 5.8: Pore volume distribution over pore diameter of the granular activated carbons.

5.3.3.3.2 External mass transfer

The transport of pollutants from the mainstream toward the exterior surface of the adsorbent granule is the external (boundary layer) mass transfer. This mass transfer resistance is sequential with two internal resistances (see Fig. 5.6). The boundary-layer-controlled diffusion model (BLCDM) is used when the external mass transfer controls the process [16].

$$\rho_p \frac{\partial \bar{\bar{q}}}{\partial t} = \frac{3K_C(1-\varepsilon_b)}{R_p \varepsilon_b}(C - C^*) \tag{5.19}$$

The BLCDM model considers no resistance inside the granule, so the concentration inside the granule is only time-dependent. The relative importance of external mass transfer versus internal one was investigated, at the concentration of 0.1 ppm, through a comparison of the outcomes of the comprehensive model (Model V-A) and the BLCDM (Model V-D) used by Pei and Zhang [24] (see Fig. 5.9 and Table 5.3). Various behaviours are observed

for different systems of adsorbate and adsorbent. There is no significant deviation between the models' predictions for the adsorption of limonene and toluene through filter type 1 and type 3, respectively. The deviation increases for the adsorption of toluene through filter type 1, and the highest deviation is for the removal of MEK through filter types 1 and 3. This can be explained by the high adsorption affinity (the equilibrium ratio of the adsorbed-phase concentration to the gas-phase concentration) of limonene compared with toluene or toluene compared with MEK [133]. The high affinity results in a high ratio of mass transfer through the adsorbed phase (surface diffusion) to the external mass transfer. Consequently, the mass transfer is mainly controlled by external mass transfer. However, surface diffusion plays a more important role in the mass transfer for MEK, which is a polar compound with the lowest affinity toward activated carbon compared with toluene and limonene. Also, as mentioned, the deviation for the removal of toluene from filter type 1 is higher than its removal by filter type 3. The reason is that filter type 3 has a higher number of pores with a size of less than 13.08 Å (narrow micropores). The adsorption energy (or affinity) for the adsorption of toluene by these pores, which can be in the range of toluene diameters, is high because of the increased overlap in potential between the pore walls [134].

The Bi_{s0} number, which is the ratio of resistance in surface diffusion to boundary layer mass transfer resistance, is used to show the effect of each mass transfer step on the adsorption of VOCs.

$$Bi_{s0} = \frac{St}{Ed_s} = \frac{K_C R_p}{\varepsilon_p D_{s0} D_g} \tag{5.20}$$

The values of Bi_{s0} at the concentration of 0.1 ppm, are 1.41, 0.60, 0.55, 3.73, and 1.62 for toluene-filter type 1, toluene-filter type 3, limonene-filter type 1, MEK-filter type 1, and

MEK-filter type 3, respectively. This shows that external mass transfer is more important for the adsorption of toluene through filter type 3 and limonene through filter type 1 than other adsorbate-adsorbent systems. Therefore, the conclusion made by Pei and Zhang [24], which assumed the external mass transfer as a rate-limiting step, cannot be generalized to all adsorbate-adsorbent systems.

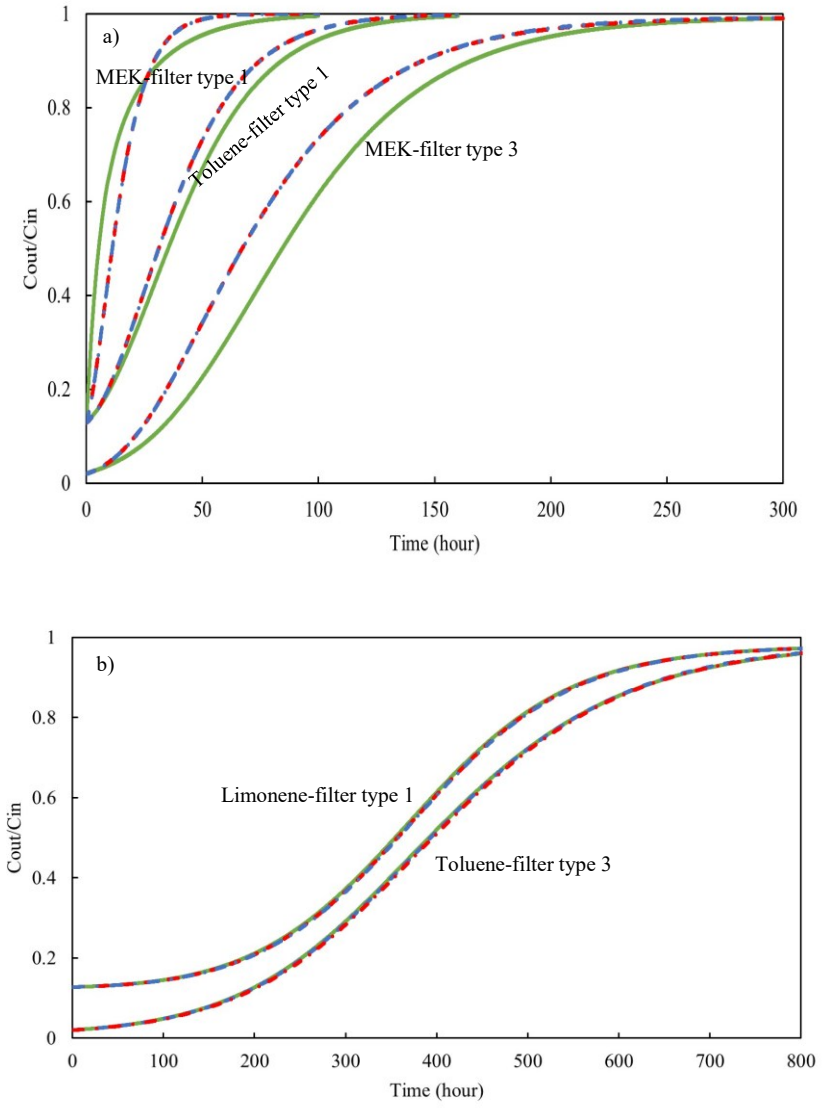

Fig. 5.9: Comparing model predictions for Models V-A (solid green lines), V-D (dashed blue lines), and V-E (dashed red lines) at the concentration of 0.1 ppm. a) MEK-filter type 1 and 2 and Toluene-filter type 1 and b) Toluene and Limonene-filter type 3.

5.3.3.3.3 Surface diffusivity variation

The comprehensive model considers concentration dependency of surface diffusivity using Darken model (Eq. (3.38)). To investigate the importance of changing surface diffusion coefficient by load, the comprehensive model (Model V-A) was compared with PSDM with constant surface diffusivity (Model V-E) [31]:

$$\varepsilon_p \frac{\partial C_p}{\partial t} + \rho_p \frac{\partial q}{\partial t} = \varepsilon_p D_p \left(\frac{\partial^2 C_p}{\partial r^2} + \frac{2}{r} \frac{\partial C_p}{\partial r} \right) + \rho_p D_s \left(\frac{\partial^2 q}{\partial r^2} + \frac{2}{r} \frac{\partial q}{\partial r} \right) \tag{5.21}$$

Model V-E uses identical initial and boundary conditions as Model V-A. Also, the unknown parameter of Model V-E (D_s) was measured by fitting the model into experimental data at the same concentrations that were used for the comprehensive model. Fig. 5.9 compares Models V-A, V-D, and V-E predictions for VOCs removal with different filters at the concentration of 0.1 ppm. The results of Model V-E are quite similar to Model V-D. It means that applying surface diffusivity measured by fitting the model to experimental data at ppm level into lower concentrations (ppb range) results in the overestimation of surface diffusion. Consequently, the adsorption is wrongly interpreted as being only limited by external mass transfers.

Vizhemehr et al. [19] used a model similar to Model V-E using surface diffusivity values from the literature. Also, the Langmuir isotherm, which gave the best fit to their experimental data at concentrations ranging from 15 to 300 ppm, was used in their dynamic modelling. There was a significant deviation between their experimental results and model predictions. Besides the unreliable value of surface diffusivity, the proper fitting of Langmuir isotherm to experimental data at a certain range of concentration for a specific adsorbent does not imply its applicability to other concentration ranges [35]. Therefore, the

Langmuir isotherm may fail to represent the adsorption data for lower concentrations. It is worth mentioning that because of the highly microporous structure of activated carbon fibres, there is great potential for the applicability of the proposed model using D-R isotherm to fibrous filters. However, different correlations may be required to measure the external mass transfer and axial dispersion coefficients for activated carbon fibres than those utilized in this study.

5.3.4 Sensitivity analysis

The sensitivity analysis was performed to show how various non-dimensional numbers influence the system. These numbers represent various physical designs and operating parameters. The analysis provides information on the performance of the filter on different scales. Several runs were performed by varying Pe, St, Ed_p, Ed_s, and D_g values to determine the impact of specific model parameters on the filter performance. It is worth mentioning that there is a limit to changing each non-dimensional number for given values of other numbers. This is because there is an implicit relation between them [135].

5.3.4.1 Effect of Peclet number

The Pe number is the ratio of convection to dispersion. Increasing the Pe number value decreases the importance of axial dispersion. Fig. 5.10 depicts the dimensionless 50% breakthrough time ($\bar{t}_{50\%}$) versus the Pe number at different Ed_s and D_g numbers. The figure illustrates the importance of axial dispersion at Pe numbers less than 100, where by increasing Pe, the removal efficiency of the filter increases. In other words, the $\bar{t}_{50\%}$ increases as the Pe number increases. Therefore, the presence of axial dispersion reduces filter usefulness [32]. The figure also shows that for Ed_s numbers less than 1, the 50% breakthrough time is highly sensitive to the Ed_s number. This confirms the importance of

surface diffusion in the mass transfer process over that range of Ed_s. In addition, the figure demonstrates that as the distribution parameters (affinities) increase, the filter's performance improves.

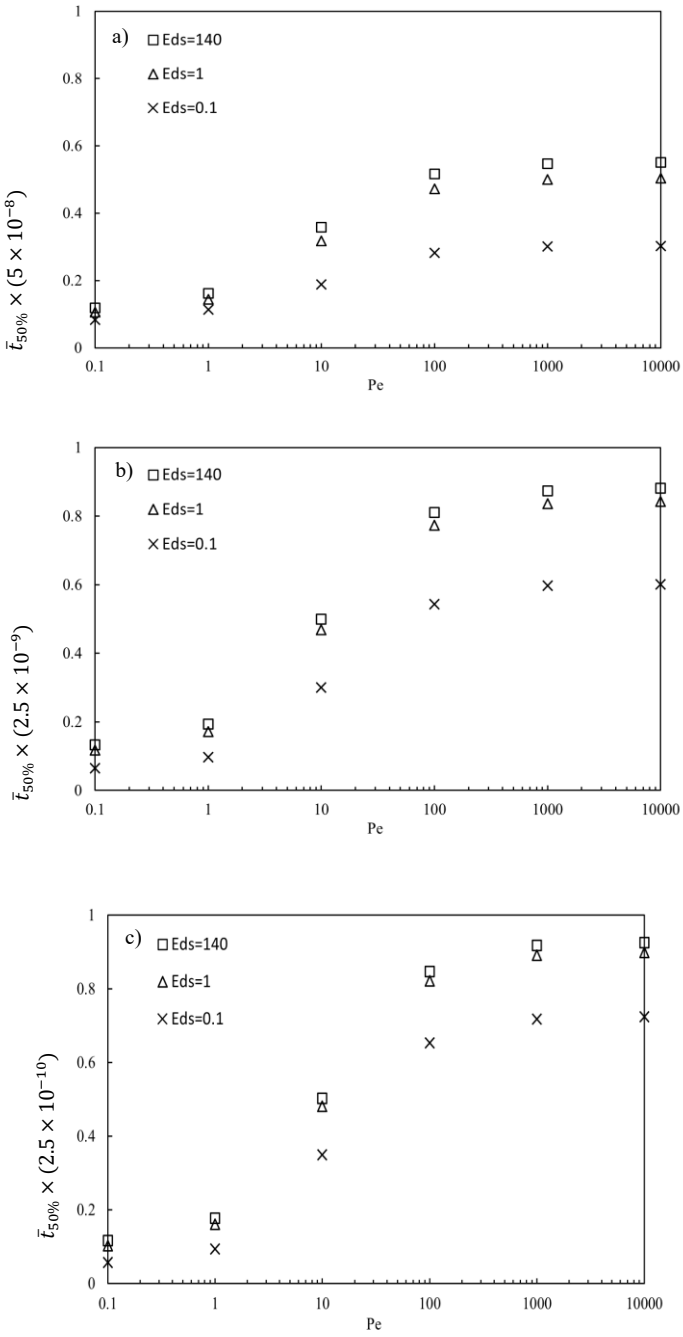

Fig. 5.10: Effect of Pe number on the removal performance at various Ed_s number (St=8, $Ed_p = 0.01$, and $\varphi = 0.5$). a) $D_g = 5 \times 10^6$, b) $D_g = 10^8$, and c) $D_g = 10^9$.

5.3.4.2 Effect of Stanton number

The Stanton (St) number measures the external mass transport rate into the mass transport by convection. Fig. 5.11 shows the effect of the St number on the filter performance at Ed_s of 0.1 and 140 at various values of D_g. For $Ed_s = 0.1$, only the beginning of the removal process is sensitive to the St number. The reason is that adsorption mainly happens on the particles' external surface at the early stage of the removal process; therefore, the external transfer becomes important [24]. However, at the $Ed_s = 140$, by changing the St number the whole parts of the breakthrough curve change except the final part, which is mostly limited by the adsorption capacity of the adsorbent [27].

5.3.4.3 Effect of Diffusion Modulus

The diffusion modulus (Ed_p and Ed_s) represents the ratio of the internal mass transfer to convection. Fig. 5.12 exhibits how the performance of the filter changes by changing Ed_p at various values of Ed_s and D_g. When the Ed_s is equal to 140, there is no difference in the breakthrough curves of the filter at different values of Ed_p. Therefore, the transfer of VOCs within the adsorbent particles is mainly controlled with surface diffusion. The figure shows that the importance of gas-phase diffusion increases by decreasing the value of Ed_s. It can be seen that at $Ed_s = 0.1$, the efficiency of the filter changes continuously by changing the amount of Ed_p number. This can happen for activated carbon particles with pore sizes bigger than tested granules.

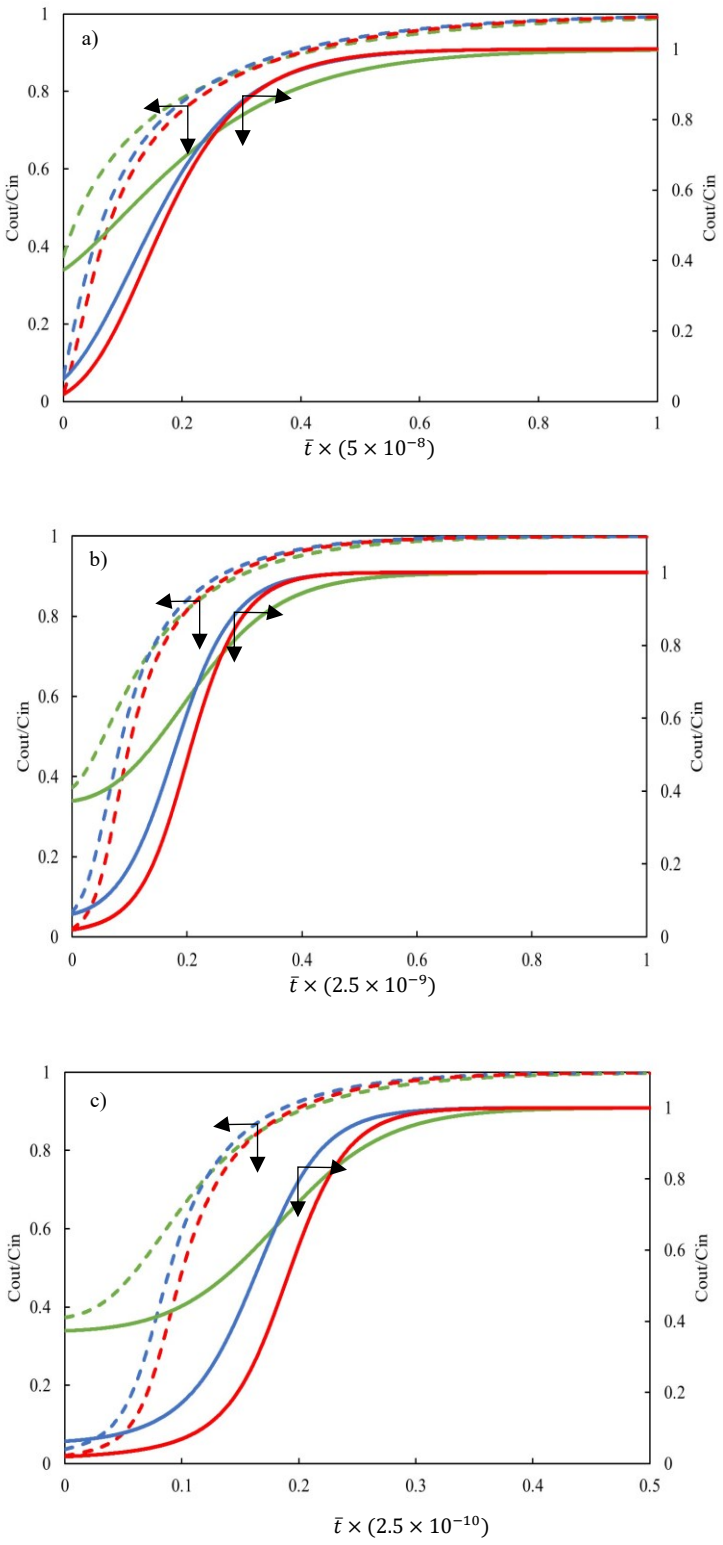

Fig. 5.11: Effect of St number on the removal performance (Pe=1, $Ed_p = 0.01$, and $\varphi = 0.5$) (solid lines: $Ed_s = 140$, dashed lines: $Ed_s = 0.1$, green lines: St=1, blue lines: St=5, and red lines: St=10). a) $D_g = 5 \times 10^6$, b) $D_g = 10^8$, and c) $D_g = 10^9$.

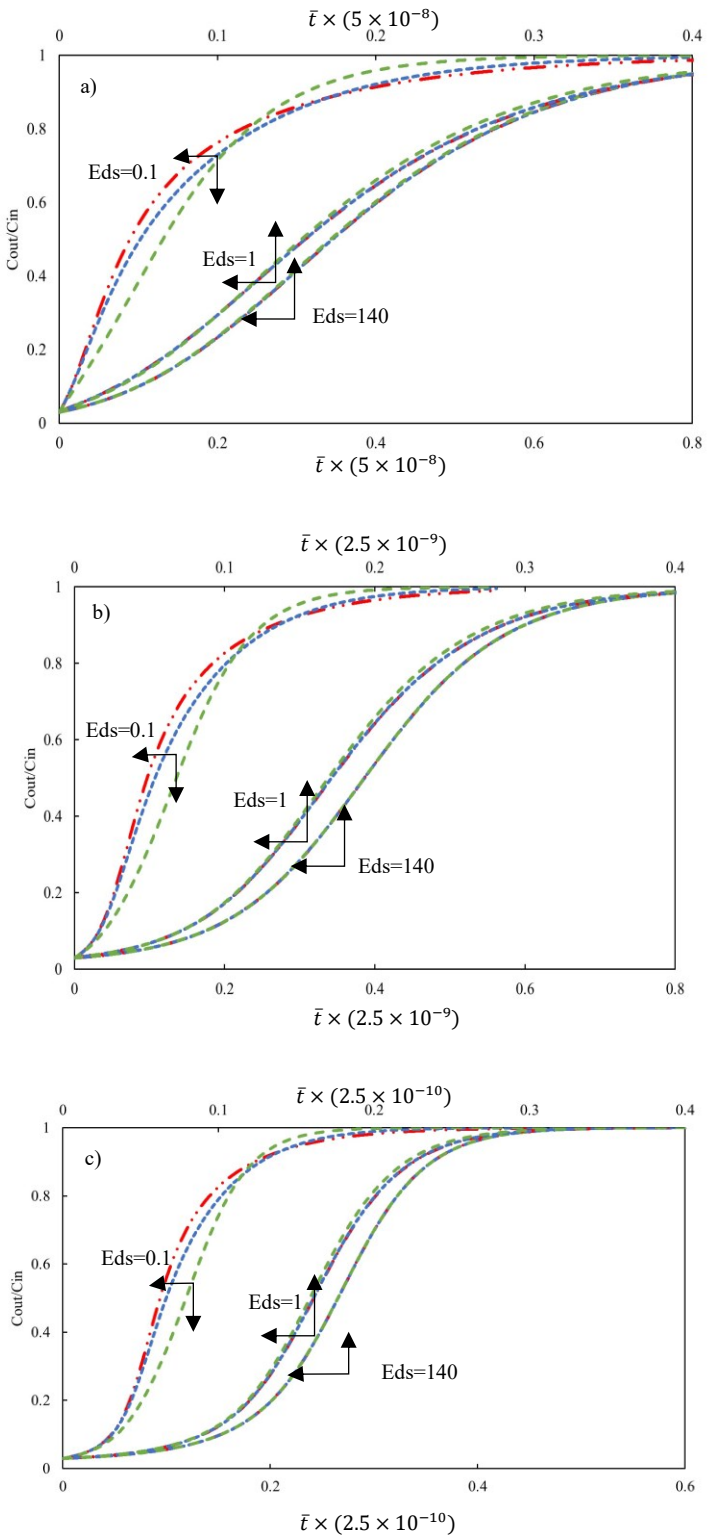

Fig. 5.12: Effect of Ed_p number on the removal performance at various Ed_s numbers (Pe=1, $St = 8$, and $\varphi = 0.5$) (green lines: $Ed_p = 1$, blue lines: $Ed_p = 0.1$, and red lines: $Ed_p = 0.01$). a) $D_g = 5 \times 10^6$, b) $D_g = 10^8$, and c) $D_g = 10^9$.

5.4 Summary

This chapter aimed to validate a dynamic model for predicting carbon-based filters' service life for removing VOCs at ppb concentration levels. The model considered axially dispersed plug flow to transfer pollutants within the adsorbent bed. The transport of pollutants from bulk to the internal adsorption sites was modelled by the external mass transfer in sequential with two internal mass transfers. The D-R isotherm was employed to represent the adsorption equilibrium. Also, the Darken model was applied to the D-R isotherm to show the concentration dependency of surface diffusivity.

The developed model with the model parameters measured at concentrations ranging from 9 to 90 ppm and a flow rate of 30 l/min could correctly predict the filter's performance at lower concentrations (5 ppm, 1 ppm, and 0.1 ppm) for all adsorbate-adsorbent systems. The model also showed accurate prediction for the filter efficiency at a higher flow rate (60 l/min).

The comparison between the PSDM and HSDM with variable surface diffusivity and PDM showed that the surface diffusion rate is quite faster than the gas-phase diffusion rate for the studied adsorbents. Also, the comparison between the comprehensive model and BLCDM revealed that the surface diffusion rate was comparable with the external mass transfer rate at ppb level concentration for the removal of MEK through filter type 1 and 3 and toluene through filter type 1 in opposite to removal of limonene by filter type 1 and toluene by filter type 3, so they should be considered for the dynamic modelling of adsorbent filters. Finally, the importance of surface diffusivity variation with concentration was determined using the Darken model in PSDM with variable surface diffusivity and comparing it to PSDM.

The non-dimensional analysis indicated that for Pe number less than 100, by decreasing the axial dispersion, the performance of the filters increases. Moreover, it revealed that for Ed_s less than 1, the adsorption process was mainly controlled with surface diffusion for the highly microporous adsorbents. However, at larger pore sizes, the gas-phase diffusion appeared to be effective for internal mass transfer. Also, the sensitivity analysis on the St number exhibited the importance of external mass transfer on the initial parts of breakthrough curves, even at low internal mass transfer rates.

6 Dynamic Modelling of Removal of Binary Mixtures of VOCs from Indoor Air through a Carbon-based Filter[1]

Indoor environments, in reality, comprise a variety of VOCs. Consequently, relying on a single component as a challenge gas leads to unreliable estimations of the service life of filters. To examine the impact of VOC mixtures on the performance of carbon filters, two critical characteristics to consider are adsorption competition and displacement phenomena. The equilibrium behaviour of adsorption, as illustrated by adsorption isotherms, is the most significant property that can vary significantly from single- to multi-component adsorption [22]. The prediction of filter efficiency in removing mixtures of VOCs has been achieved through the development of numerous mathematical models [22,33,62,64,68,69,136–139]; however, limited studies have been carried out at low indoor concentrations.

Safari et al. [62] modelled the removal of a binary mixture of VOCs (hexane and MEK) through a granular activated carbon filter in ppm concentration ranges. However, there was a significant discrepancy between the model prediction and experimental data, mainly because the extended Langmuir model was used as a multi-component adsorption isotherm. Popescu et al. [22] also developed a model for predicting the performance of granular activated carbon in removing a mixture of VOCs (ethanol, acetaldehyde, acetone,

[1] Mohamad Ghamangiz Khararoodi, Jiping Zhu, Chang-Seo Lee, Jianjun Niu, and Fariborz Haghighat. "Dynamic modelling of removal of binary mixtures of VOCs from indoor air through a carbon-based filter." Chemical Engineering Journal (2023): 144792.

toluene, cyclohexane, and 1,1,1,2-Tetrafluoroethane) with concentrations slightly above their indoor levels. Although valuable, there existed a difference between the model and experiment results for some compounds in the mixture. Similar to the work of Safari et al. [62], one probable reason for this observation was their use of the extended Langmuir model. The extended Langmuir model considers full competition between adsorbates for all active sites, a feature which is not accurate for most adsorbates and adsorbent systems. To address this issue, Tefera et al. [64] employed the extended Jain and Snoeyink's Langmuir-like isotherm to describe multi-component (n-butanol, n-butyl acetate, 2-heptanone, 2-butoxyethanol, n-decane, 1,2,4-trimethylbenzene, indane, and 2,2-dimethylpropylbenzene) adsorption equilibria at around 62.5 ppm for each compound. This isotherm supposes that the quantity of active sites available for adsorption in the absence of competition is proportionate to the difference between the maximum adsorption capacities of the compounds [63]. While the modelling outcomes agreed with the experiment results, the error was observed to be considerably high for the VOCs with lower molecular weights. The probable reason is that, similar to the extended Langmuir model, the extended Jain and Snoeyink's Langmuir-like isotherm does not consider the variation in interaction energies between mixed adsorbates [35]. Moreover, none of the proposed models have been validated for low indoor concentrations. The main limitation of applying the Langmuir-like isotherm for low indoor concentrations is that a satisfactory correlation between the experimental data and the isotherm model within a particular concentration range for a given adsorbent does not necessarily extend to other concentration ranges [35]. Therefore, it would be advantageous to explore alternative potential-based adsorption theories such as Dubinin-Astakhov (D-A) or D-R isotherms [71]. This chapter shows the

applicability of the developed model (Eqs. (3.3) to (3.6), Eqs. (3.33) to (3.38), Eqs. (5.10) to (5.13), and the D-Y isotherm model) for binary mixtures of VOCs.

6.1 Methodology

Filter type 1 and two binary mixtures (toluene and limonene; and toluene and MEK) were utilized as an adsorbent and adsorbates, respectively. The proposed model was evaluated using experimental data from mixture tests at different concentrations. A modified isotherm model (iterative method) was presented for showing the equilibrium behaviour of non-ideal mixtures (MEK and toluene). Comparative modelling was conducted to assess the importance of gas-phase diffusion. Also, the importance of Fick's diffusion was investigated by comparing the predictions of the proposed model with those of two other models which use approximate solutions (linear and quadratic driving force models) for intraparticle mass transfer. Finally, a parametric study was performed to evaluate the effect of some operational and design parameters on filter efficiency.

6.2 Results and discussion

6.2.1 Model validation

For verification of the proposed model (Model VVA-1), that integrates Eqs. (3.3) to (3.6), Eqs. (3.33) to (3.38), and Eqs. (5.10) to (5.13)), and the D-Y isotherm, first, the simulation results were compared with the experimental data at various concentrations for different binary mixtures. Then, an improved model (Model VVA-2) was proposed based on the corrected isotherm constants. Furthermore, an investigation was conducted to assess gas-phase diffusion. Finally, the importance of using Fickian diffusion within the particles was investigated by comparing the results of the proposed model with those of two other

models, which use approximate solutions of Fickian diffusion for intraparticle mass transfer. It is worth mentioning that Eqs. (3.3) to (3.6) were employed in all predictive models for interparticle mass transfer.

6.2.1.1 Comparison with experimental data

To validate the model's prediction, simulation results were compared to the results of experiments conducted in the setup complying with ISO standard 10121-1 (see Fig. 3.1) at two different concentrations (9 and 0.1 ppm). Fig. 6.1-a to Fig. 6.1-d exhibit that the model can estimate the breakthrough curve of the toluene and limonene binary mixture correctly. However, in the case of the toluene and MEK mixture, the model overestimates the filter performance for both concentrations. The probable reason is the use of the D-Y model for extending the adsorption isotherm model. Although the D-Y model considers the reduction in maximum available pore volume, it does not consider lateral interactions among the adsorbed molecules (the values of $K_{DR,i}$ are assumed to be constant) [140]. This can be applied correctly to the ideal mixture or a mixture quite close to the ideal one. Ideal mixtures can occur between two highly similar adsorbates or, in other words, between molecules with similar intermolecular forces. Contrary to limonene, MEK is a polar compound, forming a non-ideal mixture with toluene. For a non-ideal mixture, the lateral interactions between adsorbate species significantly differ from the self-interaction; therefore, the lateral interactions must be considered [35]. Since the adsorbed molecules repel each other, negative lateral interactions occur between them, leading to weaker binding and looser packing [141]. This can lead to a reduction in the adsorption. Therefore, using the D-Y model for non-ideal mixtures can result in an overestimation of filter performance. Also, it is expected that as the number of adsorbates increases, the

interactions between them become more significant (likelihood of lateral interactions between the adsorbate species increases) [142], leading to more pronounced deviations from ideality (higher overestimation).

The figures illustrate that the filter exhibits the highest performance to remove limonene, with a 50% breakthrough occurring after 1.78 hours at a concentration of 9 ppm, while it takes 0.80 hours for toluene in the toluene-limonene mixture. Furthermore, the efficiency of the filter to remove toluene is demonstrated to be superior to that of the removal of MEK in a mixture of the two compounds. The observed phenomenon can be attributed to the surface characteristics of the activated carbon and the physical characteristics of adsorbates [71]. The non-polar character of the activated carbon surface leads to a higher affinity for adsorbing non-polar volatile organic compounds, such as limonene and toluene, rather than polar compounds, such as MEK [128]. Additionally, the induced dipole-induced dipole attraction (London dispersion force) between activated carbons and volatile organic compounds varies, with limonene exhibiting the highest level of attraction and MEK the lowest [71].

The performance of the filter for the removal of each compound is lower in the binary mixtures compared with that of single compound tests, which is because of the competition phenomenon and the higher load of total contaminants. The absence of the overshoot phenomenon indicates that the thickness of the filter is less than the critical thickness, beyond which the displaced compound adds to the peak height, and its concentration reaches higher than the inlet concentration [143].

Moreover, the model is evaluated using the experimental data of Safari et al [62] conducted in a small-scale setup complying with the ASHRAE Standard 145.1 [46]. The experiments involved passing a mixture of n-hexane and MEK with a concentration of 100 ppm through a glass cylinder filled with 25 grams of granular activated carbon at a face velocity of 0.25 m/s. The diameter and length of adsorbent particles were 2.5 mm and 6 mm, respectively. The adsorption isotherm parameters are presented in Table 6.1. Fig. 6.1-e shows that although there are slight deviations between the model and experimental data, possibly due to differences in intermolecular forces among adsorbates, as stated earlier, model VVA-1 is still able to predict the overall trend.

Table 6.1: D-R isotherm parameters for different VOCs (Safari et al. [62]).

Parameters	n-hexane	MEK
$K_{DR} \times 10^9$	2.92	3.02
q_{max}	486.88	299.71

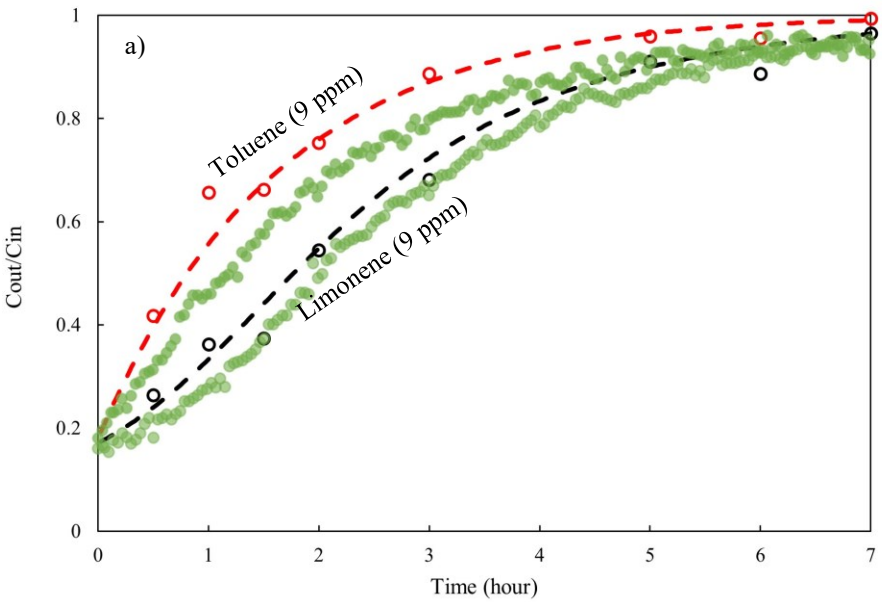

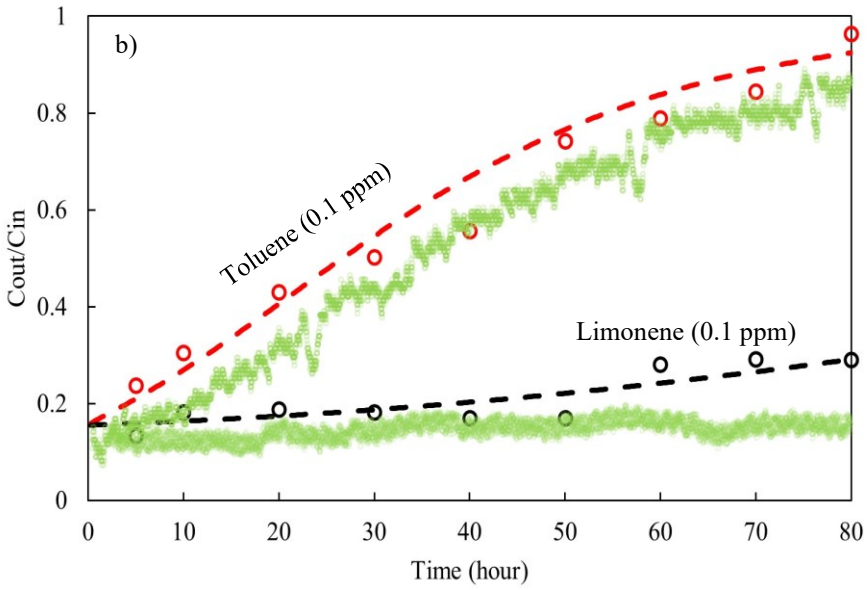
b)
Toluene (0.1 ppm)
Limonene (0.1 ppm)
Cout/Cin
Time (hour)
0
0.2
0.4
0.6
0.8
1
0
10
20
30
40
50
60
70
80

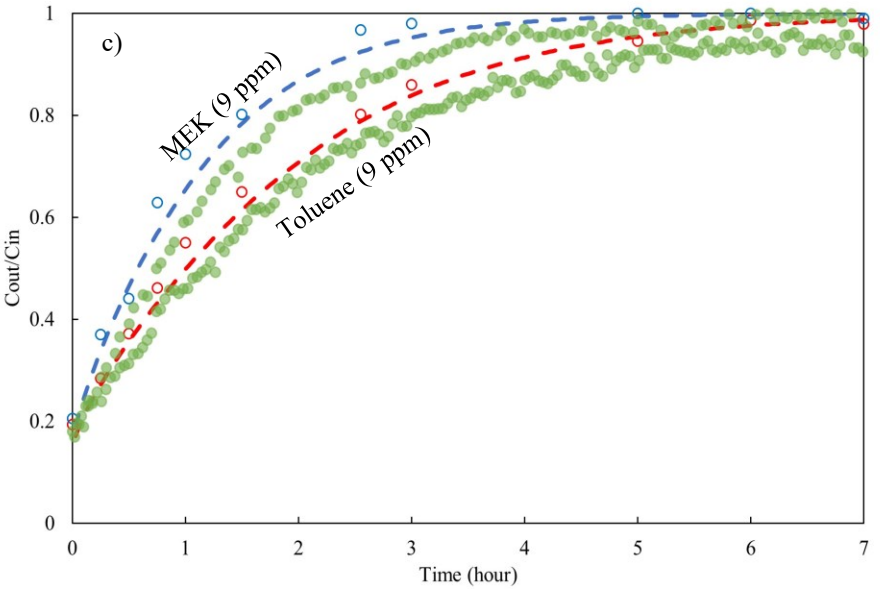
c)
MEK (9 ppm)
Toluene (9 ppm)
Cout/Cin
Time (hour)
0
0.2
0.4
0.6
0.8
1
0
1
2
3
4
5
6
7

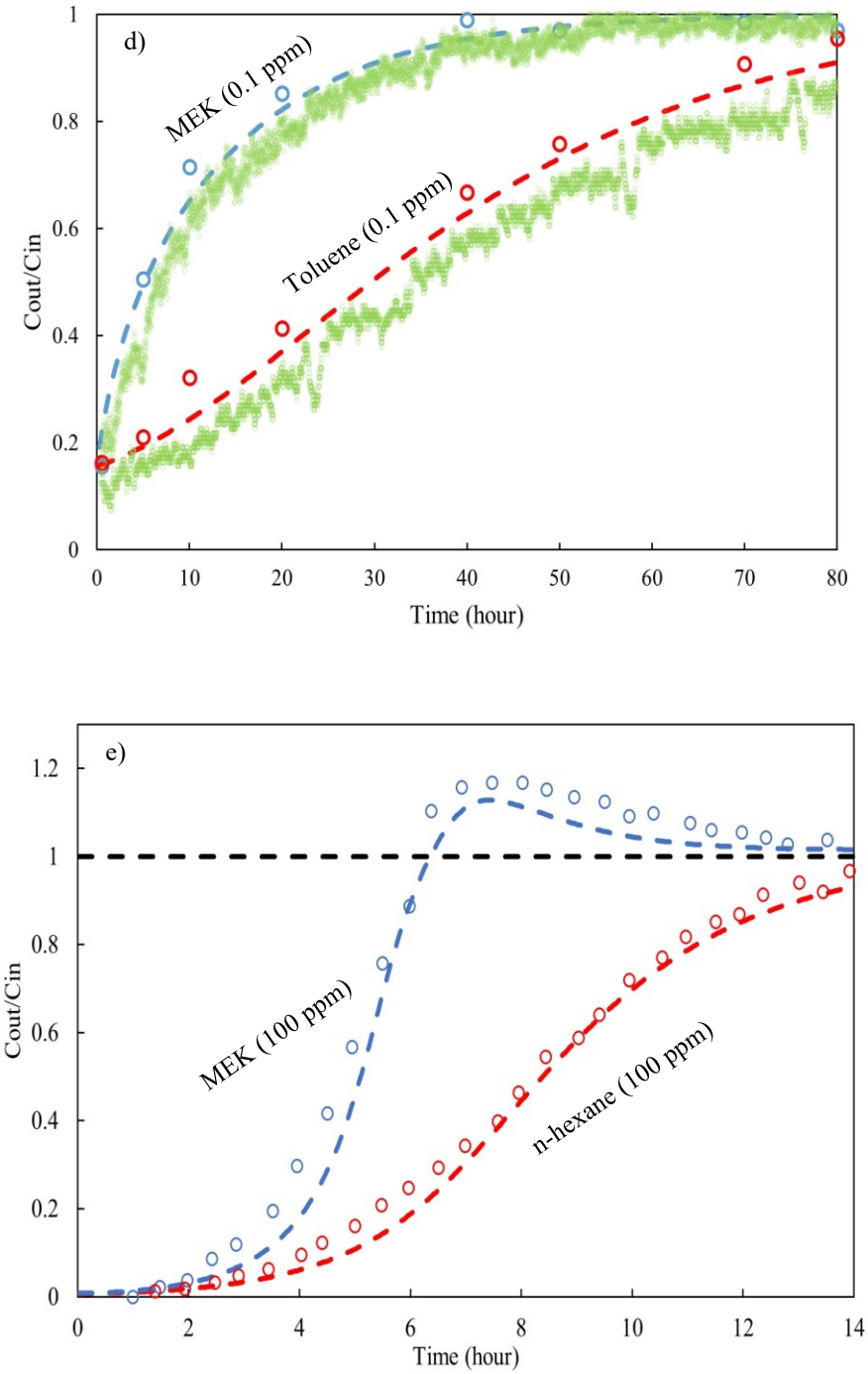

Fig. 6.1: Comparison of single experimental data (green dots) [71], binary experimental data (black, red, and blue dots) and predictions of Model VVA-1 for binary mixtures (lines) on breakthrough curves of filters. a) toluene-limonene (9 ppm), b) toluene-limonene (0.1 ppm), c) toluene-MEK (9 ppm), d) toluene-MEK (0.1 ppm), and e) n-hexane-MEK (100 ppm).

6.2.1.2 Comparison with iterative adsorption models

The D-Y model is a non-iterative method which uses single compound adsorption data. An iterative method should be utilized to apply the lateral interactions among the adsorbed molecules. Applying these models requires experimental data from mixture tests. The values of $K_{DR,i}$ were determined by fitting the proposed model to the experimental results at 9 ppm. The fitted values were used to predict the filter performance for removing binary mixtures at 0.1 ppm concentration. Fig. 6.2 depicts the relevant results for binary mixtures of toluene and MEK, and Table 6.2 lists $K_{DR,i}$ and R^2. Compared to the initial D-R isotherm parameter (see Table 5.1) the values of K_{DR} increase for both compounds; this is due to the lateral interactions between the adsorbed MEK and toluene molecules.

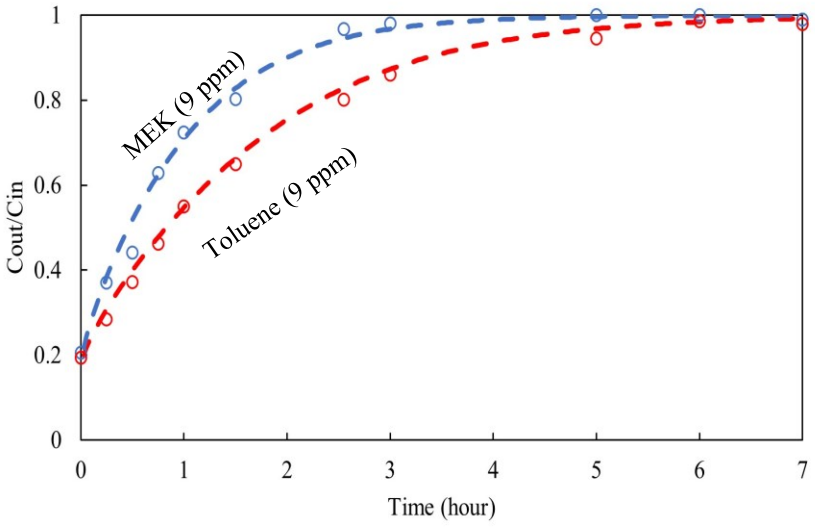

Fig. 6.2: A representation of the experimental results (dots) and fitted models (lines) at 9 ppm for the mixture of toluene and MEK.

Table 6.2: The values of $K_{DR,i}$, and R^2 for the mixture of toluene and MEK.

Parameters	Toluene	MEK
$K_{DR} \times 10^9$	3.61	3.91
R^2	0.9942	

The predictions made by Models VVA-1 and VVA-2 employing non-iterative and iterative isotherms, respectively, were compared with the experimental data at 0.1 ppm for the mixture of toluene and MEK (see Fig. 6.3). It shows the simulation results are improved by correcting the amounts of $K_{DR,i}$. As stated earlier, estimation of the iterative isotherm parameters requires experimental data from mixture tests, which is a challenging and costly procedure. Therefore, developing and using a new method that uses single-component test results to show the mixture's equilibrium behaviour is suggested for future research.

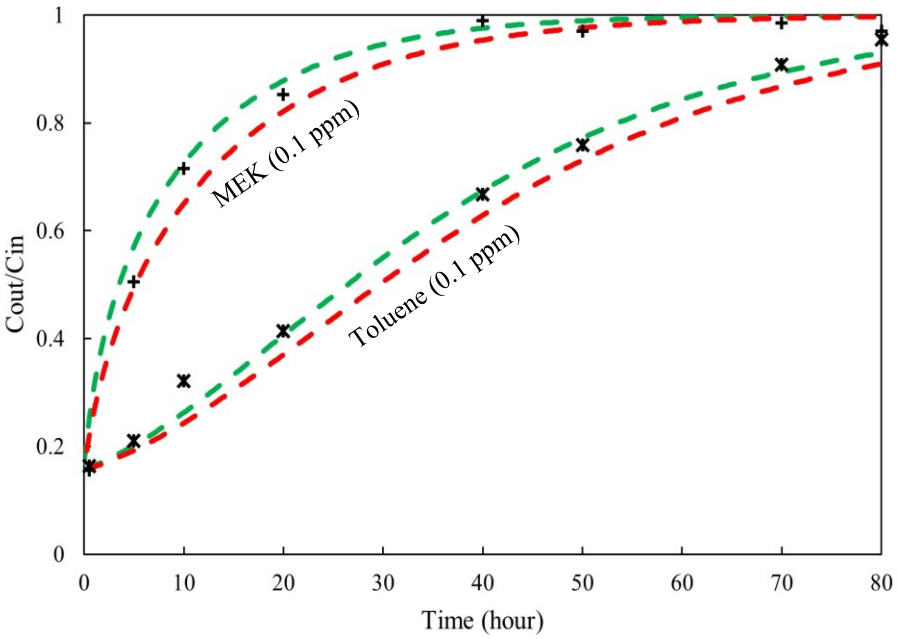

Fig. 6.3: Comparing model predictions and experimental results at 0.1 ppm for the mixture of toluene and MEK: A graphical representation of Model VVA-1 (red lines), Model VVA-2 (green lines), and experiments (dots).

6.2.1.3 Effect of gas-phase diffusion

It was shown that the gas-phase diffusion contribution is insignificant compared with the surface diffusion for the removal of the single-component systems of toluene, limonene,

and MEK in chapter 5. However, as mentioned, the equilibrium behaviour of the gaseous mixture is different from that of the single-component system. Therefore, the surface diffusion flux, which is significantly affected by the adsorption equilibrium, changes. Consequently, the gas-phase diffusion may be comparable with the surface diffusion for multi-component adsorption, even when the gas-phase diffusion is insignificant for single-component adsorption. For investigating the importance of gas-phase diffusion, Model VVA which uses HSDM with varying surface diffusivity for intraparticle mass transfer was compared with VVB and VVC which use the PSDM with varying surface diffusivity (Eqs. (3.17) to (3.20)) and the PDM (Eqs. (5.14) to (5.17)), respectively.

Fig. 6.4 compares the predictions made by Models VVA-1, VVB-1 (non-iterative), and VVC-1 (non-iterative) for the mixture of toluene and limonene and Models VVA-2, VVB-2 (iterative), and VVC-2 (iterative) for the mixture of toluene and MEK. It shows that the PDSM (Models VVB-1 and VVB-2) has a similar prediction to the HSDM (Models VVA-1 and VVA-2), but the PDM (Models VVC-1 and VVC-2) cannot estimate the filter performance correctly. These results confirm that the gas-phase diffusion is negligible compared with the surface diffusion.

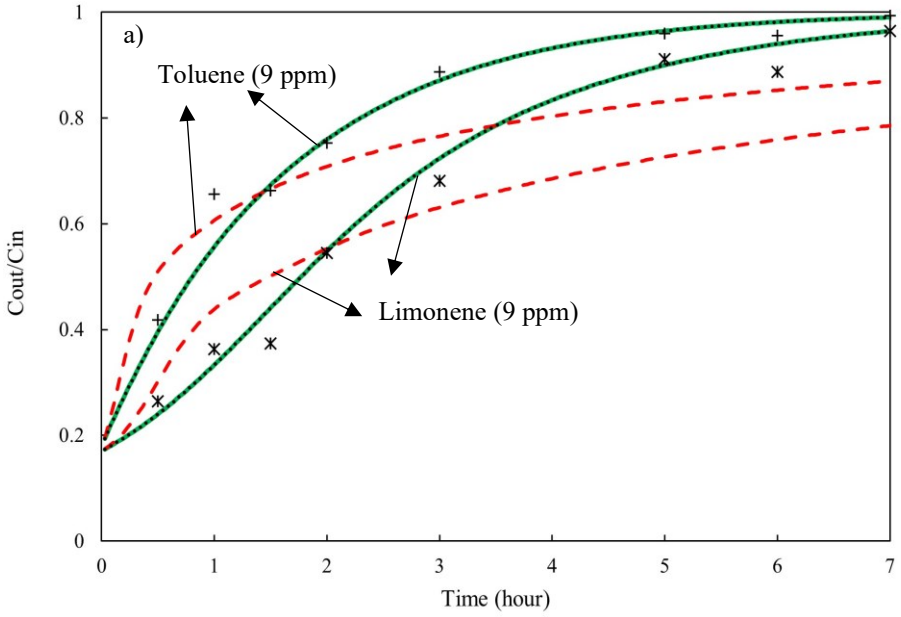
a)
Toluene (9 ppm)
Limonene (9 ppm)
Cout/Cin
Time (hour)
0
0.2
0.4
0.6
0.8
1
0
1
2
3
4
5
6
7

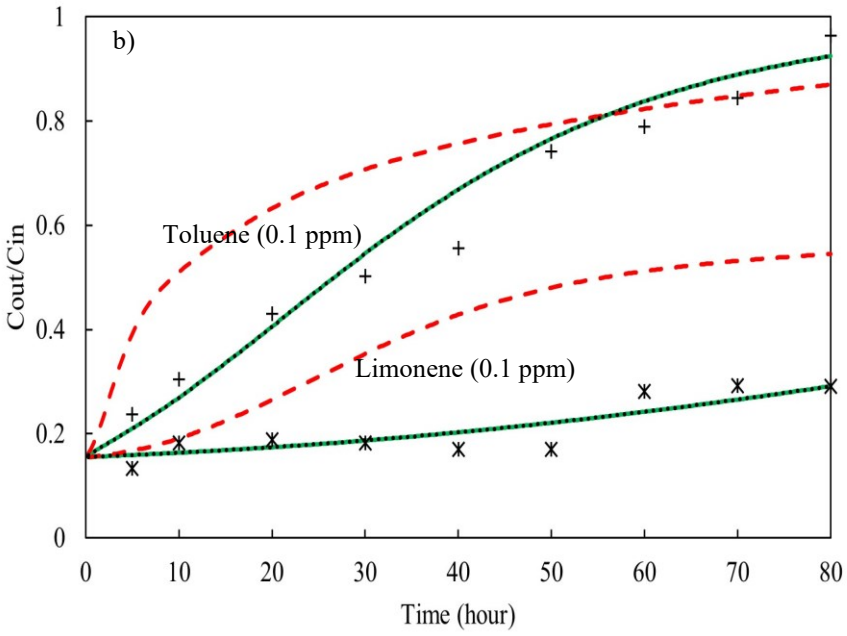
b)
Toluene (0.1 ppm)
Limonene (0.1 ppm)
Cout/Cin
Time (hour)
0
0.2
0.4
0.6
0.8
1
0
10
20
30
40
50
60
70
80

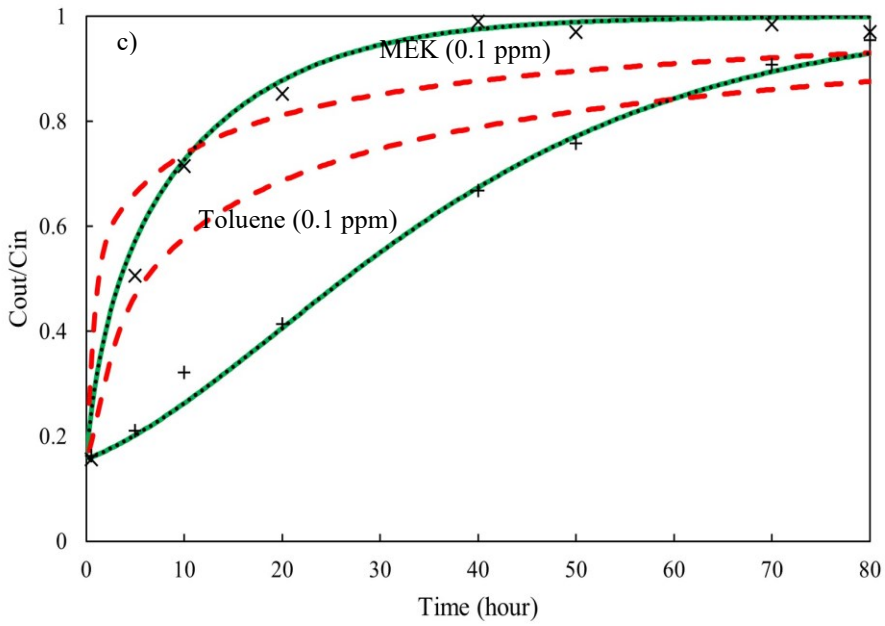

Fig. 6.4: Comparison of experimental data (dots) and model outcomes. a) A mixture of toluene and limonene (9 ppm) (models VVA-1 (green lines), VVB-1 (black dots), and VVC-1 (red lines)); b) A mixture of toluene and limonene (0.1 ppm) (models VVA-1 (green lines), VVB-1 (black dots), and VVC-1 (red lines)); and c) A mixture of toluene and MEK (0.1 ppm) (models VVA-2 (green lines), VVB-2 (black dots), and VVC-2 (red lines)).

6.2.1.4 Linear and quadratic driving force models versus diffusion models

The Fick's diffusion (FD) models described earlier are closer to reality, but they are computationally demanding. The LDF or Vermeulen model are approximate solutions of Fickian diffusion, which can reduce the computational time significantly, especially for a large number of adsorbates. The LDF model (Model VVD-1 for non-iterative and VVD-2 for iterative) considers a linear approximation for the internal mass transfer [35]:

$$\frac{\partial \bar{\bar{q}}_i}{\partial t} = k_{p,i}(q_i^* - \bar{\bar{q}}_i) \tag{6.1}$$

where q_i^* is the concentration at the particles' exterior surface. The values of $k_{p,i}$ contain the overall resistance to mass transfer within the particle. For a spherical particle, a theoretical correlation for $k_{p,i}$ was developed as [31]:

$$k_{p,i} = \frac{15 D_{e,i}}{R_p^2} \tag{6.2}$$

where effective intraparticle diffusivity ($D_{e,i}$) when the surface diffusion is the controlling mechanism is defined as [31]:

$$D_{e,i} = D_{s,i} \tag{6.3}$$

The Vermeulen model (Model VVE-1 for non-iterative and VVE-2 for iterative) is a quadratic driving force (QDF) approximation [35].

$$\frac{\partial \bar{\bar{q}}_i}{\partial t} = \frac{\pi^2 D_{e,i}}{R_p^2} \left(\frac{q_i^{*2} - \bar{\bar{q}}_i^{\,2}}{2\bar{\bar{q}}_i} \right) \tag{6.4}$$

For both the VVD-2 and VVE-2 models, the $K_{DR,i}$ values for toluene and MEK in their binary mixtures were determined at 9 ppm utilizing the iterative isotherm, as was the case with Model VVA-2. Fig. 6.5 compares the results of all models, and Table 6.3 shows the ARE.

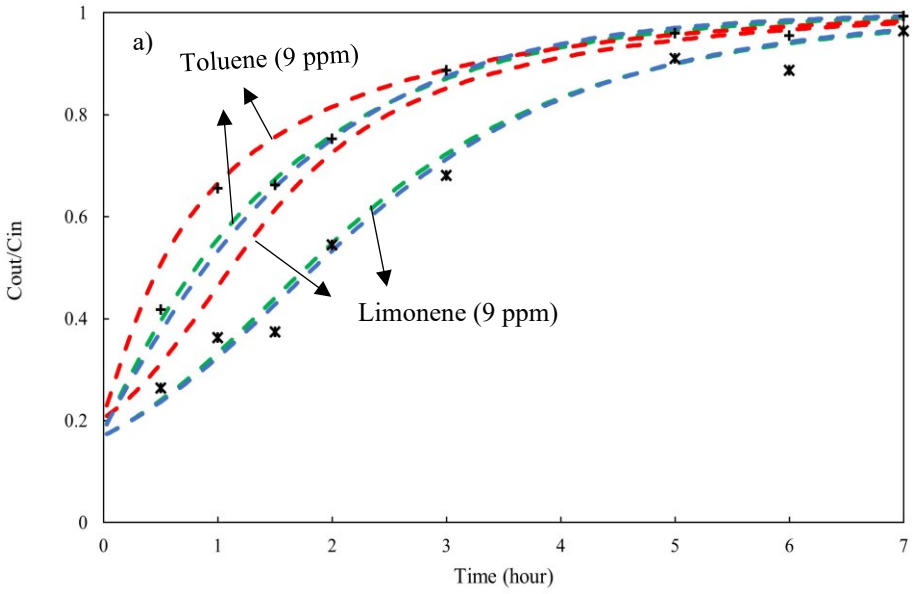
a)
Toluene (9 ppm)
Limonene (9 ppm)
Cout/Cin
Time (hour)
0
0.2
0.4
0.6
0.8
1
0
1
2
3
4
5
6
7

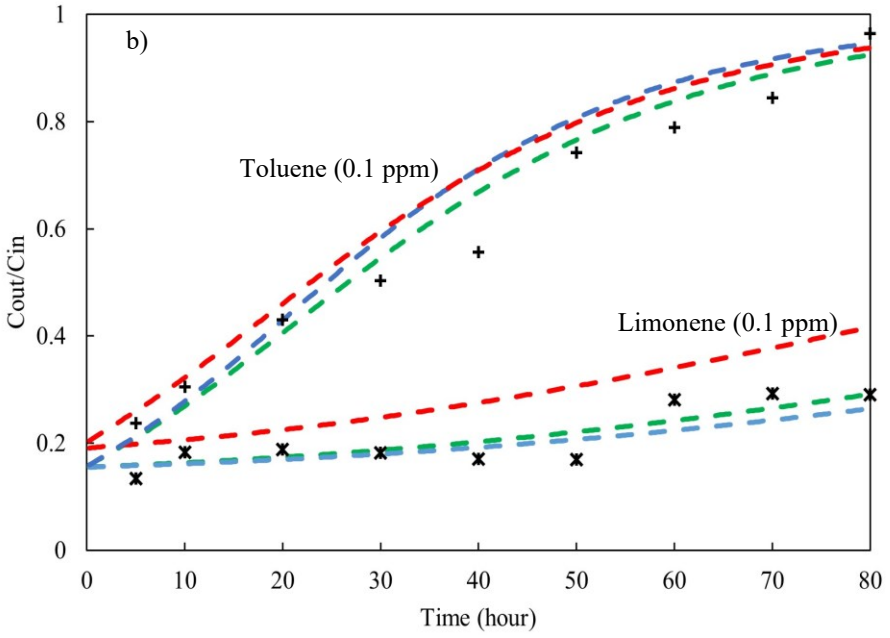
b)
Toluene (0.1 ppm)
Limonene (0.1 ppm)
Cout/Cin
Time (hour)
0
0.2
0.4
0.6
0.8
1
0
10
20
30
40
50
60
70
80

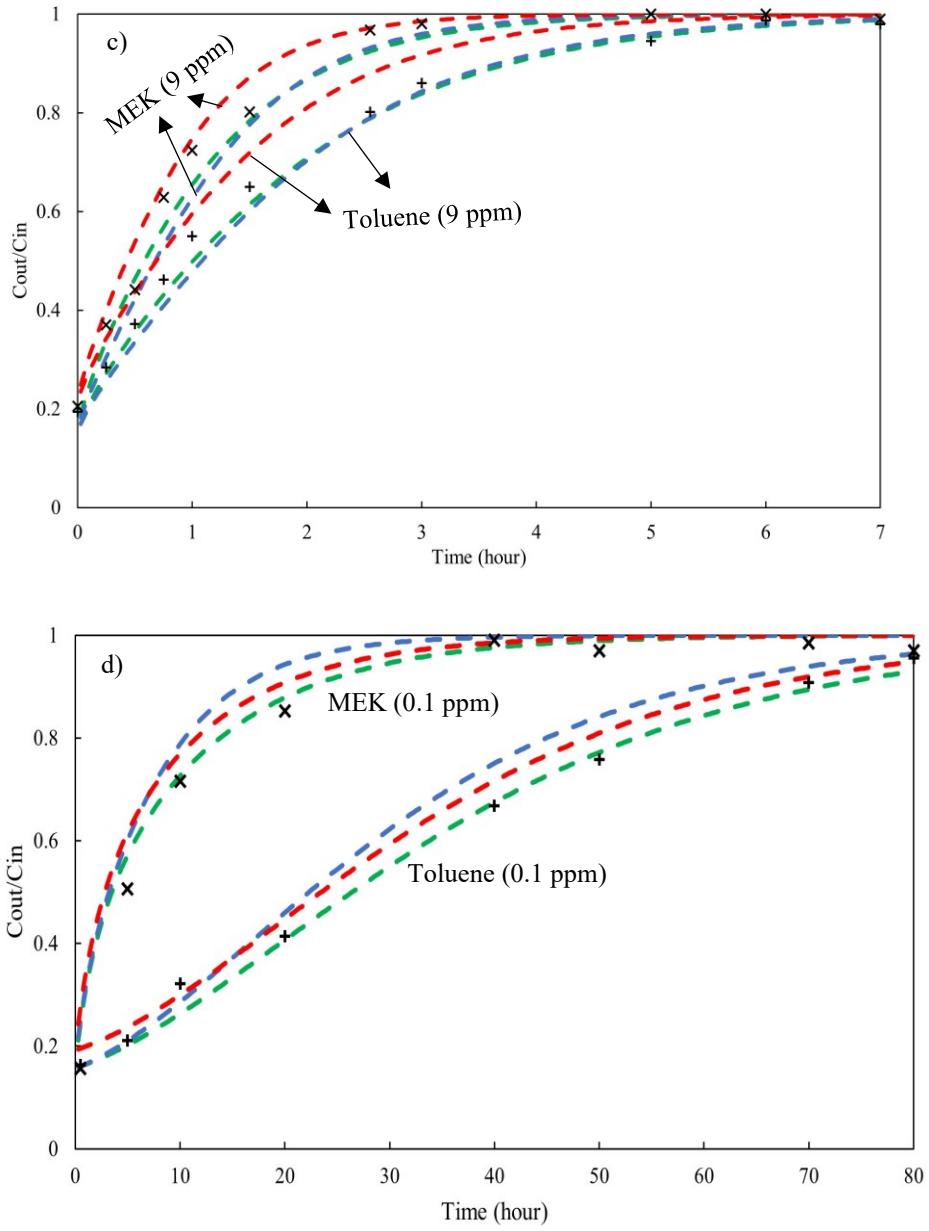

Fig. 6.5: Comparison of model outcomes for Models VVA (green lines), VVD (red lines), and VVE (blue lines) and experimental data. a) A mixture of toluene and limonene (9 ppm) (Models VVA-1, VVD-1, and VVE-1); b) A mixture of toluene and limonene (0.1 ppm) (Models VVA-1, VVD-1, and VVE-1); c) A mixture of toluene and MEK (9 ppm) (Models VVA-1, VVD-1, and VVE-1); and d) A mixture of toluene and MEK (0.1 ppm) (Models VVA-2, VVD-2, and VVE-2).

Table 6.3: Comparison of average relative errors for different models (%).

Models	Concentration (ppm)	Mixture of toluene and limonene		Mixture of toluene and MEK	
		Toluene	Limonene	Toluene	MEK
VVA-1	9	3.55	4.13	6.60	4.76
VVA-1	0.1	7.49	8.88	6.44	15.14
VVA-2	0.1	N/A	N/A	4.02	9.50
VVD-1	9	6.02	15.98	9.01	5.54
VVD-1	0.1	10.56	35.56	N/A	N/A
VVD-2	0.1	N/A	N/A	6.38	12.48
VVE-1	9	4.47	4.20	7.10	8.25
VVE-1	0.1	10.30	9.80	N/A	N/A
VVE-2	0.1	N/A	N/A	7.93	13.55

A detailed examination of the precision of various models reveals a complex interplay between multiple factors, including the type of VOC, the type of mixture, and the concentration. It is observed that the QDF model consistently demonstrates superior accuracy for limonene at upstream concentrations of both 9 and 0.1 ppm, as well as for toluene at the upstream concentration of 9 ppm. In contrast, for the specific case of MEK at the upstream concentrations of 0.1 ppm, the LDF approximation outperforms the QDF model. For the remaining cases, their accuracy is comparable. This variability in the performance of the two models can be attributed to the curvature of the adsorption isotherm (or equilibrium factor (β)). For the system without any initial pollutants within the adsorbent, the equilibrium factor is given by [130]:

$$\beta_i = \left(\frac{C_i}{C_{in,i} - C_i}\right)\left(\frac{q_{in,i} - q_i}{q_i}\right) \tag{6.5}$$

where $q_{in,i}$ is the concentration in the sorbed phase in equilibrium with C_{in}. When the equilibrium factor is lower than 0.5, between 0.5 and 1, and higher than 1, the isotherm is

highly favourable, moderately favourable, and unfavourable, respectively. Fig. 6.6 shows the value of β at different concentrations for various adsorbates. For example, for limonene at upstream concentrations of 9 ppm, the isotherm shows highly favourable behaviour. This is why the LDF model fails to estimate the filter efficiency in opposition to the QDF model. The QDF model was developed by assuming step-function changes in concentration [35]. Therefore, it is appropriate for a very steep isotherm. On the other hand, the LDF considers a diffuse front, which happens for unfavourable and moderately favourable isotherms [35]. Also, the high deviation of the LDF model for limonene compared with toluene from the FD model can be explained by the magnitude of β, which is because of the high affinity of limonene towards activated carbon. Additionally, increasing the values of β by decreasing the upstream concentration indicates the probable applicability of the LDF model for internal mass transfer in Henry's law region [35]. These results highlight the importance of considering the specific characteristics of the adsorption isotherm in the selection and application of appropriate models for a given scenario.

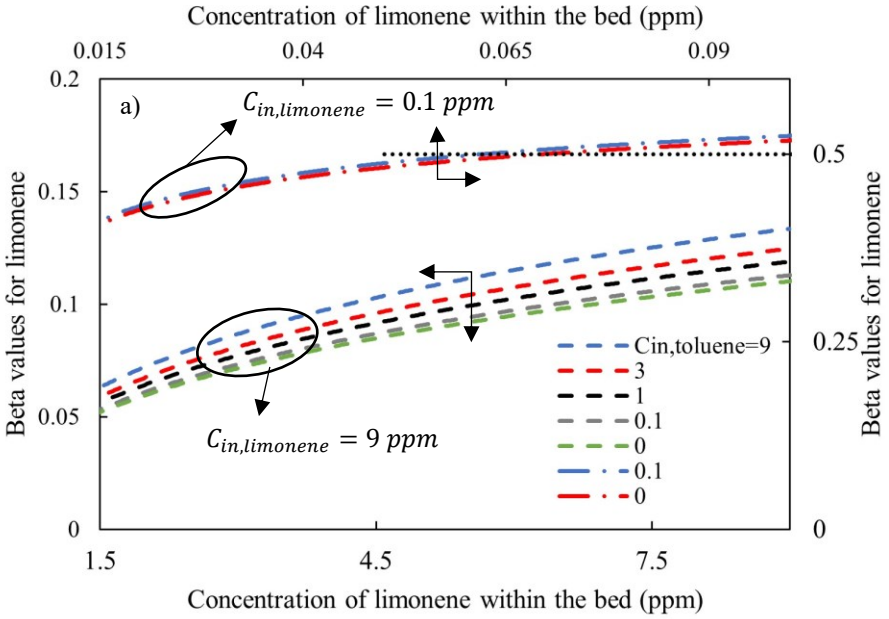
Concentration of limonene within the bed (ppm)
0.015
0.04
0.065
0.09
a)
$C_{in,limonene} = 0.1\ ppm$
$C_{in,limonene} = 9\ ppm$
Beta values for limonene
Beta values for limonene
0.2
0.15
0.1
0.05
0
0.5
0.25
0
1.5
4.5
7.5
Concentration of limonene within the bed (ppm)
Cin,toluene=9
3
1
0.1
0
0.1
0

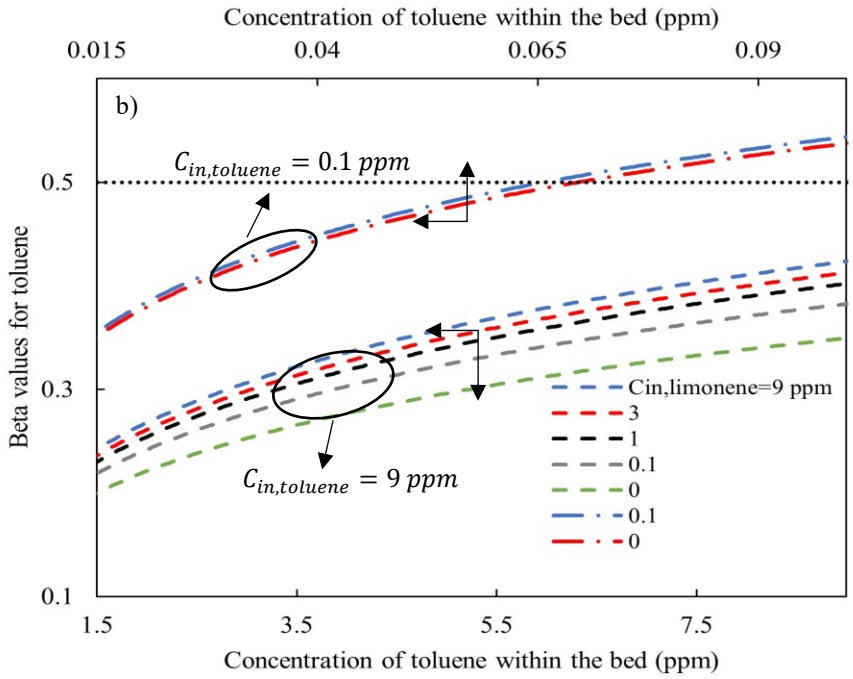
Concentration of toluene within the bed (ppm)
0.015
0.04
0.065
0.09
b)
$C_{in,toluene} = 0.1\ ppm$
$C_{in,toluene} = 9\ ppm$
Beta values for toluene
0.5
0.3
0.1
1.5
3.5
5.5
7.5
Concentration of toluene within the bed (ppm)
Cin,limonene=9 ppm
3
1
0.1
0
0.1
0

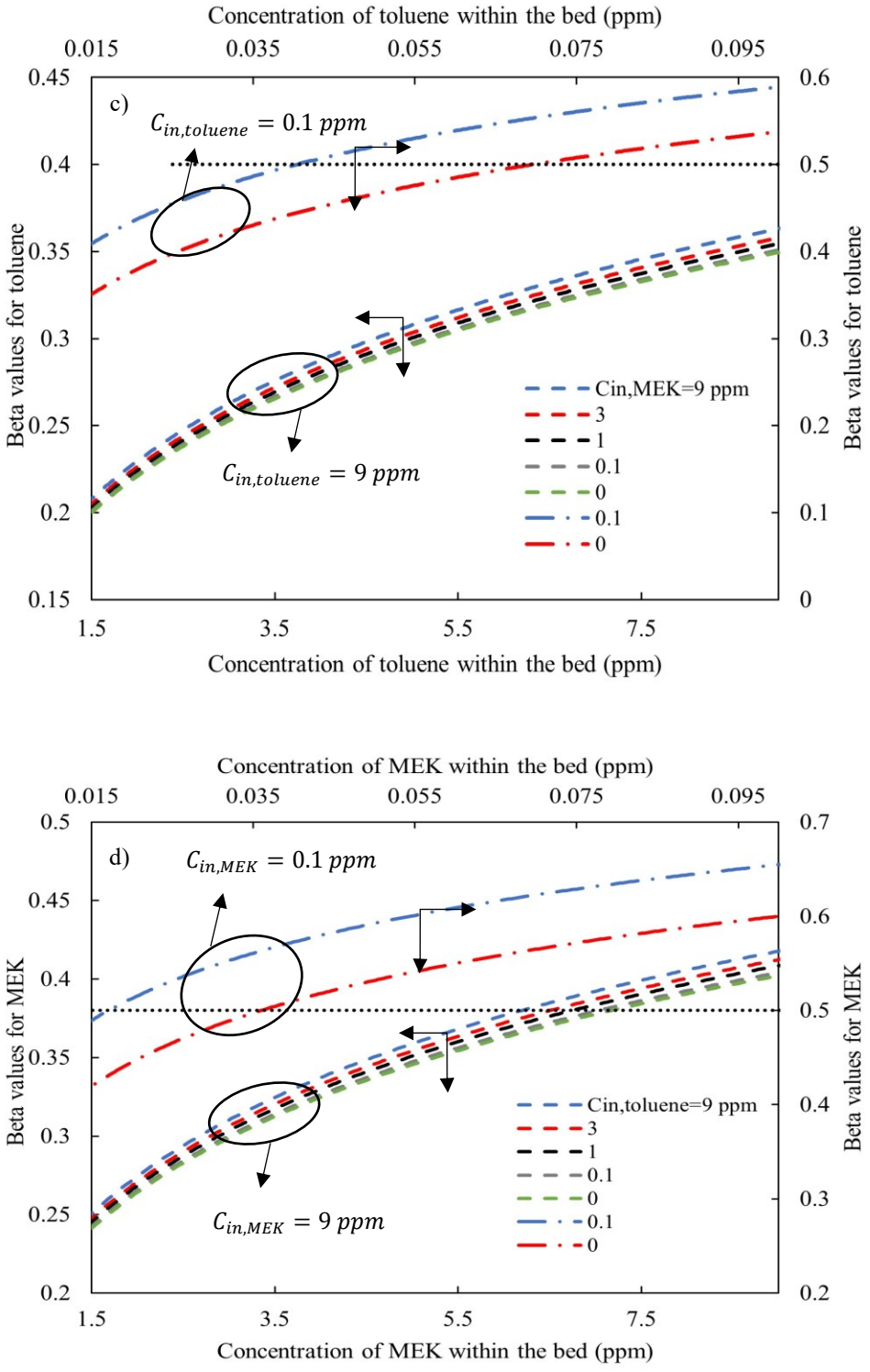

Fig. 6.6: A representation of the change in β values at different concentrations for various adsorbates. a) limonene in the mixture of toluene and limonene; b) toluene in the mixture of toluene and limonene; c) toluene in the mixture of toluene and MEK; and d) MEK in the mixture of toluene and MEK. The axes are shown by arrows.

6.2.2 Parametric study

After verifying Model VVA, a parametric analysis was performed to examine the impact of changing design and operational parameters on the filter's breakthrough curve. This work examined the effect of air velocity, inlet concentration, particle size, and filter thickness on the breakthrough curves using model VVA-1 for the toluene and limonene mixture, and model VVA-2 for the toluene and MEK mixture. For this purpose, all parameters aside from the one being analyzed were kept constant.

6.2.2.1 Air velocity

One of the most important factors affecting the efficiency of the adsorptive filter is air velocity. The study of velocity was performed at three face velocities of 0.05 m/s, 0.1 m/s, and 0.2 m/s. Fig. 6.7 shows that an increase in air velocity is associated with a decrease in filter performance. For instance, after 100 hours, the filter efficiencies are around 75 % and 45 % for limonene when the air velocity was 0.05 m/s and 0.1 m/s, respectively. As mentioned, the air velocity affects the performance of the adsorptive filter mainly in two ways: 1) change in the residence time, and 2) change in the external mass transfer [144]. A higher air velocity means a lower residence time, resulting in less time for pollutants to reach the adsorption sites [24,145]. However, by increasing the air velocity, the external mass transfer coefficient increases. Fig. 6.8 shows the impact of the external mass transfer coefficient on the performance of the filter. The values of the external mass transfer coefficient were measured using the Wakao and Funazkri correlation (Eq. (3.34)) at face velocities of 0.05, 0.1, and 0.2 m/s. By increasing the external mass transfer coefficient, the initial breakthrough and the saturation time decrease (steeper breakthrough curve), which is because of decreases in the external mass transfer resistance [112]. Comparing

Fig. 6.7 and Fig. 6.8 confirms that the filter performance is more sensitive to residence time than the external mass transfer.

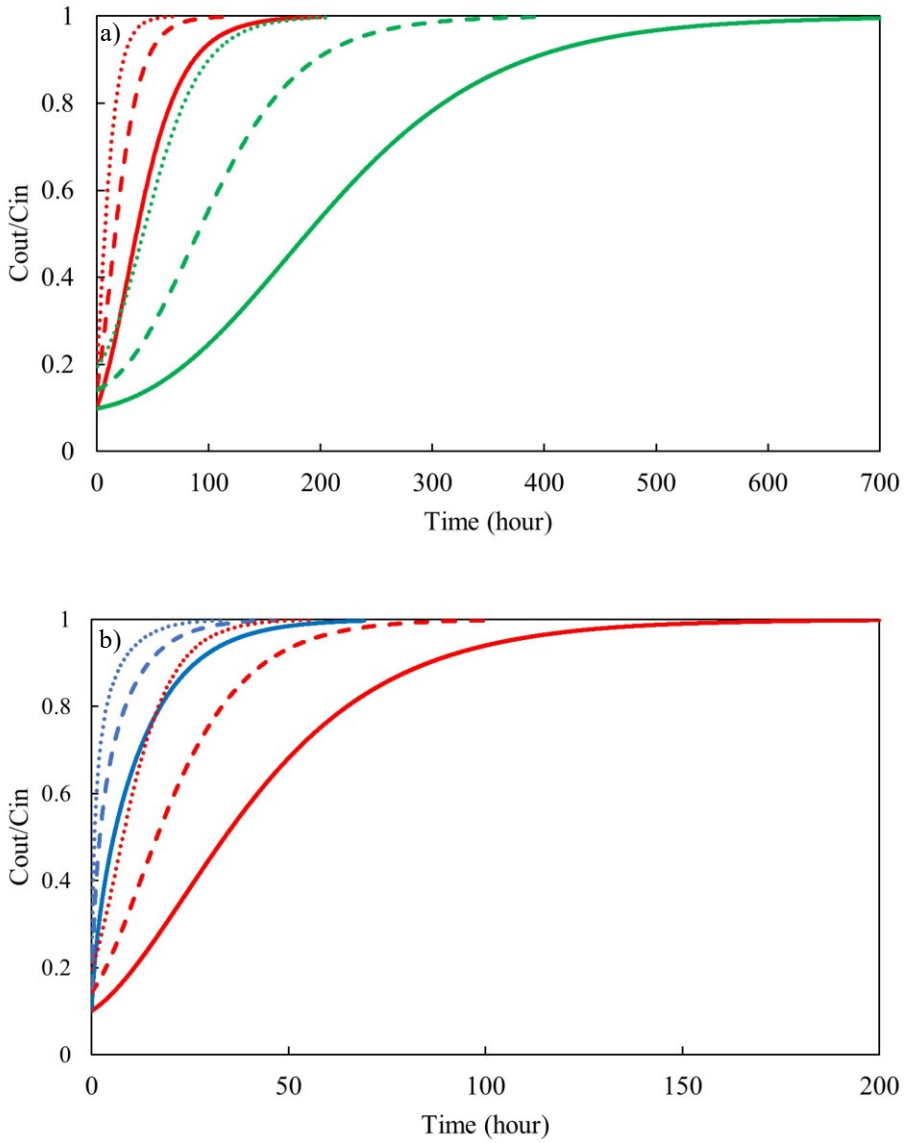

Fig. 6.7: Effect of changing air velocity on filter performance (concentration=0.1 ppm, filter thickness=1 mm, and particle size=0.5 mm) (green lines: limonene, red lines: toluene, blue lines: MEK, solid lines: 0.05 m/s, dashed lines: 0.1 m/s, and dots: 0.2 m/s). a) A mixture of toluene and limonene; b) A mixture of toluene and MEK.

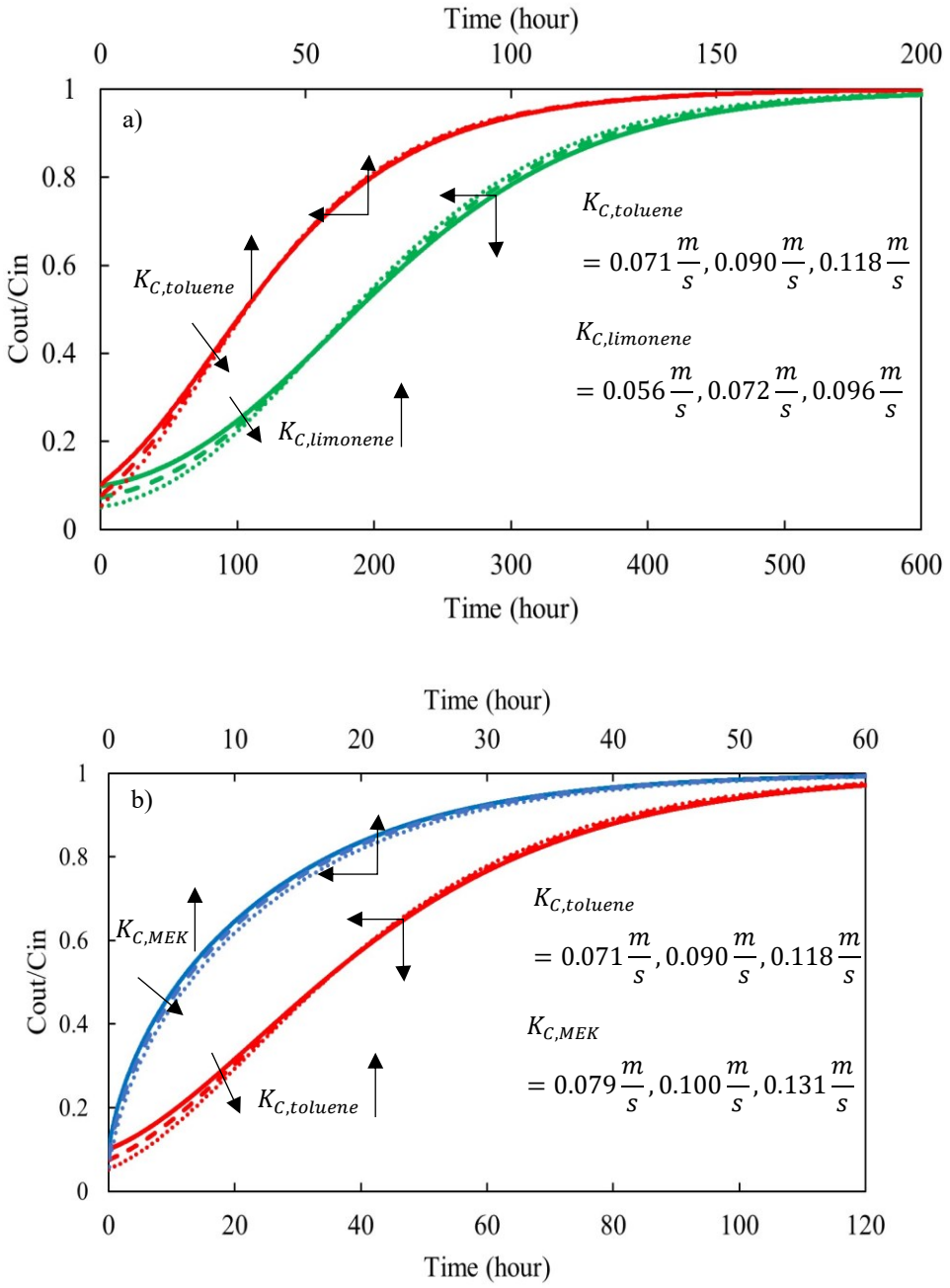

Fig. 6.8: Impact of changing external mass transfer coefficient on filter performance when the residence time was kept constant (concentration=0.1 ppm, filter thickness=1 mm, and particle size=0.5 mm) (green lines: limonene, red lines: toluene, blue lines: MEK). a) A mixture of toluene and limonene; b) A mixture of toluene and MEK.

6.2.2.2 Inlet concentration

Depending on the ventilation conditions, and the kind and quantity of pollution sources, the indoor concentration of VOC varies with time and location. Fig. 6.9 shows the breakthrough curves at various concentrations for two binary mixtures. At higher inlet concentrations, breakthrough curves are steeper, and the breakthrough times are lower because of the increased concentration gradient [111]. For example, for toluene in the toluene and limonene mixture, the 50% breakthrough time decreases from 50 hours to 35 hours when the concentration increases from 0.05 ppm to 0.1 ppm.

6.2.3 Particle size

The size of the adsorbent particles is a critical factor that can strongly influence the adsorption process. The size of the particles was varied from 0.5 to 0.7 mm while maintaining all other parameters constant, even the porosity of the bed. In practice, this can be achieved by changing the number of particles in the bed. Fig. 6.10 illustrates that as the particle diameter increases, the breakthrough curve becomes wider, and the initial breakthrough and saturation times also increase. For instance, for toluene in the toluene and MEK mixture, the initial breakthroughs for the filter at the particle sizes of 0.5, 0.6, and 0.7 mm are approximately 10, 14, and 17 %, respectively. Increasing particle size can affect both the external and internal mass transfer. With larger particle diameters, there is an increased distance for molecules to diffuse within the adsorbent particles (a higher diffusion path) [145]. Also, an increase in the diameter of particles results in a reduction of the external mass transfer [38]. This can be attributed to the consequent increase in boundary layer thickness that occurs as the particle diameter increases [38]. However, it is

worth mentioning that smaller particles can be more difficult to handle and have a higher pressure drop, which can affect the overall design of the adsorption system.

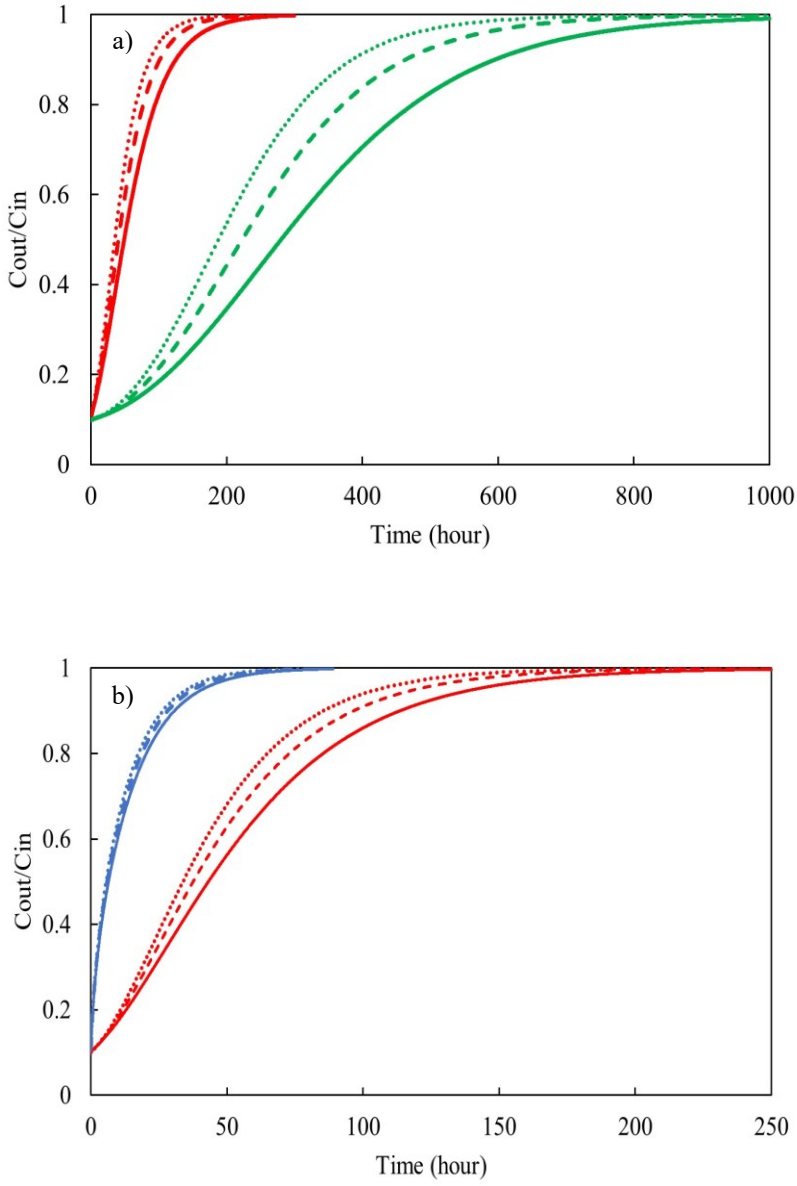

Fig. 6.9: Impact of inlet concentration on filter performance (face velocity =0.05 m/s, filter thickness=1 mm, and particle size=0.5 mm) (green lines: limonene, red lines: toluene, blue lines: MEK, solid lines: 0.05 ppm, dashed lines: 0.075 ppm, and dots: 0.1 ppm). a) A mixture of toluene and limonene; b) A mixture of toluene and MEK.

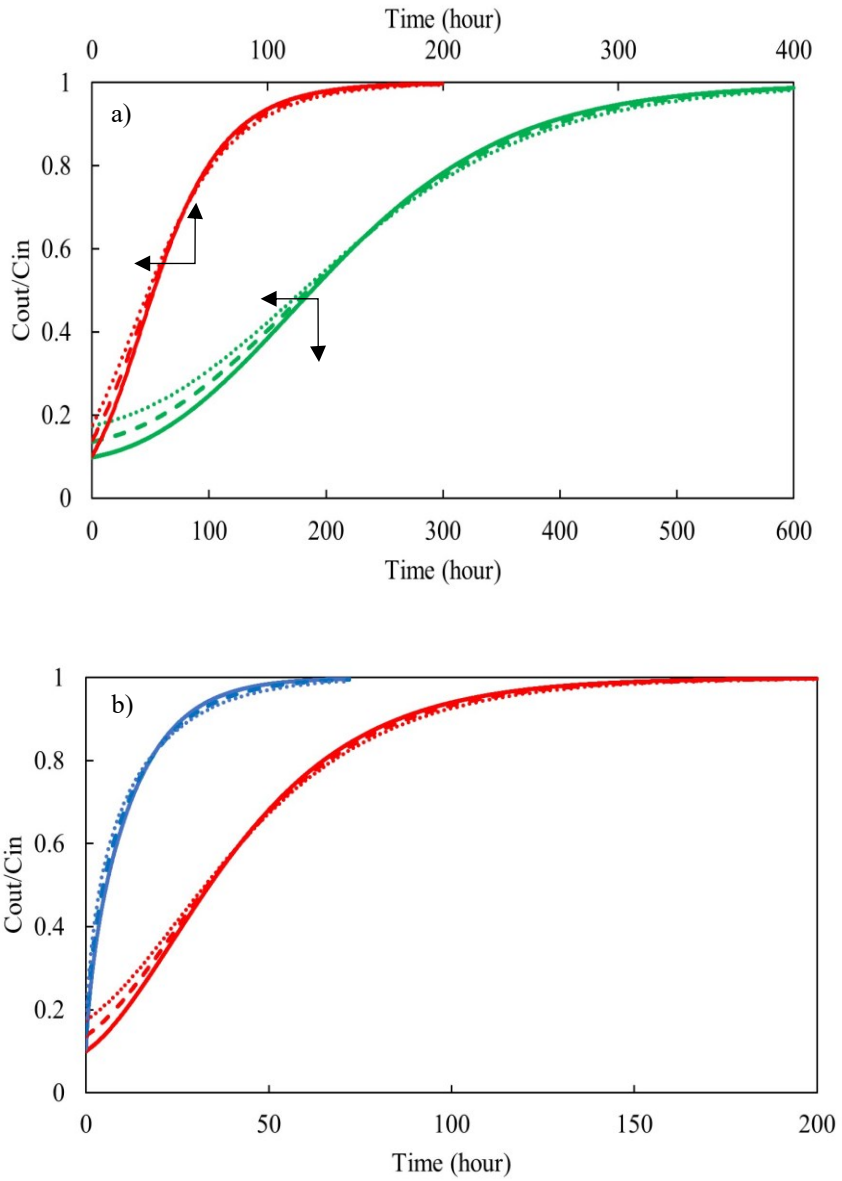

Fig. 6.10: The impact of altering the size of particles on filter performance (face velocity =0.05 m/s, concentration=0.1 ppm, and filter thickness=1 mm) (green lines: limonene, red lines: toluene, blue lines: MEK, solid lines: 0.5 mm, dashed lines: 0.6 mm, and dots: 0.7 mm). a) A mixture of toluene and limonene; b) A mixture of toluene and MEK.

6.2.4 Filter thickness

The thickness of filters is another design parameter that can significantly affect their removal performance. Fig. 6.11 illustrates the performance of the filter for thicknesses of

1, 5, and 7 mm, at the concentration of 0.1 ppm. By increasing the filter thickness, the efficiency of the filter increases, which is because of the increased residence time (contact time) [111]. At greater thicknesses, there is a reduction in the initial breakthrough, indicative of an increase in the ratio of the thickness of the filter to the length of the mass transfer zone. The overshoot phenomenon is detected at higher thicknesses, which should be greater than the critical thickness of the filter. Also, by increasing the thickness from 5 to 7, the overshoot peak and time interval increase. The reason for this is that when filter thickness increases, a greater number of less strongly adsorbed molecules are adsorbed and must be displaced [143]. Fig. 6.12 shows the breakthrough curves of the filter to remove binary mixtures when the concentrations of the VOCs with higher and lower affinities toward activated carbon are 0.2 ppm and 0.1 ppm, respectively. The comparison between Fig. 6.11 and Fig. 6.12 reveals that when the concentration of the component with higher affinity increases, the overshoot peak and time interval increase and decrease, respectively. The reason is that, at greater concentrations, compounds with high affinity can displace a certain amount of previously adsorbed low-affinity compounds in a shorter time [143]. Furthermore, compounds with higher affinity gain a stronger competitive edge at higher concentrations, displacing a greater number of low-affinity compounds [143]. Moreover, it is worth mentioning that in addition to the filter's service life, several other elements, including the pressure drop, space requirements, weight, and cost of the filter material, should be considered when determining the filter’s optimal thickness. Therefore, it is important to carefully consider these trade-offs and choose a filter thickness that meets the specific application's needs.

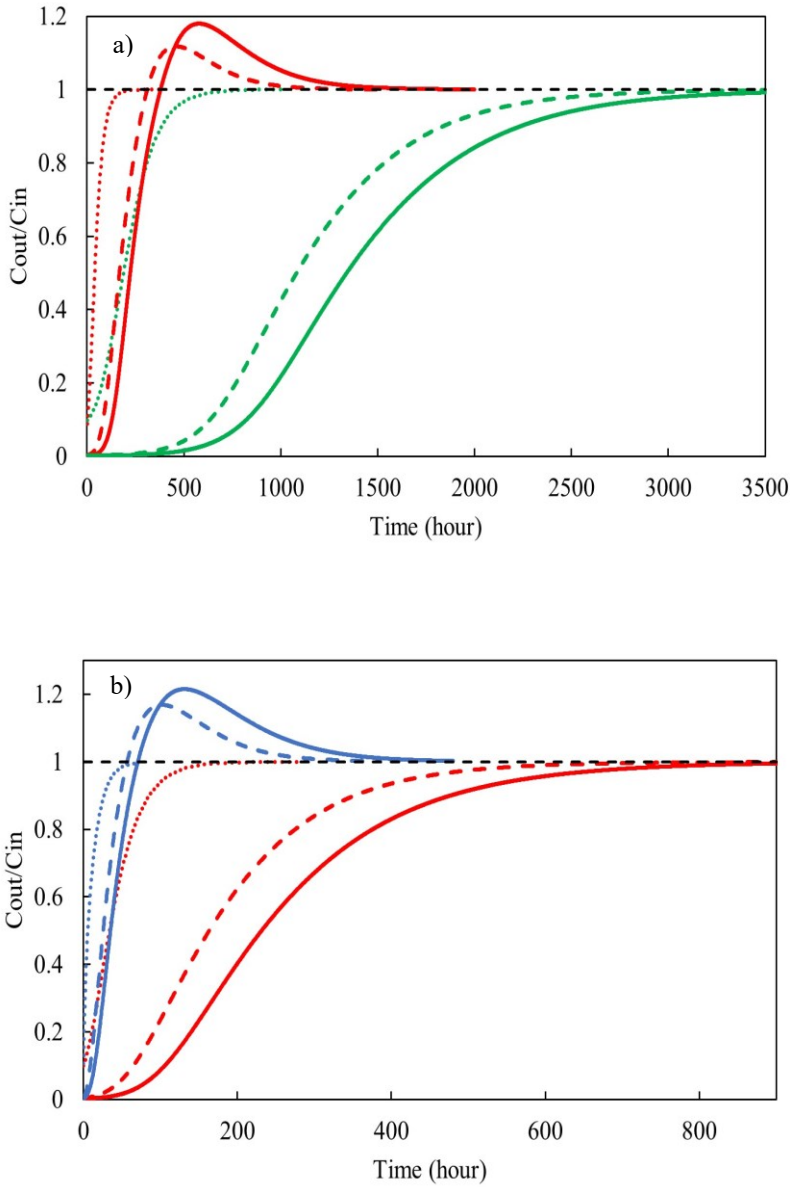

Fig. 6.11: The effect of the thickness of the filter on its breakthrough (face velocity =0.05 m/s, concentration= 0.1 ppm, and particle size=0.5 mm) (green lines: limonene, red lines: toluene, blue lines: MEK, solid lines: 7 mm, dashed lines: 5 mm, and dots: 1 mm). a) A mixture of toluene and limonene; b) A mixture of toluene and MEK.

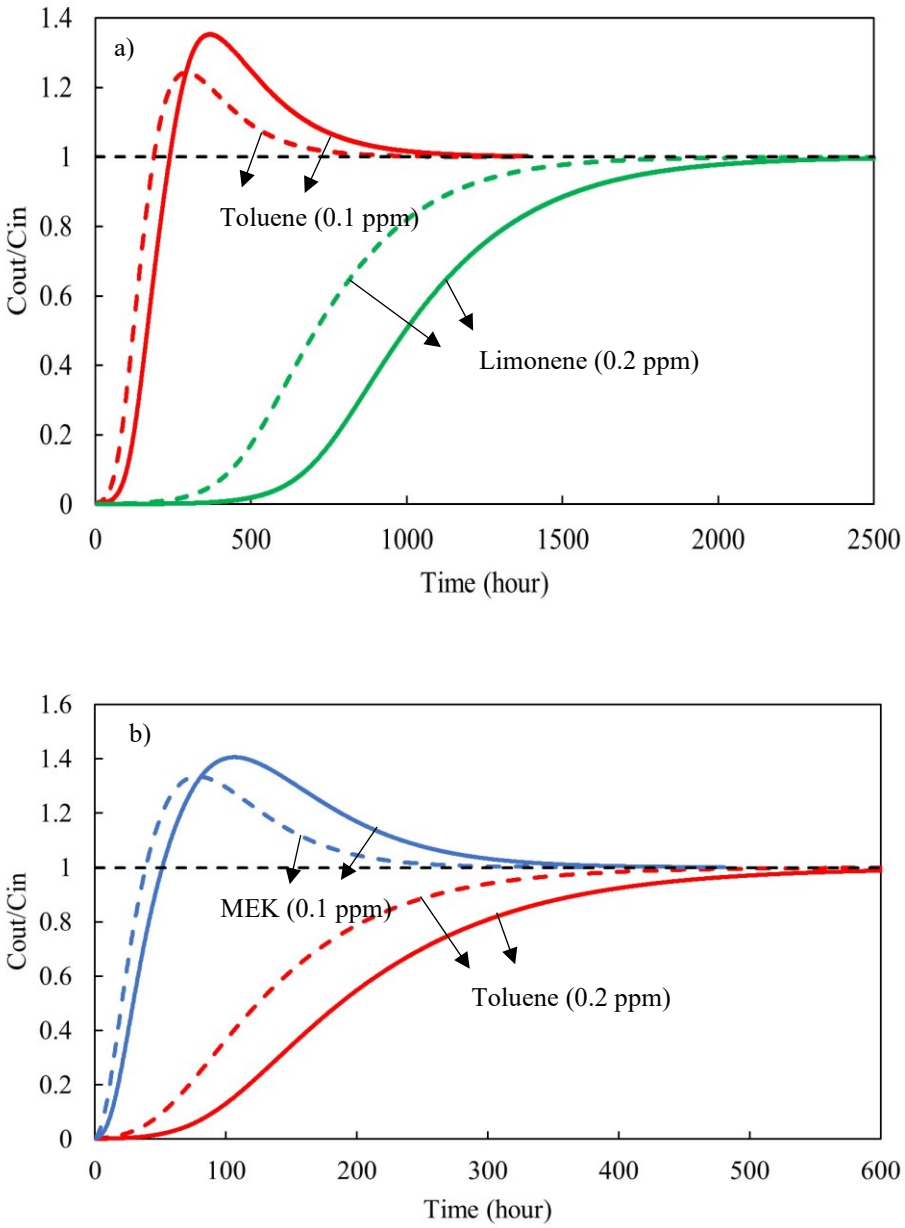

Fig. 6.12: The effect of the thickness of the filter on its breakthrough. (face velocity =0.05 m/s, and particle size=0.5 mm) (solid lines: 7 mm and dashed lines: 5 mm). a) A mixture of toluene and limonene; b) A mixture of toluene and MEK.

6.3 Summary

An advanced mathematical model (Model VVA) was developed to estimate a carbon-based filter's performance for removing the nearly ideal and non-ideal binary mixtures based on the original (non-iterative) and improved (iterative) D-Y models, respectively. The proposed model can be applied to more complex mixtures of VOCs, provided that surface diffusivities at zero loading and adsorption isotherm constants are available.

The inter-model comparison showed the insignificant effects of gas-phase diffusion for the tested carbon filter media. Also, it highlighted the importance of considering the types of compounds, the types of mixtures, and the concentrations of the compounds (the curvature of the adsorption isotherm) when selecting appropriate approximations (linear and quadratic driving force models) for intraparticle mass transfer. The conducted parametric study on design and operational parameters (air velocity, inlet concentration, particle size, and filter thickness) can be used to identify optimal conditions that lead to the most effective and efficient adsorption.

It should be kept in mind that the presence of inorganic gaseous pollutants (like O_3, NO_X, and SO_2) in real-world conditions can change the adsorption behaviour of VOCs and the surface properties of the activated carbon. This part was not investigated in this chapter. Moreover, some VOCs, such as terpenes, exhibit a high propensity to react with oxidizers like ozone, leading to the production of several secondary by-products.

7 Removal of Binary and Ternary Mixtures of Ozone and VOCs by Activated Carbon Filter: Mathematical Modelling[1]

Exposure to indoor environments containing inorganic and organic gaseous compounds has been proven to pose considerable risks to human well-being. VOCs are one of the major indoor gaseous pollutants. On the other hand, ozone, as a typical outdoor gaseous pollutant, can enter indoor spaces through natural or mechanical ventilation or infiltration. In chapters 3 and 4, ozone removal was modelled by incorporating both chemisorption and catalytic reaction mechanisms (Model OA). A comprehensive model (Model VA) was developed to evaluate the removal of single VOCs (toluene, limonene, and MEK) in chapters 3 and 5. The model successfully predicted the breakthrough of filters under various concentrations, velocities, and experimental setups. Also, the model was extended for binary mixtures of VOCs using the D-Y isotherm in chapter 6 (Model VVA). The Model VVA could predict the filter performance for both the nearly ideal mixture (toluene-limonene) and the non-ideal (toluene-MEK) mixture with high accuracy. Throughout the literature, there is no model to predict the adsorbent filters' performance for the removal of a mixture of ozone and VOCs. Experimental tests indicated that ozone oxidation of activated carbon surfaces can change surface oxygen functional groups, increasing their polarity [13,55]. Consequently, activated carbon's affinity for organic compounds is altered [13,55].

[1] Mohamad G. Khararoodi, Jiping Zhu, Chang-Seo Lee, Jianjun Niu, and Fariborz Haghighat. "Modelling the performance of the carbon-based filters to remove a mixture of ozone and VOCs from indoor air." (Reviewer Comments Received).

Furthermore, the adsorption of VOCs on the adsorbent surface causes a decrease in surface accessibility for ozone reactions [146]. Another potential interaction between ozone and VOCs is the occurrence of heterogeneous reactions on the activated carbon surface [14]. The reaction byproducts have the potential to accumulate on the adsorbent surface [14], potentially poisoning the activated carbon surface and affecting its removal performance. The objective of this chapter is to exhibit the application of the comprehensive proposed model (Eqs. (3.3) to (3.6), Eqs. (3.10) and (3.11), and Eqs. (3.17) to (3.38)) for removing mixtures of ozone and VOCs through an activated carbon filter.

7.1 Methodology

The adsorbent (Filter type 1) was exposed to binary and ternary mixtures of toluene, limonene, and ozone. The experiment results for binary and ternary mixtures at various concentrations were used to validate the proposed model. The inter-modal comparison assessed the importance of the by-products and the homogeneous reaction between ozone and limonene. A sensitivity analysis was carried out to evaluate the impacts of adsorption isotherm and reaction rate parameters on the filter's performance.

7.2 Results and discussion

7.2.1 Determining adsorption isotherm parameters

As mentioned, activated carbon can undergo two distinct reaction mechanisms for the removal of ozone. The first mechanism involves a rapid transformation of ozone into surface functional groups containing oxygen, followed by the gasification of carbon. The gasification leads to the release of carbon monoxide (CO) and carbon dioxide (CO_2) [147].

The second mechanism is a slower process that entails the catalytic conversion of ozone into molecular oxygen [147].

Surface functional groups have a significant influence on the properties of carbons [13,55]. Upon exposure to ozone, hydroxyl, carbonyl, and carboxyl groups are typically formed on the surface of activated carbon [104]. These oxygen-containing surface functional groups enhance the polarity of activated carbon [148]. Furthermore, they can cover the pore walls of activated carbon, thereby affecting its surface area and pore volume [55,115].

The aforementioned changes in the activated carbon, such as surface polarity, surface area, and pore volume, can significantly impact its adsorption behavior. Consequently, the isotherm constants obtained for a single VOC may not be applicable to a mixture of VOC and ozone. To address this limitation, the filter was pre-exposed to ozone at a concentration of 0.1 ppm before conducting the adsorption test. The adsorption tests were performed for toluene and limonene at concentrations of 9, 30, 50, 70, and 90 ppm. The ozone exposure time for each concentration was half the duration it took for the fresh filter to become saturated at that particular concentration, as determined in section 5.3.1. This was an estimation to achieve the average change in the properties of the activated carbon. The procedures for calculating the isotherm constants were similar to those used for a single VOC [71].

Fig. 7.1 illustrates the D-R curves alongside the experimental data, and Table 7.1 presents the D-R isotherm parameters and R^2.

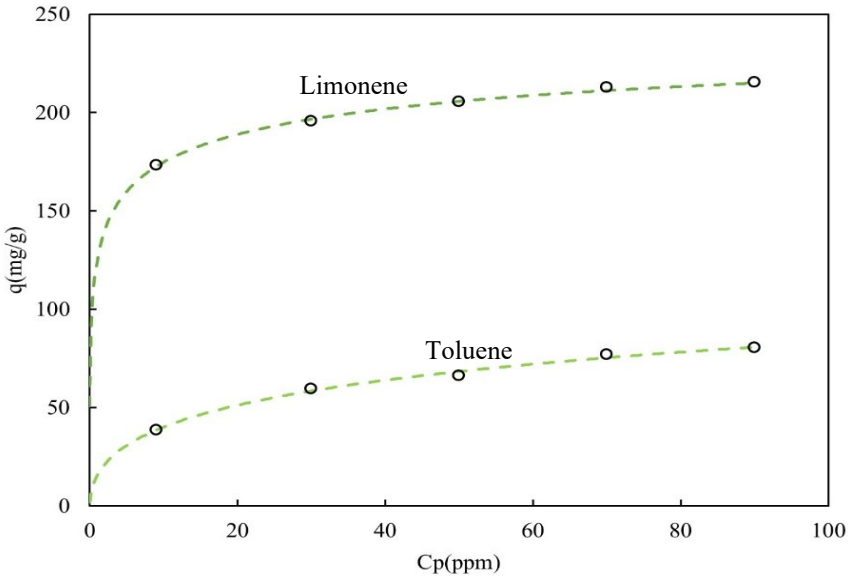

Fig. 7.1: Experimental data and D-R isotherm for toluene and limonene.

Table 7.1: The parameters of the D-R isotherm for toluene and limonene and reaction parameters for the heterogeneous reaction between ozone and limonene.

Parameters	toluene	limonene	Limonene and ozone
$K_{DR} \times 10^9$	3.71	1.95	N/A
q_{max}	182	238	N/A
R^2	0.9926	0.9966	0.9914
$k_2 \times 10^8$	N/A	N/A	8.57

Similar to fresh activated carbon, the D-R isotherm is able to present the equilibrium behaviour of VOCs on ozone-exposed carbon. However, compared to the values in Table 5.1 the values of q_{max} and K_{DR} decrease and increase when the filter has been treated with ozone, respectively. The decrease in the values of q_{max} can be related to a reduction in surface area or pore volume, potentially caused by the presence of surface functional groups that cover the walls of the pores [55,114,115]. The surface area measured using BET method and the total pore volume obtained from the volume of N_2 adsorbed show that the surface area and pore volume decrease by 14% and 13%, respectively, after 80 hours

of exposure to 0.1 ppm of ozone. The increase in the amounts of K_{DR} can be explained by a decrease in the activated carbon characteristic energy towards the toluene and limonene (E). In fact, K_{DR} is equal to $\frac{1}{E^2}$ [48], and by forming surface functional groups, the affinity of toluene and limonene towards the activated carbon decreases. Therefore, the characteristic energy decreases (K_{DR} increases).

7.2.2 Determining the reaction kinetic constant

The only parameter that remains unknown in the proposed model is the heterogeneous reaction constant (k_2) for the ozone-limonene reaction on the surface of activated carbon. The parameter was calculated by fitting the developed model into the experimental results of a binary mixture of ozone (0.1 ppm) and limonene (9 ppm) (see Fig. 7.2).

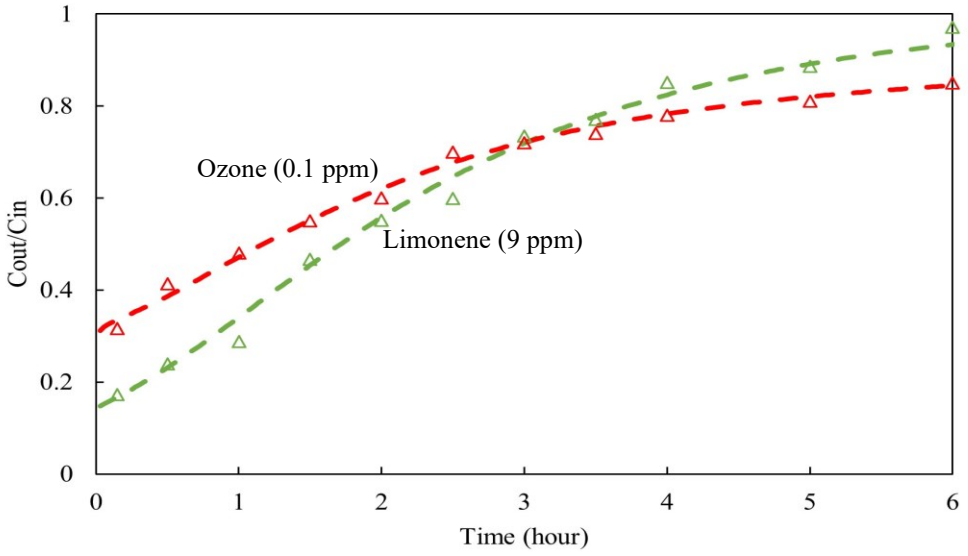

Fig. 7.2: Experimental results and the fitted model.

Table 7.1 presents the value of the reaction constant and the corresponding R^2. The model exhibits an excellent fit, as indicated by the high R^2 value and the presence of randomly scattered residuals in Fig. 7.2.

7.2.3 Model validation

The proposed model was verified in two stages. In the first stage, the predicted outcomes of the model were compared with the experimental results obtained from binary and ternary mixtures of ozone and VOCs at different concentrations. In the second stage, an inter-model comparison was performed by contrasting the proposed model with two other models. The first model considers the gas-phase reaction between ozone and limonene, while the second model neglects the generated by-products.

7.2.3.1 Comparison with experimental data

Fig. 7.3 compares the experimental results and the model's predictions for the binary and ternary mixtures of ozone and VOCs at various concentrations. It is evident that a strong agreement exists between the model's predictions and the experiment's results. This further confirms the assumption that the reaction between ozone and toluene can be considered negligible.

The figure demonstrates that the presence of ozone diminishes the efficiency of the filter in removing VOCs and vice versa. As mentioned earlier, the decrease in filter efficiency for VOC removal is attributed to the formation of functional groups, as well as the reduction in surface area and pore volume [55,114,115]. The difference between the filter's performance to remove VOCs in the presence of ozone and without ozone is the lowest in the first stage of adsorption. As time passes, the change in the adsorbent properties increases, and the difference becomes greater.

On the other hand, the adsorbed molecules block the surface of the adsorbent, reducing the accessibility of the surface for ozone. This effect is initially minimal but becomes more significant over time due to increased surface load. The impact of limonene on the efficiency of activated carbon in ozone removal surpasses that of toluene, which is consistent with earlier studies [146]. For instance, in a binary mixture with limonene (0.1 ppm) and toluene (0.1 ppm), the 50% breakthrough for ozone removal at 0.1 ppm occurs after 22 and 33 hours, respectively. This difference is attributed to the fact that activated carbon's surface has a higher affinity for limonene, resulting in a higher loading. Furthermore, it is evident that the cumulative effect of toluene and limonene on the breakthrough curve of ozone in the ternary mixture (see Fig. 7.3-d) is greater than their effect in the binary mixture with ozone (see Fig. 7.3-b and Fig. 7.3-c).

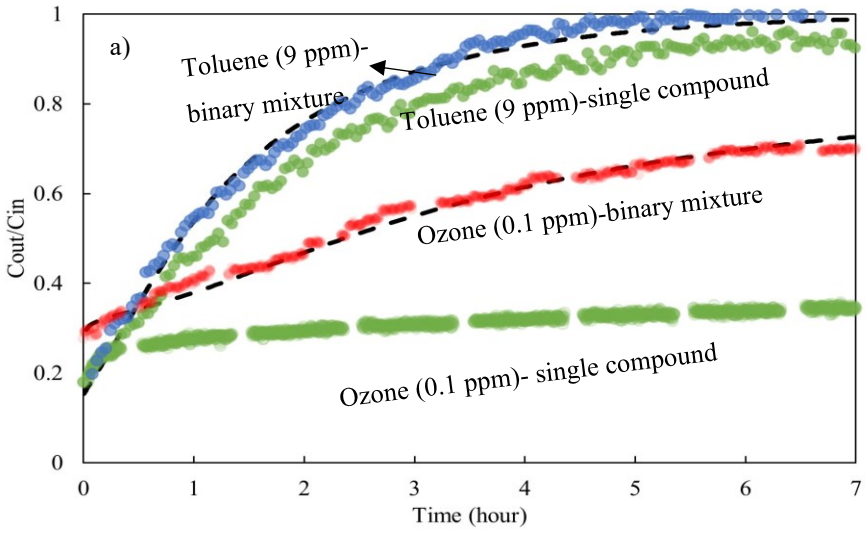

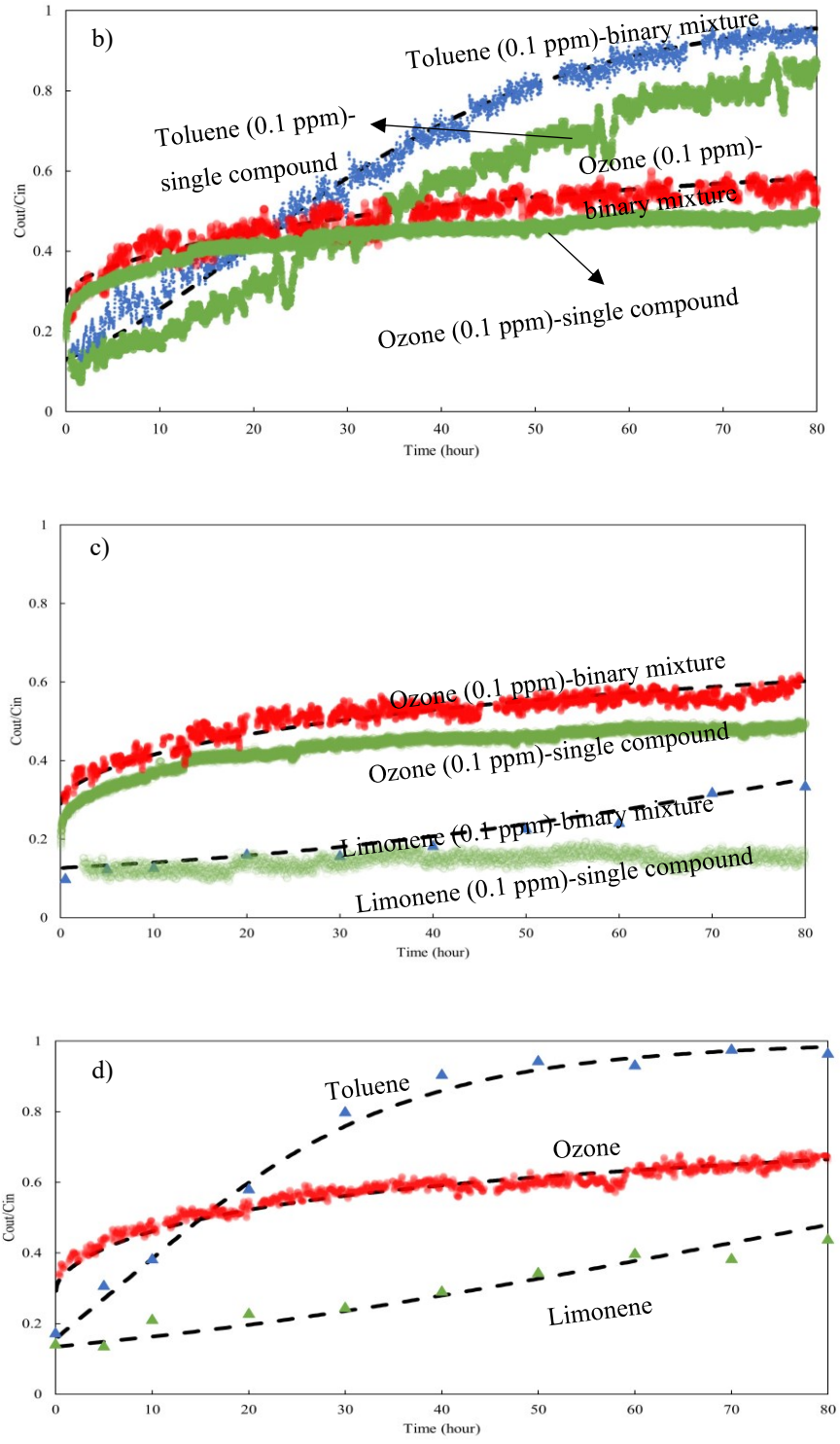

Fig. 7.3: Comparing experimental results (dots) and model's predictions (lines). a) toluene-ozone (9 ppm-0.1 ppm), b) toluene-ozone (0.1 ppm), c) limonene-ozone (0.1 ppm), and d) toluene-limonene-ozone (0.1 ppm).

7.2.3.2 Effect of gas-phase reaction

The analytical method employed did not detect any by-products resulting from the reaction between ozone and limonene in the test without the filter. However, as mentioned, the method does not have the capability to identify certain potential by-products. As a result, the proposed model (Model OVA) was compared to another model that considers the gas-phase reaction between ozone and limonene (Model OVB).

Three zones—the upstream zone (before the filter), the filter bed, and the downstream zone (after the filter)—were considered for the transfer of ozone and limonene in Model OVB. In fact, the reactor was modelled as a series of three plug and axial dispersed plug flow reactors. In the investigation of the upstream zone for limonene and ozone, it was postulated that the system undergoes one-dimensional mass transport and is in a steady-state condition. Under these assumptions, the equations governing the mass transfer are expressed as follows:

$$-u\frac{\partial C_i}{\partial x} + r_3 = 0 \tag{7.1}$$

$$C_i(x = 0) = C_{inlet,i} \tag{7.2}$$

where C_{inlet} and r_3 are the inlet concentration of the duct and the homogeneous reaction rate between ozone and limonene, respectively. Assuming a second-order reaction, r_3 is described as follows:

$$-r_3 = k_3 C_{ozone} C_{limonene} \tag{7.3}$$

where k_3 is the homogeneous reaction rate constant obtained from the literature ($k_3 = 9.29 \times 10^{-4}\frac{m^3}{mg.s}$) [149]. As the reaction rate constant associated with the toluene-ozone

reaction is deemed to be negligible [90], it is reasonable to disregard the reaction between these two compounds. Therefore, there is no change in the upstream concentration of toluene. The interparticle and intraparticle mass transfers for Model OVB are similar to Model OVA, except that the term " r_3 " needs to be included on the right side of Eq. (3.3), and the term " $r_3\varepsilon_p$ " on the right side of Eqs. (3.21) and (3.26).

Finally, the mass transfer model within the downstream zone for limonene and ozone is presented as follows:

$$\frac{\partial C_i}{\partial t} = -u\frac{\partial C_i}{\partial x} + r_3 \tag{7.4}$$

$$C_i(t = 0, x) = 0 \tag{7.5}$$

$$C_i(t, x = L_1 + L) = C_{out,i} \tag{7.6}$$

where L_1 is the upstream zone length. As mentioned, the concentration of toluene remains constant in the upstream and downstream zones.

Fig. 7.4 depicts that there is no significant difference between the predictions of Models OVA and OVB (Eqs. (3.3) to (3.6), Eqs. (3.10) and (3.11), Eqs. (3.17) to (3.38), and Eqs. (7.1) to (7.6)). It means that the gas-phase reaction rate is too slow to result in any significant conversion within the used experimental duct, with a residence time of approximately 20 seconds.

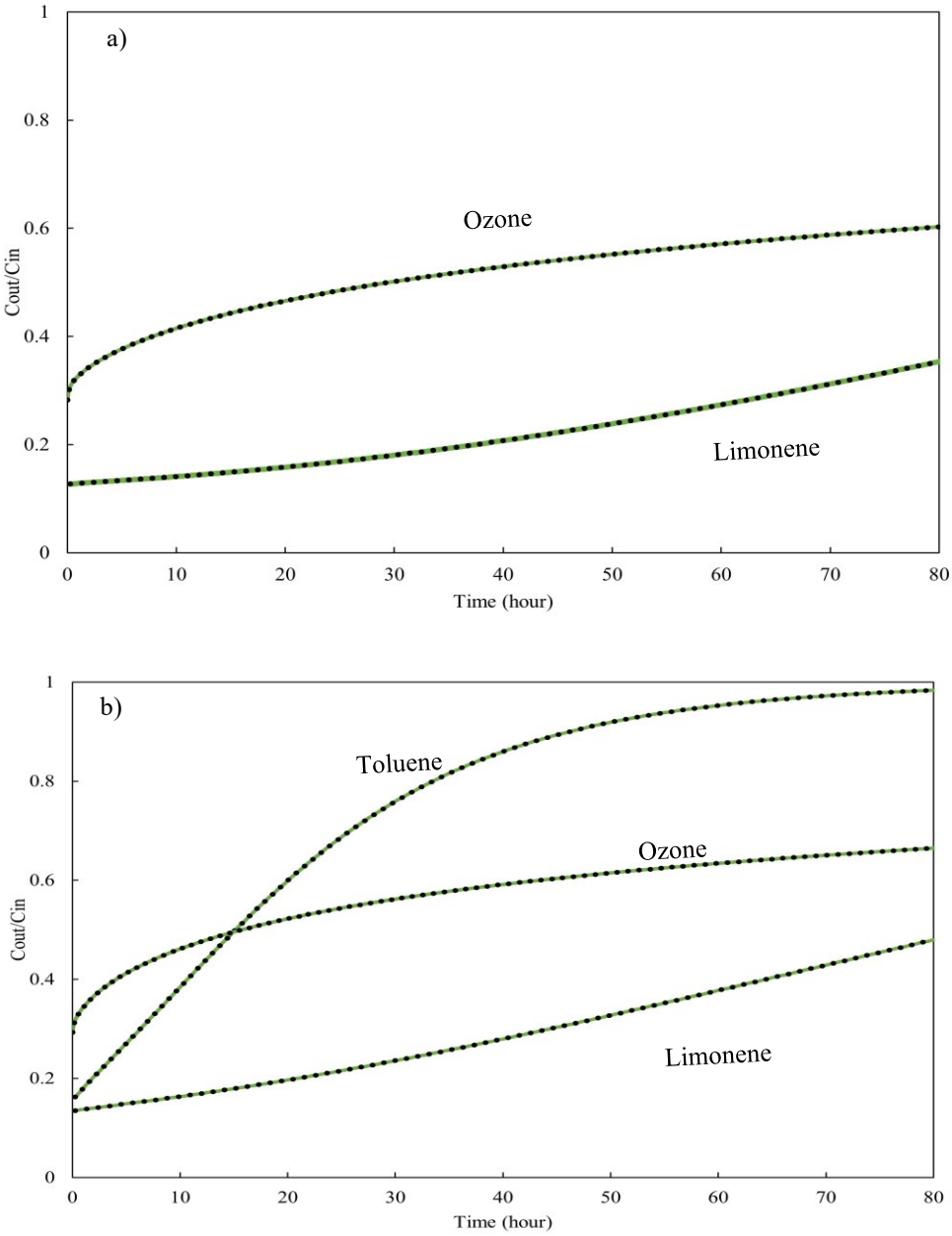

Fig. 7.4: Comparison of the predictions of Models OVA (green lines) and OVB (black dots). a) binary mixture of limonene and ozone (0.1 ppm), b) ternary mixture of limonene, toluene, and ozone (0.1 ppm).

7.2.4 Effect of by-products

The effect of by-products was considered in the proposed model to estimate the filter's efficiency in removing both VOCs and ozone. Also, it was assumed that all reaction products were maintained on the surface of activated carbon. Although no reaction products were detected in the downstream samples, it might be because of the fact that the presence of the challenging VOCs would impact the detection limit of the samples, rendering it too high to effectively identify the byproducts. However, from an application perspective, this assumption is a conservative and safe approach. Moreover, the results are consistent with the work of Metts [19], where it was shown that 99% of the detected by-products (keto-limonene and limonene oxides) remained on the surface of activated carbon.

The by-products detected on the surface of activated carbon were keto-limonene (4-acetyl-1-methylcyclohexene (AMCH)) and carvone based on the GC-MS library. For the production of keto-limonene, ozone reacts with the external double bond of limonene and produces primary ozonide [150]. Primary ozonide cleaves to form keto-limonene and an energy-rich excited Criegee intermediate (CI*). Also, this intermediate (CI*) can become a stabilized Criegee intermediate (SCI) by quenching. The stabilized Criegee intermediate can react further with water and produce keto-limonene [150, 151]. On the other hand, the allylic oxidation of limonene results in the production of carveol [152]. Carveol can undergo oxidative dehydrogenation, which produces carvone (see Fig. 7.5) [152]. Therefore, the reaction rate constant (k_2) is equal to the sum of the reaction constants of the competitive parallel reactions.

For investigating the importance of considering the by-products in the filter's efficiency, the prediction made by the proposed model (Model OVA) was compared with the

prediction made by a model which does not consider the by-products (Model OVC- Eqs. (3.3) to (3.6), Eqs. (3.10) and (3.11), Eqs. (3.17) to (3.38), and $V_i = 0$ for by-products). Fig. 7.6 compares the predictions of Models OVA and OVC for the binary mixture of ozone and limonene, as well as the ternary mixture of ozone, limonene, and toluene. Since Model OVC does not consider by-products adsorption on the surface, it overestimates the filter's performance for the removal of all compounds. Also, the difference between Model OVA and Model OVC increases with the load of by-products.

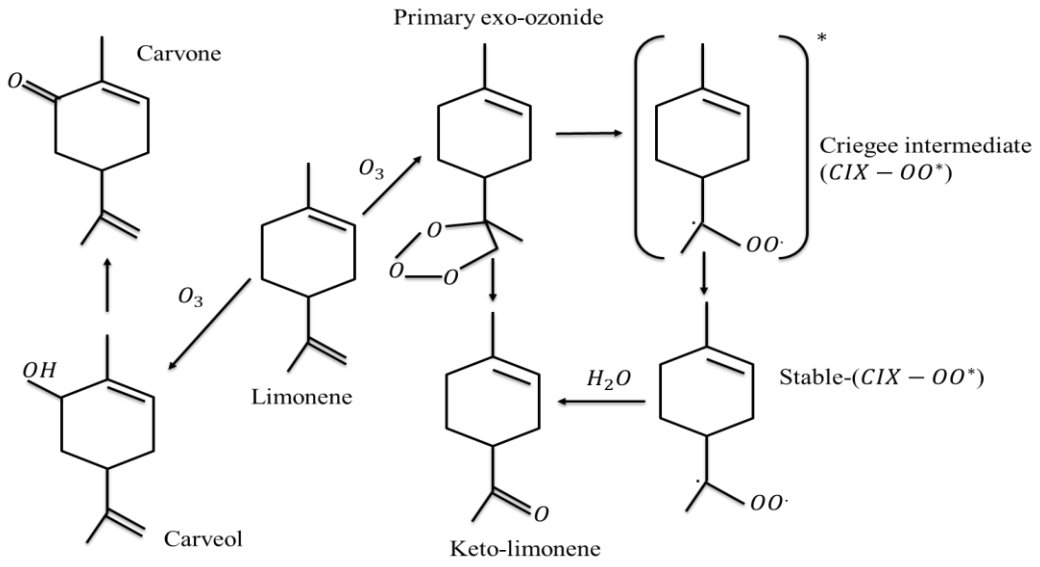

Fig. 7.5: Reaction pathways to produce keto-limonene and carvone.

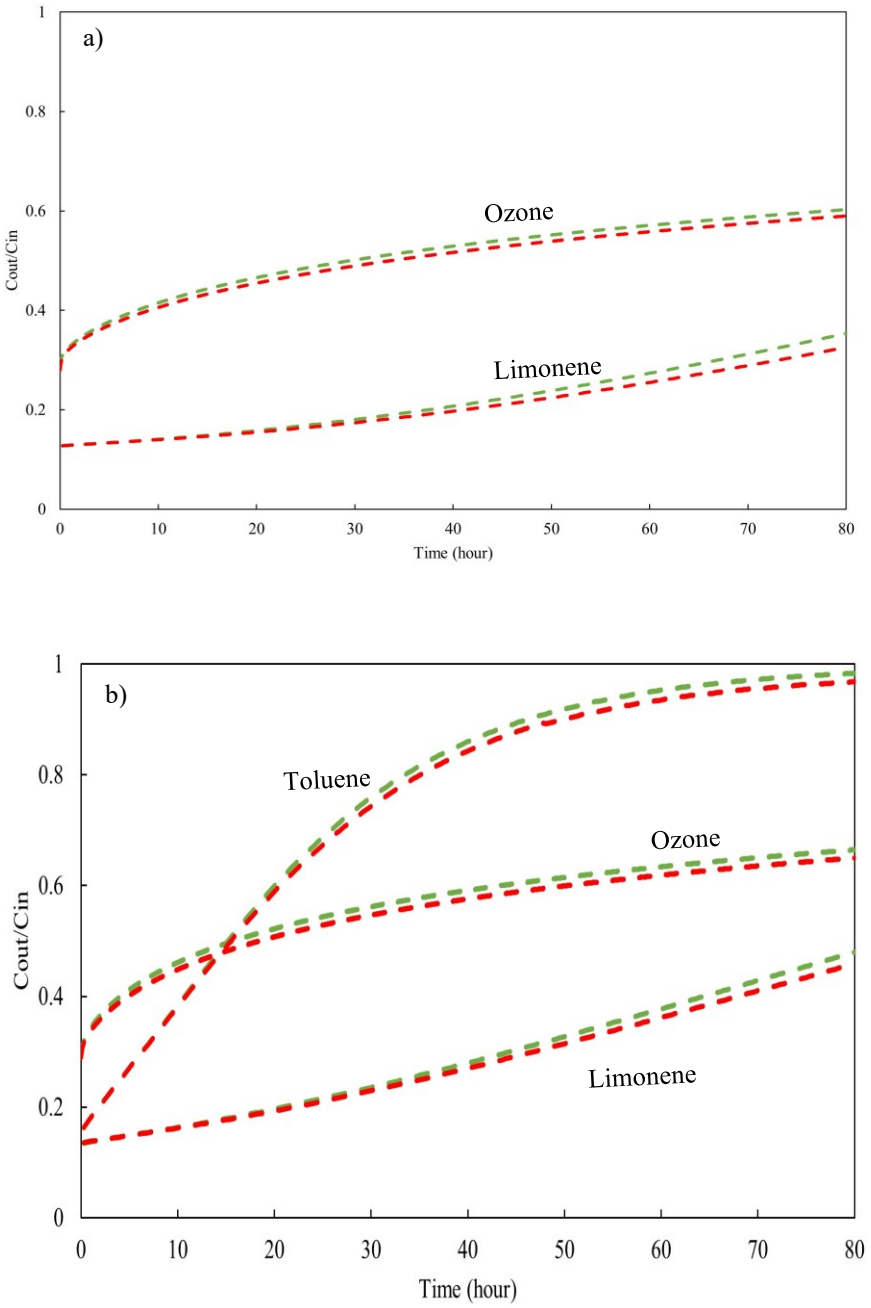

Fig. 7.6: Comparing the predictions of Models OVA (green lines) and OVC (red lines). a) binary mixture of limonene and ozone (0.1 ppm), b) ternary mixture of limonene, toluene, and ozone (0.1 ppm).

7.2.5 Sensitivity analysis

A sensitivity analysis was conducted on the adsorption isotherm and reaction kinetic parameters to evaluate the robustness of the proposed model. These parameters were susceptible to experimental measurement errors (q_{max} and K_{DR}) or fitting the model to experiment results (k_2). To determine the relative importance of the parameters in the model's prediction, a comparison was made by altering each parameter and analyzing the corresponding ARE while keeping all other parameters constant.

7.2.5.1 Reaction rate constant

The sensitivity analysis conducted in section 4.2.3.1 focused on the reaction rate parameters of the ozone-activated carbon surface reaction (k_1, k_d, n and m). However, this study specifically investigated the effect of the reaction rate constant for the ozone-limonene reaction (k_2) on the model's accuracy. For this purpose, k_2 was modified by a factor up to 80% and 120% relative to its fitted value. Fig. 7.7 depicts that the model is not highly sensitive to the reaction constant. For example, the increase in ARE for ozone was 0.7% when there was a 20% decrease in k_2 values. It is worth mentioning that any changes in the model's prediction for toluene removal in the ternary mixture are a result of changing the concentration of limonene, which is in equilibrium with toluene and the by-products production.

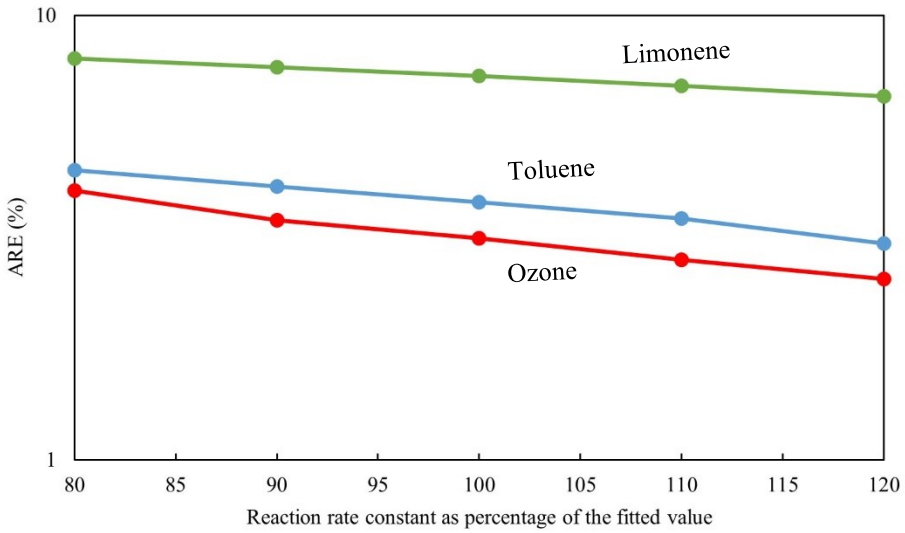

Fig. 7.7: Sensitivity analysis on the reaction constants for the removal of limonene, toluene, and ozone through the filter.

7.2.6 Adsorption isotherm parameters

The impact of adsorption isotherm parameters (K_{DR} and q_{max}) on the model's prediction is demonstrated in Fig. 7.8 for the ternary mixture of toluene, limonene, and ozone. The figure shows that by changing the adsorption parameters for the VOC with a lower affinity towards activated carbon (toluene (Fig. 7.8-a)), the ARE only increases significantly for that VOC. On the other hand, modifying the adsorption parameters for the VOC with a higher affinity towards activated carbon (limonene (Fig. 7.8-b)) not only affects the model's prediction for that VOC but also has a considerable impact on the filter's performance for the removal of ozone and toluene.

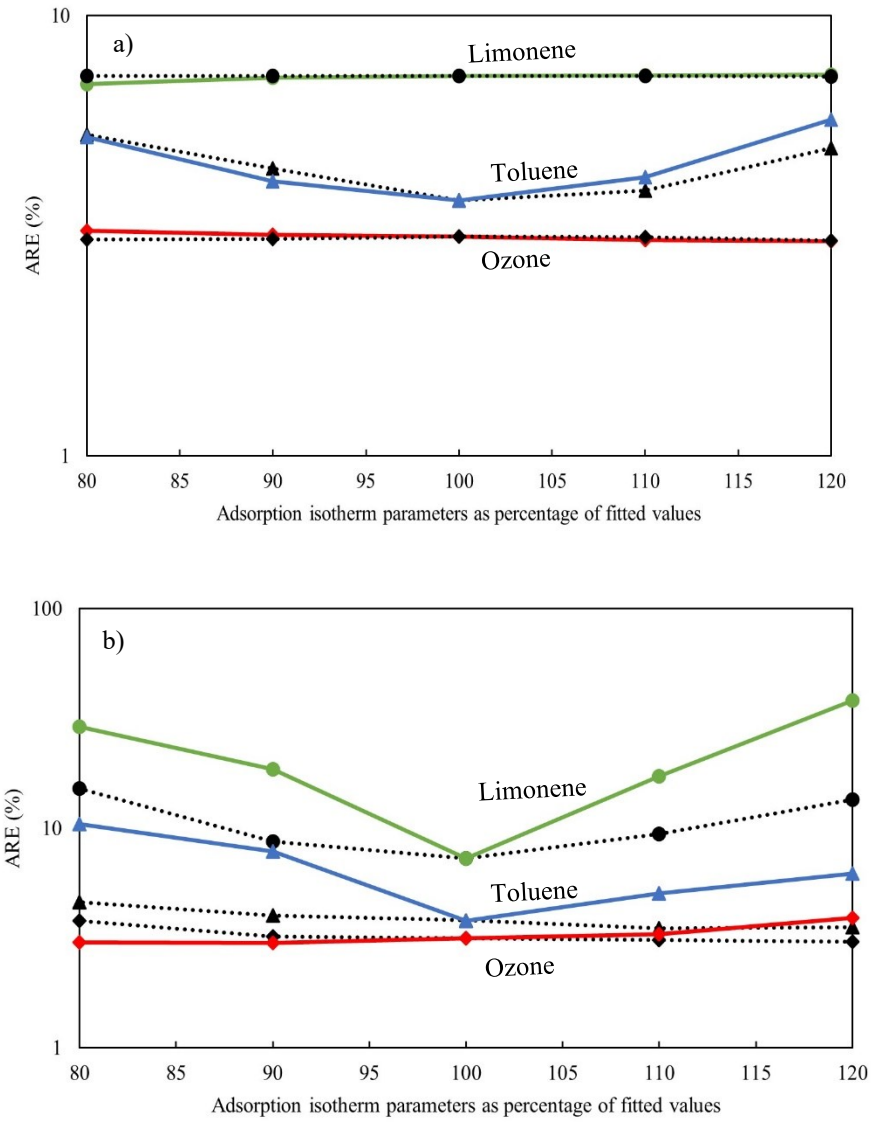

Fig. 7.8: Sensitivity analysis on the adsorption isotherm parameters for the removal of limonene, toluene, and ozone through the filter. q_{max} (dots lines) and K_{DR} (solid lines). a) D-R isotherm constants for toluene and a) D-R isotherm constants for limonene.

7.3 Summary

The dynamic performance of an activated carbon filter in removing mixtures of ozone and VOCs (toluene and limonene) was predicted using a comprehensive mathematical model (Model OVA). The E-R mechanism was considered for the heterogeneous reaction between ozone and the more reactive VOC (limonene). The D-R isotherm was improved by using the volume exclusion theory to consider the effect of the produced by-products. Also, the effect of the adsorbed VOCs and the reaction by-products, which result in a decrease in the accessibility of the surface for the ozone-activated carbon reaction, was considered.

The developed model showed high accuracy in predicting the filter's efficiency in removing binary and ternary mixtures of ozone and VOCs. The results indicated that the coexistence of ozone and VOCs exerts a notable influence on the efficiency of the filtration system in eliminating both compounds. The information is essential in planning the regeneration or replacement time of the filter.

The homogeneous reaction between ozone and limonene was confirmed to be insignificant for the duct with a high residence time. Additionally, the heterogeneous reaction exhibited a higher rate than the homogenous reaction. In fact, carbon acts as a catalyst and speeds up the rate of reaction. Based on the sensitivity analysis, it was determined that the model's sensitivity is higher towards the adsorption isotherm parameters when compared to the reaction kinetic parameter for ozone and limonene.

8 Conclusions and Recommendations

8.1 Conclusion

The presence of inorganic and organic gaseous in indoor environments has been shown to cause significant harm to human wellness. VOCs and ozone are two of the major indoor and outdoor gaseous pollutants, respectively, and exposure to such pollutants has been linked to respiratory illness, headaches, and other associated health concerns. Activated carbon, owing to its effective ability to remove ozone and the majority of VOCs, has emerged as the most commonly employed adsorbent for indoor air quality control. While they can be effectively removed by carbon-based filters, the carbon can become saturated due to adsorption or even exhausted due to irreversible reactions during the purification process. Therefore, evaluating the filter's performance in removing these pollutants is essential to determining the filter maintenance schedule.

The main objective of this research was the development and validation of a comprehensive model for predicting carbon-based filters' performance for the removal of a mixture of ozone and VOCs. The axially dispersed plug flow considers convection, dispersion, accumulation in the bulk of the filter, and mass transfer through the boundary layer for all compounds. For intraparticle transfer of ozone, the pore diffusion model considers accumulation and diffusion in the pores of particles. Also, it was augmented by two reaction rates: 1) Ozone-carbon reaction rate that considered the deactivation of activated carbon, and 2) Heterogeneous reaction between ozone and limonene based on the E-R mechanism. On the other hand, the PSDM with variable surface diffusivity was used for the intraparticle transfer of VOCs. The D-R isotherm was employed to represent the

adsorption equilibrium. Also, the Darken model was applied to the D-R isotherm to show the concentration dependency of surface diffusivity. For the binary mixture of VOCs, the D-Y model showed equilibrium behaviour. Finally, the D-R isotherm was improved by using the volume exclusion theory to consider the effect of the generated by-products. Moreover, the effect of the adsorbed VOCs and the reaction by-products, which result in a decrease in the accessibility of the surface for the ozone-activated carbon reaction, was considered.

The prediction made by the model was in good agreement with the experimental data for the concentration level observed indoors for all tested filters. Additionally, the model correctly predicted the experimental results collected using a full-scale setup. Also, it was able to predict the lower efficiency and steeper initial breakthrough curve at a higher velocity.

The inter-model comparison showed the importance of axial dispersion and pore gas-phase diffusion for the removal of ozone through the tested filters. Also, the model was highly sensitive to the reaction parameters for the reaction between ozone and the activated carbon surface, in contrast to the ozone-limonene reaction parameter. For ozone removal, only the initial stage of the removal process is influenced by the external mass transfer.

The inter-model comparison for the removal of VOCs depicted that surface diffusion is the dominant internal mass transfer. On the other hand, considering the importance of surface diffusivity variation revealed that depending on the type of adsorbate-adsorbent systems, the ratio of surface diffusion rate and external mass transfer rate changes significantly. In a case where surface diffusion is substantially higher than the external mass transfer, the

internal mass transfer can be considered instantaneous. It means that there is no limitation on mass transfer within the particles. For the binary mixtures of VOCs, since the original D-Y method does not consider the effect of lateral interactions, it was only able to predict the equilibrium behaviour of multi-component adsorption of VOCs with similar intermolecular forces. Furthermore, the curvature of the adsorption isotherm should be considered when applying appropriate approximations (linear and quadratic driving force models) for intraparticle mass transfer instead of using Fick's law of diffusion.

The experiments conducted in this study showed that the coexistence of ozone and VOCs significantly impacts the efficiency of filtration systems in eliminating these compounds. Specifically, the presence of VOCs hindered the accessibility of the surface for ozone reactions. Also, the interaction of ozone with the carbon surface influenced important parameters such as pore volume, surface area, and the carbon's affinity towards VOCs. Additionally, the formation of byproducts resulting from the ozone-limonene reaction on the surface of activated carbon (keto-limonene and carvone) adversely affected the performance of the filtration system in removing both VOCs and ozone.

By considering the above-mentioned interactions, the proposed model offered a comprehensive framework for assessing the effectiveness of filtration systems in removing both VOCs and ozone. Moreover, the model can be used to investigate the effects of the operational and design parameters, including the inlet concentration, air velocity, filter thickness, filter porosity, particle size, and particle porosity, on the filter's performance. This information can be utilized to make informed decisions regarding the design and selection of optimal filters, ensuring the removal of VOCs and ozone to improve the overall air quality in indoor environments.

8.2 Recommendations for further work

Based on the study's findings and limitations, here are some suggestions for future modelling work.

1) The improved D-Y model is effective in depicting the equilibrium behaviour of adsorption for non-ideal mixtures, but it comes at the cost of losing one of the key benefits of the non-iterative approach, which is not requiring mixture testing for measuring isotherm parameters. Therefore, it is recommended that future investigations explore the development and implementation of a novel approach that utilizes results from single-component adsorption tests to show the equilibrium behaviour of non-ideal mixtures.
2) The proposed model assumes that the detected reaction by-products are totally adsorbed on the surface of the carbon. From an application perspective, the assumption is conservative and safe. However, if a substantial fraction of the reaction by-products departs from the activated carbon surface, it is imperative to conduct adsorption experiments individually on each by-product to determine their equilibrium behaviour. Also, since the exact concentration of each by-product is required, the reaction constants for both pathways for the ozone and limonene reactions should be measured.
3) Permanganate-impregnated alumina media are often used in combination with activated carbon for the removal of certain gaseous pollutants which cannot be effectively removed by activated carbon alone, such as nitrogen oxides, oxides of sulphur, acetaldehyde, and formaldehyde. Predicting the performance of multi-media for the removal of a more comprehensive range of gaseous

compounds is suggested for future studies. In doing so, the model should be expanded to consider the interactions of compounds with the surface of media (adsorption or reaction) and their effect on the removal of other gaseous pollutants.

4) The tested filters (combined filters) are designed to remove particles in addition to gaseous compounds. Therefore, there is a need to develop a predictive model for assessing the efficiency of combined filters in the simultaneous removal of particulate matter and gaseous compounds. One of the most important considerations should be the soiling of the carbon by particles, which can affect its performance in removing gaseous compounds.

References

[1] USEPA, “Indoor Air Quality.” https://www.epa.gov/report-environment/indoor-air-quality (accessed Aug. 18, 2021).

[2] ASHRAE, *ASHRAE handbook : fundamentals*, SI. Atlanta: ASHRAE, 2013.

[3] USEPA, “Introduction to Indoor Air Quality.” https://www.epa.gov/indoor-air-quality-iaq/introduction-indoor-air-quality (accessed Jun. 13, 2023).

[4] F. Haghighat, C. S. Lee, B. Pant, G. Bolourani, N. Lakdawala, and A. Bastani, “Evaluation of various activated carbons for air cleaning - Towards design of immune and sustainable buildings,” *Atmos. Environ.*, vol. 42, no. 35, pp. 8176–8184, 2008.

[5] Z. Shayegan, C. S. Lee, and F. Haghighat, “TiO2 photocatalyst for removal of volatile organic compounds in gas phase – A review,” *Chem. Eng. J.*, vol. 334, no. September 2017, pp. 2408–2439, 2018.

[6] A. H. Mamaghani, F. Haghighat, and C. S. Lee, “Photocatalytic oxidation technology for indoor environment air purification: The state-of-the-art,” *Appl. Catal. B Environ.*, vol. 203, pp. 247–269, 2017.

[7] M. Malayeri, F. Haghighat, and C. S. Lee, “Modeling of volatile organic compounds degradation by photocatalytic oxidation reactor in indoor air: A review,” *Build. Environ.*, vol. 154, no. February, pp. 309–323, 2019.

[8] M. Bahri and F. Haghighat, “Plasma-based indoor air cleaning technologies: The state of the art-review,” *Clean - Soil, Air, Water*, vol. 42, no. 12, pp. 1667–1680,

2014.

[9] A. Luengas, A. Barona, C. Hort, G. Gallastegui, V. Platel, and A. Elias, “A review of indoor air treatment technologies,” *Rev. Environ. Sci. Biotechnol.*, vol. 14, no. 3, pp. 499–522, 2015.

[10] USEPA, “Residential Air Cleaners A Technical Summary 3rd Edition Portable Air Cleaners Furnace and HVAC Filters,” 2018. https://www.epa.gov/sites/default/files/2018-07/documents/residential_air_cleaners_-_a_technical_summary_3rd_edition.pdf (accessed Aug. 19, 2021).

[11] ASHRAE, *ASHRAE handbook : heating, ventilating, and air-conditioning applications*, I-P. ASHRAE, 2015.

[12] D. W. Vanosdell, C. E. Rodes, and M. K. Owen, “Laboratory Testing of Full-Scale In-Duct Gas Air Cleaners,” vol. 112, 2006.

[13] M. L. Kingsley and J. H. Davidson, “Adsorption of toluene onto activated carbons exposed to 100áppb ozone,” *Carbon N. Y.*, vol. 44, no. 3, pp. 560–564, 2006.

[14] T. A. Metts and S. A. Batterman, “Heterogeneous reactions of ozone and D-limonene on activated carbon.,” *Indoor Air*, vol. 17, no. 5, pp. 362–371, 2007.

[15] J. R. Smith, *Theory of Chemisorption*. Springer-Verlag Berlin Heidelberg, 1980.

[16] Axley JW, “Tools for the analysis of gas-phase air-cleaning systems in buildings,” 1994.

[17] M. S. Shafeeyan, W. M. A. Wan Daud, and A. Shamiri, “A review of

mathematical modeling of fixed-bed columns for carbon dioxide adsorption," *Chem. Eng. Res. Des.*, vol. 92, no. 5, pp. 961–988, 2014.

[18] M. H. Chahbani and D. Tondeur, "Mass transfer kinetics in pressure swing adsorption," *Sep. Purif. Technol.*, vol. 20, no. 2–3, pp. 185–196, 2000.

[19] A. K. Vizhemehr and F. Haghighat, "Modeling of gas-phase filter model for high- and low-challenge gas concentrations," *Build. Environ.*, vol. 80, pp. 192–203, 2014.

[20] A. K. Vizhemehr, F. Haghighat, and C. S. Lee, "Predicting gas-phase air-cleaning system efficiency at low concentration using high concentration results: Development of a framework," *Build. Environ.*, vol. 68, pp. 12–21, 2013.

[21] C. He, "Model-Based Testing and Evaluation of Sorption Media for Removing Volatile Organic Compounds in Indoor Air," Syracuse University, 2018.

[22] R. S. Popescu, P. Blondeau, E. Jouandon, J. C. Costes, and J. L. Fanlo, "Elemental modeling of adsorption filter efficiency for indoor air quality applications," *Build. Environ.*, vol. 66, pp. 11–22, 2013.

[23] C. He, W. Chen, K. Han, B. Guo, J. Pei, and J. S. Zhang, "Evaluation of filter media performance: Correlation between high and low challenge concentration tests for toluene and formaldehyde (ASHRAE RP-1557)," *HVAC R Res.*, vol. 20, no. 5, pp. 508–521, 2014.

[24] J. Pei and J. Zhang, "Modeling of sorbent-based gas filters: Development, verification and experimental validation," *Build. Simul.*, vol. 3, no. 1, pp. 75–86,

2010.

[25] T. Cheng, Y. Jiang, Y. Zhang, and S. Liu, “Prediction of breakthrough curves for adsorption on activated carbon fibers in a fixed bed,” *Carbon N. Y.*, vol. 42, no. 15, pp. 3081–3085, 2004.

[26] M. Yao, Q. Zhang, D. W. Hand, and R. Taylor, “Modeling of Adsorption and Regeneration of Volatile Organic Compounds on Activated Carbon Fiber Cloth,” *J. Environ. Eng.*, vol. 135, no. 12, pp. 1371–1379, 2009.

[27] J. Pei, “Physical adsorption, chemisorption and catalytic oxidization for indoor VOCs removal,” Syracuse University, 2011.

[28] A. Poursaeidesfahani *et al.*, “Prediction of adsorption isotherms from breakthrough curves,” *Microporous Mesoporous Mater.*, vol. 277, no. March 2018, pp. 237–244, 2019.

[29] D. M. Ruthven, *Principles of adsorption and adsorption processes*. Wiley-Interscience, 1984.

[30] O. Levenspiel, *Chemical Reaction Engineering*. Wiley, 1999.

[31] C. Tien, *Adsorption calculations and modeling*. Butterworth-Heinemann, 1994.

[32] M. Malayeri, C. S. Lee, and F. Haghighat, “Modeling of photocatalytic oxidation reactor for methyl ethyl ketone removal from indoor environment: Systematic model development and validation,” *Chem. Eng. J.*, vol. 409, no. September 2020, p. 128265, 2021.

[33] F. J. Gutiérrez Ortiz, M. Barragán Rodríguez, and R. T. Yang, “Modeling of fixed-

bed columns for gas physical adsorption," *Chem. Eng. J.*, vol. 378, no. June, p. 121985, 2019.

[34] S. O. Rastegar and T. Gu, "Empirical correlations for axial dispersion coefficient and Peclet number in fixed-bed columns," *J. Chromatogr. A*, vol. 1490, pp. 133–137, 2017.

[35] R. T. Yang, *Gas Separation by Adsorption Processes*. Butterworth-Heinemann, 1987.

[36] L. Fournel, P. Mocho, R. Brown, and P. Le Cloirec, "Modeling breakthrough curves of volatile organic compounds on activated carbon fibers," *Adsorption*, vol. 16, no. 3, pp. 147–153, 2010.

[37] H. S. Fogler, *Elements of Chemical Reaction Engineering*, Fifth. Prentice Hall, 2016.

[38] R. E. Treybal, *mass transfer operations*. McGraw Hill, 1980.

[39] N. Wakao and T. Funazkri, "Effect of fluid dispersion coefficients on particle-to-fluid mass transfer coefficients in packed beds: correlation of Sherwood numbers," *Chem. Eng. Sci.*, pp. 1375–1384, 1978.

[40] P. N. Dwlvedi and S. N. Upadhyay, "Particle-Fluid Mass Transfer in Fixed and Fluidized Beds," *Ind. Eng. Chem. Process Des. Dev.*, vol. 16, no. 2, pp. 157–165, 1977.

[41] W. Ranz and W. R. Marshall, "Evaporation from drops," *Chem. eng. prog*, no. 48, pp. 141–146, 1952.

[42] M. Malayeri, C. S. Lee, F. Haghighat, and L. Klimes, “Modeling of gas-phase heterogeneous photocatalytic oxidation reactor in the presence of mass transfer limitation and axial dispersion,” *Chem. Eng. J.*, vol. 386, no. January, p. 124013, 2020.

[43] I. Mochida *et al.*, “Removal of SOx and NOx over activated carbon fibers,” *Carbon N. Y.*, vol. 38, no. 2, pp. 227–239, 2000.

[44] S. Giraudet and P. Le Cloirec, “Activated carbon filters for filtration–adsorption,” in *Activated carbon fiber and textiles*, Elsevier, 2017, pp. 211–243.

[45] G. Marbán, T. Valdés-Solís, and A. B. Fuertes, “Modeling the breakthrough behavior of an activated carbon fiber monolith in n-butane adsorption from diluted streams,” *Chem. Eng. Sci.*, vol. 61, no. 14, pp. 4762–4772, 2006.

[46] ASHRAE, “ANSI /ASHRAE Standard 145 .1. Laboratory Test Method for Assessing the Performance of Gas-Phase Air-Cleaning Systems: Loose Granular Media,” *2015*.

[47] ISO, “ISO 10121-1, Test Method for Assessing the Performance of Gas-phase Air Cleaning Media and Devices for General Ventilation - Part 1: Gas-phase Air Cleaning Media,” *2014*.

[48] D. D. Do, *Adsorption Analysis: Equilibria and Kinetics*, no. Imperial College Press. 1998.

[49] S. G. Chatterjee and C. Tien, “Retention of toxic gases by modified carbon in fixed beds,” *Carbon N. Y.*, vol. 28, no. 6, pp. 839–848, 1990.

[50] L. A. Graceffo, S. G. Chatterjee, H. Moon, and C. Tien, “A model for the retention of toxic gases by impregnated carbon,” *Carbon N. Y.*, vol. 27, no. 3, pp. 441–456, 1989.

[51] R. C. Soares, J. M. Loureiro, C. Serenoa, and A. E. Rodrigues, “Modeling and Simulation of Carbon Mask Adsorptive Reactors,” *Ind. Eng. Chem. Res.*, vol. 34, no. 8, pp. 2762–2768, 1995.

[52] D. K. Friday, “Breakthrough behavior of a light gas in a fixed-bed adsorptive reactor,” in *American Institute of Chemical Engineers, National Meeting*, 1988, pp. 89–93.

[53] C. C. Huang and C. H. Chen, “Dynamic Adsorption Model of H2S in a Fixed Bed of Copper Impregnated Activated Carbon,” *Sep. Sci. Technol.*, vol. 48, no. 1, pp. 148–155, 2013.

[54] P. M. Álvarez, F. J. Masa, J. Jaramillo, F. J. Beltrán, and V. Gómez-Serrano, “Kinetics of ozone decomposition by granular activated carbon,” *Ind. Eng. Chem. Res.*, vol. 47, no. 8, pp. 2545–2553, 2008.

[55] C. Subrahmanyam, D. A. Bulushev, and L. Kiwi-Minsker, “Dynamic behaviour of activated carbon catalysts during ozone decomposition at room temperature,” *Appl. Catal. B Environ.*, vol. 61, no. 1–2, pp. 98–106, 2005.

[56] K. Han, J. S. Zhang, B. Guo, and C. He, “Laboratory comparison of relative performance of gas phase filtration media at high and low O3/NO2 challenge concentrations (ASHRAE RP-1557),” *HVAC R Res.*, vol. 20, no. 5, pp. 522–531, 2014.

[57] A. K. Vizhemehr, “Predicting the Performance of Activated Carbon Filters at Low Concentrations Using Accelerated Test Data,” Concordia University, 2014.

[58] G. O. Wood, “A review of the effects of covapors on adsorption rate coefficients of organic vapors adsorbed onto activated carbon from flowing gases,” *Carbon N. Y.*, vol. 40, no. 5, pp. 685–694, 2002.

[59] M. A. Sidheswaran, H. Destaillats, D. P. Sullivan, S. Cohn, and W. J. Fisk, “Energy efficient indoor VOC air cleaning with activated carbon fiber (ACF) filters,” *Build. Environ.*, vol. 47, no. 1, pp. 357–367, 2012.

[60] X. Zhang, B. Gao, A. E. Creamer, C. Cao, and Y. Li, “Adsorption of VOCs onto engineered carbon materials: A review,” *J. Hazard. Mater.*, vol. 338, pp. 102–123, 2017.

[61] R. S. Popescu, P. Blondeau, E. Jouandon, and I. Colda, “Breakthrough time of activated-carbon filters used in residential and office buildings–modelling and comparison with experimental data,” *Proc. REHVA world Congr. CLIMA*, no. June, pp. 10–14, 2007.

[62] V. Safari, F. Haghighat, C. S. Lee, P. Blondeau, R. S. Popescu, and N. Lakdawala, “A systematic approach for evaluation of gas-phase filter model,” *HVAC R Res.*, vol. 19, no. 6, pp. 705–714, 2013.

[63] J. S. Jain and V. L. Snoeyink, “Adsorption from bisolute systems on active carbon,” *J. Water Pollut. Control Fed.*, vol. 45, no. 12, pp. 2463–2479, 1973.

[64] D. T. Tefera, Z. Hashisho, J. H. Philips, J. E. Anderson, and M. Nichols,

"Modeling competitive adsorption of mixtures of volatile organic compounds in a fixed-bed of beaded activated carbon," *Environ. Sci. Technol.*, vol. 48, no. 9, pp. 5108–5117, 2014.

[65] A. L. Myers and J. M. Prausnitz, "Thermodynamics of Mixed-Gas Adsorption," vol. 11, no. 1, pp. 121–127, 1965.

[66] K. A. Alkhamis and D. E. Wurster, "Study of multiple-component adsorption on the surface of activated carbon using a model system of benzyl alcohol and phenobarbital," *Pharm. Dev. Technol.*, vol. 8, no. 2, pp. 127–133, 2003.

[67] K. S. Walton and D. S. Sholl, "Predicting multicomponent adsorption: 50 years of the ideal adsorbed solution theory," *AIChE J.*, vol. 61, no. 9, pp. 2757–2762, 2015.

[68] F. Gironi and V. Piemonte, "VOCs removal from dilute vapour streams by adsorption onto activated carbon," *Chem. Eng. J.*, vol. 172, no. 2–3, pp. 671–677, 2011.

[69] J. H. Yun, D. K. Choi, and S. H. Kim, "Equilibria and dynamics for mixed vapors of BTX in an activated carbon bed," *AIChE J.*, vol. 45, no. 4, pp. 751–760, 1999.

[70] H. Naidu and A. P. Mathews, "Linear driving force analysis of adsorption dynamics in stratified fixed-bed adsorbers," *Sep. Purif. Technol.*, vol. 257, no. November 2020, p. 117955, 2021.

[71] M. G. Khararoodi, F. Haghighat, and C.-S. Lee, "Develop and validate a mathematical model to estimate the removal of indoor VOCs by carbon filters," *Build. Environ.*, p. 110082, 2023.

[72] M. Ghasemi, F. Haghighat, C.-S. Lee, and M. Namdari, “The effect of VOC and environmental parameters on ozone sensors performance,” *Adv. Build. Energy Res.*, pp. 1–21, 2023.

[73] J. Fick, L. Pommer, B. Andersson, and C. Nilsson, “Ozone removal in the sampling of parts per billion levels of terpenoid compounds: An evaluation of different scrubber materials,” *Environ. Sci. Technol.*, vol. 35, no. 7, pp. 1458–1462, 2001.

[74] K. Mermet *et al.*, “Optimization of a gas chromatographic unit for measuring biogenic volatile organic compounds in ambient air,” *Atmos. Meas. Tech.*, vol. 12, no. 11, pp. 6153–6171, 2019.

[75] NIOSH, “NIOSH Pocket Guide to Chemical Hazards.” https://www.cdc.gov/niosh/npg/npgd0476.html (accessed Apr. 17, 2022).

[76] C. Yaws, *The Yaws handbook of vapor pressure: Antoine coefficients*. Gulf Professional Publishing, 2015.

[77] R. Helburn, J. Albritton, G. Howe, L. Michael, and D. Franke, “Henry’s law constants for fragrance and organic solvent compounds in aqueous industrial surfactants,” *J. Chem. Eng. Data*, vol. 53, no. 5, pp. 1071–1079, 2008.

[78] S. Giraudet, P. Pré, H. Tezel, and P. Le Cloirec, “Estimation of adsorption energies using the physical characteristics of activated carbons and the molecular properties of volatile organic compounds,” *Carbon N. Y.*, vol. 44, no. 12, pp. 2413–2421, 2006.

[79] F. Qu, L. Zhu, and K. Yang, “Adsorption behaviors of volatile organic compounds (VOCs) on porous clay heterostructures (PCH),” *J. Hazard. Mater.*, vol. 170, no. 1, pp. 7–12, 2009.

[80] M. J. Lashaki, M. Fayaz, S. Niknaddaf, and Z. Hashisho, “Effect of the adsorbate kinetic diameter on the accuracy of the Dubinin–Radushkevich equation for modeling adsorption of organic vapors on activated carbon,” *J. Hazard. Mater.*, vol. 241, pp. 154–163, 2012.

[81] ASHRAE, “ANSI/ASHRAE Standard 145.2. Laboratory Test Method for Assessing the Performance of Gas-Phase Air-C lean ing Systems: Air-C lean ing Devices,” 2016.

[82] N. I. Onuoha and M. S. WA1NWRIGHT, “Catalyst deactivation in the hydrolysis of acrylonitrile to acrylamide over Raney copper,” *Chem. Eng. Commun.*, vol. 29, no. 1–6, pp. 13–25, 1984.

[83] T. S. Y. Choong, T. N. Wong, T. G. Chuah, and A. Idris, “Film-pore-concentration-dependent surface diffusion model for the adsorption of dye onto palm kernel shell activated carbon,” *J. Colloid Interface Sci.*, vol. 301, no. 2, pp. 436–440, 2006.

[84] S. J. Doong and R. T. Yang, “A simple potential-theory model for predicting mixed-gas adsorption,” *Ind. Eng. Chem. Res.*, vol. 27, no. 4, pp. 630–635, 1988.

[85] G. O. Wood, “Review and comparisons of D/R models of equilibrium adsorption of binary mixtures of organic vapors on activated carbons,” *Carbon N. Y.*, vol. 40, no. 3, pp. 231–239, 2002.

[86] B. P. Bering, V. V Serpinsky, and S. I. Surinova, “Mixed Gas Adsorption by Activated Carbons,” in *Dokl. Akad. Nauk. SSSR*, 1963, vol. 153, p. 129.

[87] R. Bai and R. T. Yang, “A Modification of the Doong− Yang Model for Gas Mixture Adsorption Using the Lewis Relationship,” *Langmuir*, vol. 21, no. 18, pp. 8326–8332, 2005.

[88] F. A. Carey, *ORGANIC CHEMISTRY*. McGraw-Hill, 2014.

[89] C. J. Weschler, “Ozone’s impact on public health: contributions from indoor exposures to ozone and products of ozone-initiated chemistry,” *Environ. Health Perspect.*, vol. 114, no. 10, pp. 1489–1496, 2006.

[90] C. J. Weschler, “Ozone in indoor environments: concentration and chemistry,” *Indoor Air*, vol. 10, no. 4, pp. 269–288, 2000.

[91] M. G. Khararoodi, F. Haghighat, and C.-S. Lee, “Removal of indoor air ozone using carbon-based filters: Systematic development and validation of a predictive model,” *Build. Environ.*, p. 109157, 2022.

[92] D. O. COONEY, “The importance of axial dispersion in liquid-phase fixed-bed adsorption operations,” *Chem. Eng. Commun.*, vol. 110, no. 1, pp. 217–231, 1991.

[93] W. J. Massman, “A review of the molecular diffusivities of H2O, CO2, CH4, CO, O3, SO2, NH3, N2O, NO, and NO2 in air, O2 and N2 near STP,” *Atmos. Environ.*, vol. 32, no. 6, pp. 1111–1127, 1998.

[94] N. Wakao and J. M. Smith, “Diffusion in catalyst pellets,” *Chem. Eng. Sci.*, vol. 17, no. 11, pp. 825–834, 1962.

[95] D. C. K. Ko, C. W. Cheung, and J. F. Porter, “A branched pore kinetic model applied to the sorption of metal ions on bone char,” *J. Chem. Technol. Biotechnol. Int. Res. Process. Environ. Clean Technol.*, vol. 80, no. 8, pp. 861–871, 2005.

[96] E. A. Celaya, J. J. A. Aguirrezabala, and P. Chatzipantelidis, “Implementation of an Adaptive BDF2 Formula and Comparison with the MATLAB Ode15s,” *Procedia Comput. Sci.*, vol. 29, pp. 1014–1026, 2014.

[97] M. Malayeri, M. Bahri, F. Haghighat, and A. Shah, “Impact of air distribution on indoor formaldehyde abatement with/without passive removal material: A CFD modeling,” *Build. Environ.*, p. 108792, 2022.

[98] J. Ju, B. Shi, Z. Yu, Y. Zhu, and Z. Zhao, “Backward Discrete State Event-Driven Approach for Simulation of Stiff Power Electronic Systems,” *IEEE Access*, vol. 9, pp. 28573–28581, 2021.

[99] L. Zhong, C.-S. Lee, and F. Haghighat, “Indoor ozone and climate change,” *Sustain. cities Soc.*, vol. 28, pp. 466–472, 2017.

[100] D. R. Gold, G. Allen, A. Damokosh, P. Serrano, C. Hayes, and M. Castiilejos, “Comparison of outdoor and classroom ozone exposures for school children in Mexico City,” *J. Air Waste Manage. Assoc.*, vol. 46, no. 4, pp. 335–342, 1996.

[101] S. International, “SAE AIR910. Ozone in High Altitude Aircraft,” *2011*.

[102] H. Canada, “Residential Indoor Air Quality Guideline: Ozone.” https://www.canada.ca/en/health-canada/services/publications/healthy-living/residential-indoor-air-quality-guideline-ozone.html (accessed Apr. 17,

2022).

[103] S. Becker, J. M. Soukup, W. Reed, J. Carson, R. B. Devlin, and T. L. Noah, "Effect of ozone on susceptibility to respiratory viral infection and virus-induced cytokine secretion," *Environ. Toxicol. Pharmacol.*, vol. 6, no. 4, pp. 257–265, 1998.

[104] P. Lee and J. Davidson, "Evaluation of activated carbon filters for removal of ozone at the PPB level," *Am. Ind. Hyg. Assoc. J.*, vol. 60, no. 5, pp. 589–600, 1999.

[105] Y. Takeuchi and T. Itoh, "Removal of ozone from air by activated carbon treatment," *Sep. Technol.*, vol. 3, no. 3, pp. 168–175, 1993.

[106] M. Ondarts, J. Outin, L. Reinert, E. Gonze, and L. Duclaux, "Removal of ozone by activated carbons modified by oxidation treatments," *Eur. Phys. J. Spec. Top.*, vol. 224, no. 9, pp. 1995–1999, 2015.

[107] R. Ligotski, U. Sager, U. Schneiderwind, C. Asbach, and F. Schmidt, "Prediction of VOC adsorption performance for estimation of service life of activated carbon based filter media for indoor air purification," *Build. Environ.*, vol. 149, pp. 146–156, 2019.

[108] E. Koessler and A. Almomani, "Hybrid particle swarm optimization and pattern search algorithm," *Optim. Eng.*, vol. 22, no. 3, pp. 1539–1555, 2021.

[109] D. S. P. Franco, J. L. S. Fagundes, J. Georgin, N. P. G. Salau, and G. L. Dotto, "A mass transfer study considering intraparticle diffusion and axial dispersion for

fixed-bed adsorption of crystal violet on pecan pericarp (Carya illinoensis),” *Chem. Eng. J.*, vol. 397, p. 125423, 2020.

[110] M. Namdari, C.-S. Lee, and F. Haghighat, “Active ozone removal technologies for a safe indoor environment: A comprehensive review,” *Build. Environ.*, vol. 187, no. September 2020, p. 107370, 2021.

[111] A. A. Ahmad and B. H. Hameed, “Fixed-bed adsorption of reactive azo dye onto granular activated carbon prepared from waste,” *J. Hazard. Mater.*, vol. 175, no. 1–3, pp. 298–303, 2010.

[112] P. G. Aguilera and F. J. Gutiérrez Ortiz, “Prediction of fixed-bed breakthrough curves for H2S adsorption from biogas: Importance of axial dispersion for design,” *Chem. Eng. J.*, vol. 289, pp. 93–98, 2016.

[113] W. D. Ellis and P. V Tometz, “Room-temperature catalytic decomposition of ozone,” *Atmos. Environ.*, vol. 6, no. 10, pp. 707–714, 1972.

[114] M. L. Kingsley, “Adsorption of Low Concentration Gaseous Mixtures on Activated Carbon,” University of Minnesota, 2004.

[115] H. Valdés, M. Sánchez-Polo, J. Rivera-Utrilla, and C. A. Zaror, “Effect of ozone treatment on surface properties of activated carbon,” *Langmuir*, vol. 18, no. 6, pp. 2111–2116, 2002.

[116] C.-Y. Wen and L. Fan, “Models for flow systems and chemical reactors,” 1975.

[117] C. S. Lee, W. B. Amorim, S. Rastan, E. Morofsky, M. Dziedzic, and F. Haghighat, “Measurements of Indoor and Outdoor Air VOC Levels of Office Buildings in

Montreal," 2009.

[118] USEPA, "Volatile Organic Compounds' Impact on Indoor Air Quality." https://www.epa.gov/indoor-air-quality-iaq/volatile-organic-compounds-impact-indoor-air-quality (accessed Apr. 10, 2022).

[119] S. K. Brown, M. R. Sim, M. J. Abramson, and C. N. Gray, "Concentrations of volatile organic compounds in indoor air–a review," *Indoor Air*, vol. 4, no. 2, pp. 123–134, 1994.

[120] M. Malayeri, J. Zhu, J. Niu, C.-S. Lee, and F. Haghighat, "Kinetic modeling of binary mixture of butyraldehyde and acetone with generated by-products in photocatalytic oxidation reactor," *Chem. Eng. J.*, vol. 443, p. 136457, 2022.

[121] Iaqscience, "Volatile Organic Compounds." https://iaqscience.lbl.gov/vocs-and-cancer (accessed Apr. 10, 2022).

[122] A. V Pimenov, A. I. Lieberman, J. L. Shmidt, and H. Y. Cheh, "Accelerated adsorption with activated carbon fiber," *Sep. Sci. Technol.*, vol. 30, no. 16, pp. 3183–3194, 1995.

[123] P. Li, G. Xiu, and A. E. Rodrigues, "Modelling diffusion and reaction for inert-core catalyst in batch and fixed bed reactors," *Can. J. Chem. Eng.*, vol. 97, no. 1, pp. 217–225, 2019.

[124] A. Shiue *et al.*, "Validation and application of adsorption breakthrough models for the chemical filters used in the make-up air unit (MAU) of a cleanroom," *Build. Environ.*, vol. 46, no. 2, pp. 468–477, 2011.

[125] J. C. Crittenden, R. R. Trussell, D. W. Hand, K. J. Howe, and G. Tchobanoglous, *MWH's water treatment: principles and design*. John Wiley & Sons, 2012.

[126] M. Yao, Q. Zhang, D. W. Hand, D. L. Perram, and R. Taylor, "Investigation of the treatability of the primary indoor volatile organic compounds on activated carbon fiber cloths at typical indoor concentrations," *J. Air Waste Manage. Assoc.*, vol. 59, no. 7, pp. 882–890, 2009.

[127] I. I. Laskar and Z. Hashisho, "Insights into modeling adsorption equilibria of single and multicomponent systems of organic and water vapors," *Sep. Purif. Technol.*, vol. 241, no. February, p. 116681, 2020.

[128] R. T. Yang, *Adsorbents: fundamentals and applications*. John Wiley & Sons, 2003.

[129] F. A. Carey, *Organic Chemistry*. McGraw-Hill Higher Education, 2000.

[130] Ruthven, "Douglas M. Ruthven - Principles of Adsorption and Adsorption Processes-Wiley-Interscience (1984).pdf." 2004.

[131] G. Marbán, L. A. Ramírez-Montoya, H. García, J. Á. Menéndez, A. Arenillas, and M. A. Montes-Morán, "Load-dependent surface diffusion model for analyzing the kinetics of protein adsorption onto mesoporous materials," *J. Colloid Interface Sci.*, vol. 511, pp. 27–38, 2018.

[132] D. Richard, M. de L. Delgado Núñez, and D. Schweich, "Adsorption of complex phenolic compounds on active charcoal: Breakthrough curves," *Chem. Eng. J.*, vol. 158, no. 2, pp. 213–219, 2010.

[133] N. J. Barrow, “The description of phosphate adsorption curves,” *J. Soil Sci.*, vol. 29, no. 4, pp. 447–462, 1978.

[134] C. L. Mangun, M. A. Daley, R. D. Braatz, and J. Economy, “Effect of pore size on adsorption of hydrocarbons in phenolic-based activated carbon fibers,” *Carbon N. Y.*, vol. 36, no. 1–2, pp. 123–129, 1998.

[135] K. C. A. Alam, B. B. Saha, Y. T. Kang, A. Akisawa, and T. Kashiwagi, “Heat exchanger design effect on the system performance of silica gel adsorption refrigeration systems,” *Int. J. Heat Mass Transf.*, vol. 43, no. 24, pp. 4419–4431, 2000.

[136] D. C. K. Ko, J. F. Porter, and G. McKay, “Application of the concentration-dependent surface diffusion model on the multicomponent fixed-bed adsorption systems,” *Chem. Eng. Sci.*, vol. 60, no. 20, pp. 5472–5479, 2005.

[137] M. J. Ahmed, A. H. A. K. Mohammed, and A. A. H. Kadhum, “Modeling of breakthrough curves for adsorption of propane, n-butane, and iso-butane mixture on 5A molecular sieve zeolite,” *Transp. porous media*, vol. 86, pp. 215–228, 2011.

[138] L. Li, Z. Liu, J. Xin, J. Song, and L. Tang, “Adsorption Modeling with Soret-Like and Dufour Effects of a Two-Component Organic Gas on Activated Carbon,” *J. Chem. Eng. Data*, vol. 57, no. 2, pp. 568–576, 2012.

[139] A. D. da Luz, S. M. de A. Guelli Ulson de Souza, C. da Luz, J. M. M. de Mello, and A. A. Ulson de Souza, “Analysis of competition between multicomponent BTX compounds for the active site of adsorption in a fixed-bed column,” *Ind. Eng. Chem. Res.*, vol. 52, no. 47, pp. 16911–16921, 2013.

[140] S. U. Rege and R. T. Yang, “A novel FTIR method for studying mixed gas adsorption at low concentrations: H2O and CO2 on NaX zeolite and γ-alumina,” *Chem. Eng. Sci.*, vol. 56, no. 12, pp. 3781–3796, 2001.

[141] P. Atkins, P. W. Atkins, and J. de Paula, *Atkins' physical chemistry*. Oxford university press, 2014.

[142] Y. G. Dobrjakov, I. M. Balashova, and G. Maurer, “Experimental results for the limiting activity coefficients in some binary and ternary mixtures of organic components,” *J. Chem. Eng. Data*, vol. 45, no. 2, pp. 185–193, 2000.

[143] A. R. Mansour, A. B. Shahalam, and N. Darwish, “A comprehensive study of parameters influencing the performance of multicomponent adsorption in fixed beds,” *Sep. Sci. Technol.*, vol. 19, no. 13–15, pp. 1087–1111, 1984.

[144] M. Namdari, C.-S. Lee, and F. Haghighat, “The effect of operational conditions on the performance of granular ozone removal media: Statistical experimental design and kinetic modeling,” *Build. Environ.*, p. 110216, 2023.

[145] G. Shaverdi, F. Haghighat, and W. Ghaly, “Development and systematic validation of an adsorption filter model,” *Build. Environ.*, vol. 73, pp. 64–74, 2014.

[146] T. A. Metts and S. A. Batterman, “Effect of VOC loading on the ozone removal efficiency of activated carbon filters,” *Chemosphere*, vol. 62, no. 1, pp. 34–44, 2006.

[147] C. Subrahmanyam, D. A. Bulushev, and L. Kiwi-Minsker, “Dynamic behaviour of activated carbon catalysts during ozone decomposition at room temperature,”

Appl. Catal. B Environ., vol. 61, no. 1–2, pp. 98–106, 2005.

[148] M. L. Kingsley and J. H. Davidson, "Adsorption of toluene onto activated carbons exposed to 100 ppb ozone," *Carbon N. Y.*, vol. 44, no. 3, pp. 560–564, 2006.

[149] R. Atkinson, D. Hasegawa, and S. M. Aschmann, "Rate constants for the gas-phase reactions of O3 with a series of monoterpenes and related compounds at 296±2 K," *Int. J. Chem. Kinet.*, vol. 22, no. 8, pp. 871–887, 1990.

[150] J. H. Kroll and J. H. Seinfeld, "Chemistry of secondary organic aerosol: Formation and evolution of low-volatility organics in the atmosphere," *Atmos. Environ.*, vol. 42, no. 16, pp. 3593–3624, 2008.

[151] B. Chuong, J. Zhang, and N. M. Donahue, "Cycloalkene ozonolysis: collisionally mediated mechanistic branching," *J. Am. Chem. Soc.*, vol. 126, no. 39, pp. 12363–12373, 2004.

[152] M. F. M. G. Resul, A. M. L. Fernández, A. Rehman, and A. P. Harvey, "Development of a selective, solvent-free epoxidation of limonene using hydrogen peroxide and a tungsten-based catalyst," *React. Chem. Eng.*, vol. 3, no. 5, pp. 747–756, 2018.

APPENDIX

Prequalification tests for bench-scale setup

The prequalification tests were done in three steps: 1) concentration uniformity test, 2) no filter test, and 3) 100 % efficiency test.

Concentration uniformity test

A uniform concentration profile is required within the duct to assure that the sample concentration represents the true concentration of pollutants in the system. A perforated mesh was used at the test duct entrance to create uniform concentrations within the duct. The uniformity test was conducted for ozone and limonene. The experimental procedure was explained in the experimental setup and analysis instrument section. The difference was that the ozone and limonene concentrations were measured at five points (see Fig. A. 1) for 5 minutes. This test was performed five times with ozone and limonene at target concentrations of 0.1 ppm and 9 ppm, respectively. The results showed that the coefficient of variation (CV) for both compounds is less than 2 percent (see Table. A. 1).

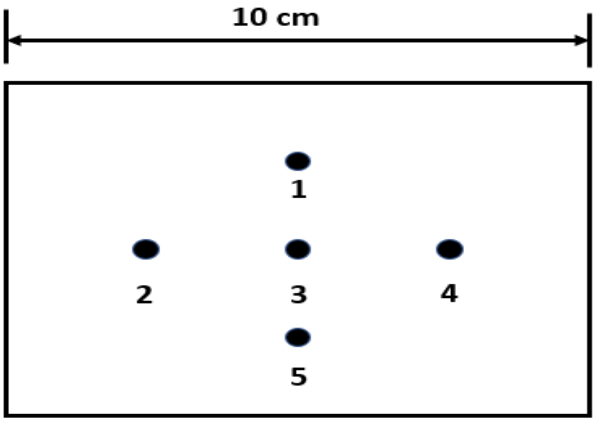

Fig. A. 1: In-duct concentration traverse points.

Table. A. 1: Experimental results for concentration uniformity test.

	Parameters	Point 1	Point 2	Point 3	Point 4	Point 5	All points
Ozone	Ave. Concentration (ppm)	0.099	0.102	0.100	0.102	0.104	0.101
	STDEV	3.8	1.7	1.5	2.5	4.0	-
	CV (%)	-	-	-	-	-	1.97
Limonene	Ave. Concentration (ppm)	9.12	9.10	8.94	9.03	8.95	9.03
	STDEV	2.9	2.0	2.1	3.0	1.8	-
	CV (%)	-	-	-	-	-	1.90

No filter test

An upstream/downstream comparison test was carried out without any filter to investigate the loss of pollutants to the test duct wall. This test was performed twice with ozone at target concentrations of 0.1 ppm and 0.5 ppm. A three-channel ozone monitor (2B Technologies Model 106-M) was employed to simultaneously measure ozone concentrations upstream and downstream of the test duct. During the test, channels one and two were connected upstream and downstream, respectively. Also, the same test was performed for limonene with a target concentration of 9 ppm (see Fig. A. 2). The measurement was done for one hour for each concentration. Table. A. 3 shows the results of all experiments. It can be seen that for both tests, the removal was less than 1%.

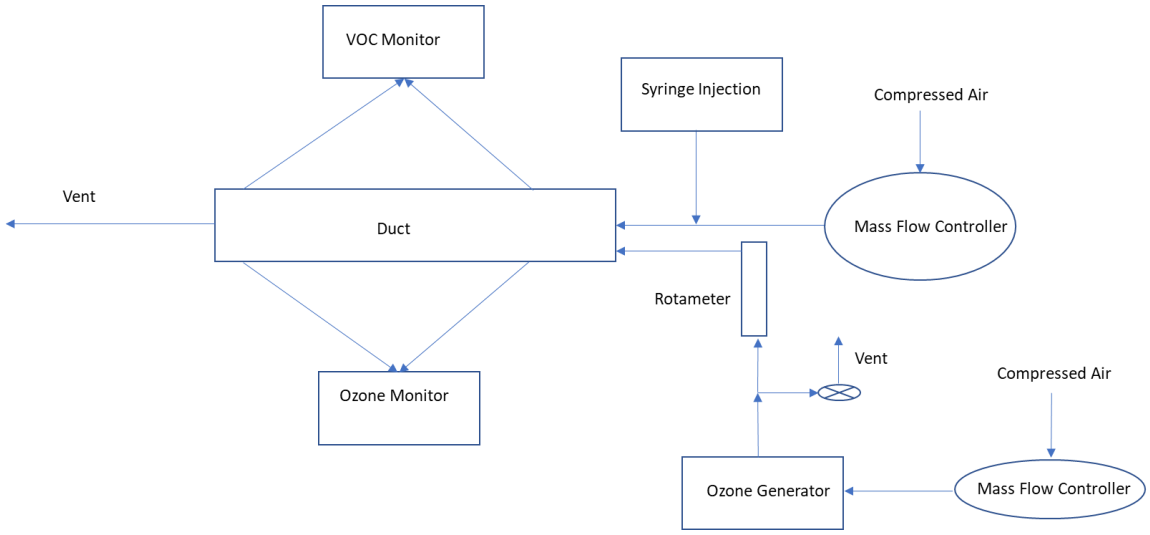

Fig. A. 2: Schematic diagram of experimental setup for no filter test.

Table. A. 2: Experimental results for no filter test.

Test Number	compound	Carrier Gas Flow Rate (L/min)	Ave. Upstream Concentration (ppm)	Ave. Downstream Concentration (ppm)	Removal (%)
1	Ozone	30.64	0.104	0.106	-1.2
2	Ozone	30.30	0.527	0.524	0.5
3	Ozone	30.55	0.110	0.109	0.7
4	Ozone	30.32	0.545	0.540	0.9
1	Limonene	30.09	9.12	9.03	0.9
2	Limonene	30.22	8.97	8.90	0.8

100% efficiency test

To investigate the possible error sources (leaks and dead spaces), an efficiency test should be carried out to show that the test duct and sampling system can provide efficiency higher than 99% [81]. A panel filter with a thickness of 2.5 cm filled with 130.4 g coconut-based granular activated carbon was utilized as an air cleaner. The filter was sealed in the test duct by a gasket to avoid leakage. This test was done twice with ozone at a target concentration of 0.5 ppm. A one-channel ozone monitor (2B Technologies Model

scrubberless 211) was used to measure the ozone concentration at the filter upstream and downstream. At first, the ozone monitor was connected downstream when the injection was started. Then, it was switched between upstream and downstream by a three-way valve during the total experiment time of 50 minutes. This test was also repeated for limonene, with a target concentration of 9 ppm. For the measurement of toluene, PID analyzer was utilized (see Fig. A. 3). Table. A. 3 shows the results of all experiments. It can be seen that in all cases, the filter's efficiency was higher than 99%.

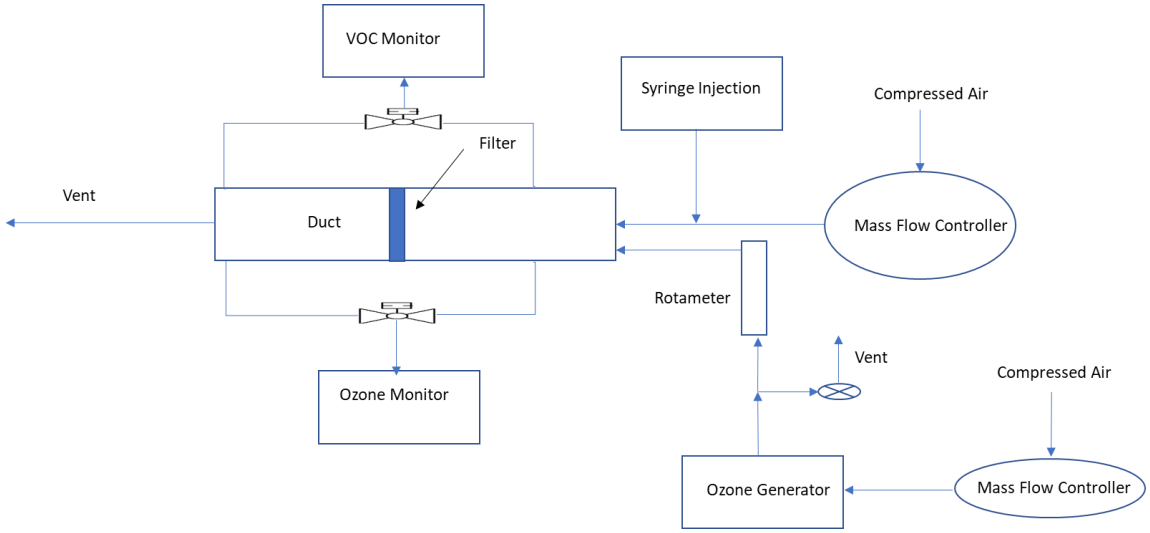

Fig. A. 3: Schematic diagram of the experimental setup for 100% efficiency test.

Table. A. 3: Experimental results for 100% efficiency test.

Test Number	compounds	Carrier Gas Flow Rate (L/min)	Ave. Upstream Concentration (ppm)	Ave. Downstream Concentration (ppm)	Efficiency of Filter (%)
1	Ozone	30.82	0.524	0.0025	99.53
2	Ozone	30.83	0.543	0.0008	99.84
1	Limonene	30.05	9.245	0.080	99.13
2	Limonene	30.30	9.320	0.085	99.09